Spring 4-2010

COMPUTATIONAL AND EXPERIMENTAL CHARACTERIZATION OF BITUMINOUS COMPOSITES BASED ON EXPERIMENTALLY DETERMINED PROPERTIES OF CONSTITUENTS

Pravat Karki
University of Nebraska at Lincoln, pravatko@utexas.edu

COMPUTATIONAL AND EXPERIMENTAL CHARACTERIZATION OF BITUMINOUS COMPOSITES BASED ON EXPERIMENTALLY DETERMINED PROPERTIES OF CONSTITUENTS

By

Pravat Karki

A THESIS

Presented to the Faculty of

The Graduate College at the University of Nebraska

In Partial Fulfillment of Requirements

For the Degree of Master of Science

Major: Civil Engineering

Under the Supervision of Professor Yong-Rak Kim

Lincoln, Nebraska

April, 2010

COMPUTATIONAL AND EXPERIMENTAL CHARACTERIZATION OF BITUMINOUS COMPOSITES BASED ON EXPERIMENTALLY DETERMINED PROPERTIES OF CONSTITUENTS

Pravat Karki, M.S.

University of Nebraska, 2010

Adviser: Yong-Rak Kim

The stiffness of asphalt concrete mixtures is characterized in terms of the dynamic modulus for designing the thickness of flexible pavements. The dynamic modulus value of asphalt concrete is either determined experimentally or predicted by using empirical, semi-empirical, analytical or computational micromechanics models. This study proposes to use a computational micromechanics model to predict the dynamic modulus of asphalt concrete mixtures based on the experimentally determined properties of the constituents in the heterogeneous microstructure. The model defines asphalt concrete mixtures as the composites of two different homogeneous isotropic components – the viscoelastic fine aggregate matrix phase and the elastic aggregate phase.

Mechanical properties are determined by oscillatory torsional shear tests of cylindrical bars of fine aggregate matrix mixtures, and quasi-static nanoindentation tests of aggregates. A protocol is developed to mix-design and fabricate the Superpave gyratory compacted fine aggregate matrix mixture as a replicate of fine aggregate matrix phase of asphalt concrete mixtures in terms of binder content, air void content and specific gravity.

The cyclic uniaxial compressive tests are computationally simulated based on the finite element method (FEM). The model uses the material properties of the two-dimensional microstructure that are obtained from digitally processed images of asphalt concrete mixtures. The results are compared with the experimentally determined dynamic modulus tests of the same cylindrical samples of asphalt concrete mixtures. FEM simulations of the dynamic modulus of rectangular microstructure agreed with the laboratory tests of cylindrical samples.

To all my beloved kiths and kin

ACKNOWLEDGEMENT

I would first like to thank my advisor and graduate committee chairperson, Dr. Yong-Rak Kim for his continuous support, trust, and encouragement during the last two years of my Master's degree. Dr. Kim was always there to listen and to give me advice whenever I had questions about my research and confusions about my future. From him, I have learnt to look for different ways to approach a research problem and the need to be persistent to accomplish any goal. It was my honor to find Dr. David H. Allen and Dr. Raymond Moore as my graduate committee members. My thanks also go to Dr. Joseph A. Turner for advising me time and again during the nanoindentation tests.

A special thanks to Dr. Junghun Lee, who was always there to help me with advice as a post-doc and an elder brother. I will always remember his contribution in my research. The next person who has contributed a lot in shaping my research so nicely is my dear friend Francisco Thiago Sacramento Aragão. As a research colleague and a brother, he helped me in understanding and solving the problems in my research and personal life. I would also like to thank Dr. Philip Abuor Yuya for helping me in conducting the nanoindentation tests in spite of his busy schedule.

My thanks also go to my research and office partners, Minki Hong and Soohyok Im, who not only shared the office but also the enthusiasm of working and succeeding continuously. My research colleagues, Dr. Hoki Ban, Jamilla Lutif, Leonardo Souza, Ingryd Pinto, Aseel Ahmad, Jun Zhang and Mohammad Haft Javaherian all have helped me in different stages of my research. I want to thank all of them. I would also like to thank Boris Mijatovic, Victor Ventorini Pontes and Ian Plummer for their help in

fabricating the samples for my tests by preparing the materials whenever I needed. With the help of these laborious friends, I could complete my research in time.

I really appreciate the support from my family back home in Nepal, namely my father Basudev Karki, my mum Laxmi Karki, the eldest brother Bhuwan Karki, sister-in-law Uma Karki and my cousin Suveskhya Karki. Without the love and blessings from them, no task would have been completed successfully. My love and respect to my brothers, Kiran Karki and Prabin Karki for understanding my busy schedule. Their stay in the States made my stay in Nebraska as if I were in Nepal.

I thank my friends, Nabaraj Banjara, Kundan Dhakal and Nischhal K.C. for their cooperation during my research. As my apartment partners, they provided me privacy, freedom and cooperation whenever and wherever I required.

Last but not least, I want to thank the Federal Highway Administration (FHWA), Western Research Institute (WRI), Asphalt Research Consortium (ARC), Texas A $& M University for their financial support for this research project. Similarly, I would like to thank all the members of Computation of Homogenized Evolutionary Stresses in Inhomogeneous Viscoelastic Entities (COHESIVE) research group for helping me at several times and ways. I thank Mr. Larry Koves, Mr. James Beason and other people in Nebraska Department of Roads (NDOR) for training me to fabricate and test asphalt concrete mixtures.

Finally, I would like to thank all my friends around the globe for their best wishes.

TABLE OF CONTENTS

ACKNOWLEDGEMENT ii
LIST OF FIGURES viii
LIST OF TABLES x
CHAPTER 1 INTRODUCTION 1
1.1 Overview 1
1.2 Research Objectives 6
1.3 Research Scope 6
1.4 Thesis Organization 7
CHAPTER 2 LITERATURE REVIEW 9
2.1 Asphalt Binder 9
2.2 Aggregates 10
2.3 Asphalt Concrete Mixtures 12
2.3.1 Background 12
2.3.2 Properties 13
2.3.3 Asphalt Concrete Characterization 20
2.4 Fine Aggregate Matrix Mixtures 28
2.4.1 Background 28
2.4.2 Properties 30
2.4.3 Fine Aggregate Matrix Characterization 31
2.5 Nanoindentation Tests for Elastic Modulus of Aggregates 34
CHAPTER 3 EXPERIMENTAL CHARACTERIZATION OF ASPHALT CONCRETE MIXTURES 43
3.1 Material Selection 43
3.1.1 Aggregates 43
3.1.2 Binder 44
3.2 Mix Design 44
3.3 Sample Fabrication 44
3.4 Dynamic Modulus Tests 45
3.4.1 Test Sample Preparation 45

3.4.2 Temperature Equilibrium 47
3.4.3 Load Profile 47
3.4.4 Cyclic Uniaxial Compressive Tests 48
3.4.5 Test Execution and Data Acquisition 49
3.5 Data Analysis 49
3.5.1 Dynamic Modulus Tests 49
3.5.2 Master Curve Development 50
3.6 Results 51
3.6.1 Sieve Analysis 51
3.6.2 Volumetric Analysis 52
3.6.3 Dynamic Modulus Tests 53
3.5.4 Master Curve Generation 54
CHAPTER 4 EXPERIMENTAL CHARACTERIZATION OF FINE AGGREGATE MATRIX 57
4.1 Material Selection 57
4.1.1 Aggregates 57
4.1.2 Binder 59
4.2 Mix Design 59
4.2.1 Binder Content 59
4.2.2 Compaction Density 62
4.3 Sample Fabrication 64
4.4 Oscillatory Frequency Sweep Tests 66
4.4.1 Test Sample Preparation 66
4.4.2 Temperature Equilibrium 66
4.4.3 Load Profile 66
4.4.4 Oscillatory Torsional Shear Tests 67
4.4.5 Data Acquisition 68
4.5 Data Analysis 68
4.5.1 Oscillatory Torsional Shear Tests 68
4.5.2 Master Curve Generation 69
4.5.3 Prony Series Coefficients 70

4.6 Results 71
4.6.1 Sieve Analysis of Aggregates 71
4.6.2 Volumetric Analysis of Mixtures 72
4.6.3 Oscillatory Torsional Shear Tests 73
4.6.4 Master Curve Development 74
4.6.5 Prony Series Coefficients 76
CHAPTER 5 EXPERIMENTAL CHARACTERIZATION OF AGGREGATES 78
5.1 Material/ Sample Selection 78
5.2 Sample Preparation 79
5.3 Nanoindentation Tests 81
5.3.1 Calibration 82
5.3.2 Selection of Points of Interest 82
5.3.3 Load Profile 84
5.3.4 Quasi Static Tests 86
5.3.5 Data Acquisition 86
5.4 Data Analysis 86
5.5 Results 88
CHAPTER 6 COMPUTATIONAL CHARACTERIZATION OF ASPHALT CONCRETE MIXTURES 93
6.1 Sampling 93
6.2 Sample Preparation 93
6.2.1 Digital Scanning 93
6.2.2 Image Treatment 93
6.2.3 Image Analysis 95
6.2.4 Finite Element Mesh Generation 96
6.3. FEM Simulations of Dynamic Modulus Tests 96
6.3.1 Material Properties 96
6.3.2 Boundary Conditions 97
6.3.3 Load Profile 98
6.3.4 Test Execution 99
6.3.5 Data Acquisition 99

6.4 Data Analysis 100
6.5 Results 101
6.5.1 Characteristics of AC Microstructure 101
6.5.2 Dynamic Modulus Tests 103
CHAPTER 7 RESULTS AND DISCUSSIONS 105
7.1 Results from Experimental Characterization of Asphalt Concrete Mixtures 105
7.2 Results from Experimental Characterization of Fine Aggregate Matrix Mixtures 106
7.2.1 Properties at the Different Locations of SGC Matrix Samples 106
7.2.2 Properties of Different Types of SGC Matrix Samples 107
7.3 Results from Experimental Characterization of Aggregates 109
7.4 Results from Computational Characterization of Asphalt Concrete Mixtures 111
7.5 Comparison between Experimental Method and Computational Model 112
CHAPTER 8 CONCLUSIONS AND RECOMMENDATIONS 115
8.1 Conclusions 115
8.2 Recommendations 117
BIBLIOGRAPHY 119

LIST OF FIGURES

Figure 1.1 Phases of Asphalt Concrete Mixtures 3
Figure 1.2 Parametric Analysis on Aggregate Stiffness (Aragão et al., 2010) 5
Figure 1.3 Flow Chart of Research Methodology 7
Figure 2.1 Components of the Complex Modulus 17
Figure 2.2 Components of the Complex Shear Modulus 31
Figure 2.3 Sphere Indenting on a Semi-Infinite Substratum 36
Figure 3.1 Sample Fabrication of Asphalt Concrete Mixtures 45
Figure 3.2 Gages in Asphalt Concrete Samples (AASHTO TP 62) 46
Figure 3.3 Installing the Asphalt Concrete Samples for Tests 46
Figure 3.4 Input and Output Signals of Dynamic Modulus Tests 48
Figure 3.5 Aggregate Proportions in AC Mixtures by (a) Type (b) Size 51
Figure 3.6 Dynamic Modulus Tests of Asphalt Concrete Mixtures 54
Figure 3.7 Dynamic Modulus Master Curve of Asphalt Mixtures 55
Figure 3.8 Shift Factors for Asphalt Concrete Mixtures 56
Figure 4.1 Aggregate Proportions in AC and FAM by Type 58
Figure 4.2 Sieve Analysis of Aggregates in AC and FAM 58
Figure 4.3 Superpave Gyratory Compaction of Fine Aggregate Matrix 64
Figure 4.4 Torsional Bars Extraction SGC Fine Aggregate Matrix 65
Figure 4.5 Input and Output Signals of Torsional Shear Tests 67
Figure 4.6 FAM Sample Installation and Test Methodology 68
Figure 4.7 Sieve Analyses of Aggregates in Fine Aggregate Matrix 72
Figure 4.8 Frequency Sweep Tests of Fine Aggregate Matrix Bars 73
Figure 4.9 Master Curve of Dynamic Shear Modulus of FAM Bars 74
Figure 4.10 FAM Master Curves (a) Shift Factors (b) Shift at 23^{o}C 75
Figure 4.11 Storage Shear Modulus of Fine Aggregate Matrix 76
Figure 4.12 Relaxation Shear Modulus of Fine Aggregate Matrix 77
Figure 5.1 Sampling of AC Mixtures for Nanoindentation 79
Figure 5.2 Assembly for Holding the Sample During, Grinding and Polishing 80
Figure 5.3 Accessories for Gluing, Grinding and Polishing 80

Figure 5.4 Grinding and Polishing for Nanoindentation 81
Figure 5.5 Nanoindentation Test Equipments and Indenter 82
Figure 5.6 Points of Interest for Nanoindentation Tests 83
Figure 5.7 Visualization of Trapezoidal Loading Profile 84
Figure 5.8 Indentation Curves from Trapezoidal Loading Profile 84
Figure 5.9 Indentation Curves from Triangular Loading Profile 85
Figure 5.10 Loading Profiles for Nanoindentation Samples 85
Figure 5.11 Load-Indentation Depth Profile in Nanoindentation 87
Figure 5.12 Images of Residual Indentations 89
Figure 5.13 Results of Nanoindentation Tests in Limestone 90
Figure 5.14 Topography and Gradients of AC Samples 91
Figure 5.15 Results of Nanoindentation Tests in AC Samples 91
Figure 6.1 Image Treatment for (a) Scanning (b) Black and White (c) Boundary 94
Figure 6.2 Boundary Conditions for FEM Test Simulations 98
Figure 6.3 Input and Output Signals of FEM Test Simulations 99
Figure 6.4 Virtual Measuring Gages in FEM Test Sample 100
Figure 6.5 Sieve Analysis by Aggregates by Areas and Weights 103
Figure 6.6 Master Curves of Dynamic Modulus from Simulations 103
Figure 7.1 Master Curve of Dynamic Modulus of Mixtures from Tests 105
Figure 7.2 Comparison of Compaction of FAM with 0.00 % Air Voids 106
Figure 7.3 Comparison of Compaction of FAM with 1.75 % Air Voids 107
Figure 7.4 Comparison of Dynamic Modulus of Different Types of Matrix 108
Figure 7.5 Comparison of Stiffness of Different Types of Matrix @ 50 rad. / sec 109
Figure 7.6 Elastic Modulus Values of Aggregates in AC Mixtures 110
Figure 7.7 Dynamic Moduli from FEM Simulations: V a = 0.00%, 1.75% 111
Figure 7.8 Comparison of Stiffness from Tests and FEM Simulations 112
Figure 7.9 Simulation Results within the Allowable Limits of Experimental Results ... 114

LIST OF TABLES

Table 1.1 Time and Equipments Required for Dynamic Modulus Tests 2
Table 3.1 Aggregate Proportions in Asphalt Concrete Mixtures..... 43
Table 3.2 Volumetric Properties of Asphalt Concrete Mixtures 52
Table 3.3 Dynamic Modulus of Asphalt Concrete Mixtures..... 53
Table 4.1 Aggregate Proportions in Fine Aggregate Matrix 57
Table 4.2 Volumetric Properties of Fine Aggregate Matrix..... 65
Table 4.3 Sieve Analysis of Aggregates in Fine Aggregate Matrix 72
Table 6.1 Sieve Analysis of Aggregate by Area and Weight 102

CHAPTER ONE

INTRODUCTION

1.1 Overview

Bituminous composites are widely used in different fields of public and private construction including airport runways, roadways, parking lots, roofs, driveways and many more. Obviously a lot of money is spent on the materials, machines and manpower for their construction and maintenance every year, particularly roadways. The United States alone spends billions of dollars every year for updating its network of highways.

Determining the best materials that can resist both short and long term distresses in pavements has been the primary strategy for minimizing this cost. Using several types of machines and methods, research engineers have proposed several methods to predict the life of pavements based on the properties and performance. There are also several prediction models based on experience and observations; however, they have not successfully predicted the properties and in-service performance of pavements with high accuracy. The objective of study was to propose a new computational micromechanics model to replace dynamic modulus tests of asphalt concrete mixtures, which are one of the longest and most expensive laboratory tests.

Dynamic modulus is an essential property of asphalt concrete mixtures that describes their responses to distresses, such as fatigue cracking, low temperature cracking, rutting or other permanent deformation, moisture damage, etc. The Mechanistic-Empirical Pavement Design Guide (MEPDG, 2004) developed by American Association of State Highway and Transportation Officials (AASHTO) requires either an experimentally

determined dynamic modulus or a predicted value based on binder properties and loading conditions using Witczak's semi-empirical model (1999, 2006) or a dynamic modulus value selected from its built-in data-base.

Although the experimental determination of the dynamic modulus is recognized as an accurate method, it is time consuming and very expensive due to the materials, laboratory equipments and skilled manpower required for the multi-step process. Table 1.1 lists the time and equipments required for the main steps of sample fabrication and subsequent dynamic modulus testing.

Table 1.1 Time and Equipments Required for Dynamic Modulus Tests

Steps	Machines	Time
Sieving	Sieves or Sieving Machine	3 days
Heating	Oven	1 day
Mixing	Mixer	
Compaction	Superpave Gyratory Compactor	
Coring	Diamond Coring Machine	1 day
Cutting	Diamond Saw Machine	
Test Preparation	Fixing Jigs, Gages, LVDTs	1 day
Equilibrium	Environmental Temperature Chamber	3 days
Testing	Universal testing Machine (UTM)	
Data Analysis	Computer	1 day

With the long time and expense required for these tests, cheaper, faster and repeatable alternative method are needed for predicting the dynamic modulus of asphalt concrete mixtures. The early predictive models were in the forms of nomograph and conversion tables, which were based on binder stiffness, and the relative proportions of binder and aggregate. These variables were later incorporated by the Asphalt Institute (AI) as inputs for semi-empirical models for predicting modulus with limited accuracy. Later,

Christensen (2003) proposed a semi-empirical model based on the contribution of stiffness by the participating constituents and their volumetrics.

Citing the expense and time required for experiments that predict dynamic modulus by semi-empirical models and several assumptions made in analytical models, several researchers have proposed different computational micromechanics models (Masad and Niranjanan, 2002, Dai and You, 2008; You, 2006; Abbas et al., 2007, Aragão et al., 2010, and others). Recently, Abbas et al. (2007) proposed a computational micromechanics model based on the discrete element method (DEM) to predict the dynamic modulus of asphalt concrete mixtures by simulating the tests conducted in a Superpave performance tester.

Most recently, Aragão et al. (2010) proposed a new computational micromechanics model based on the finite element method (FEM) to predict the dynamic modulus by simulating cyclic uniaxial compressive tests. The researchers used fine aggregate matrix mixtures and aggregates as the two distinct phases of asphalt concrete mixtures (Figure 1.1), in coherence to the phase system proposed by Kim et al. (2002, 2003, 2004 and 2007).

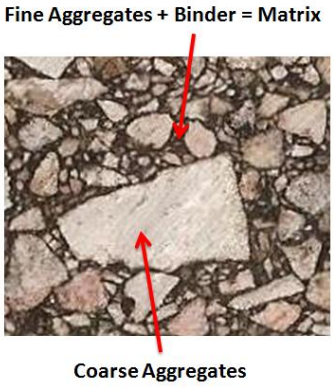

Figure 1.1 Phases of Asphalt Concrete Mixtures

The researchers concluded that their prediction of dynamic modulus was more accurate than the MEPDG model (Witczak and Bari, 2006) and the modified Hirsch's model (Christensen et al., 2003) when compared with the laboratory test results. In their predictive model, Aragão et al. (2010) used the viscoelastic properties of fine aggregate matrixes obtained from torsional shear tests and the elastic properties of aggregates obtained from nanoindentation tests. They mixed fine aggregates with the binder and determined the relative proportions of each based on the proportional sharing of binder by coarse aggregates and fine aggregates. However, they used manually applied impact loads to compact the samples in contrast to machinated gyratory compaction of the asphalt concrete mixtures.

Kim et al. (2002, 2003, 2004 and 2007) also fabricated the fine aggregate matrix with roughly estimated binder content and Ottawa sand but without using any gyratory compaction. Their study introduced and identified the use of the fine aggregate matrix as a viscoelastic phase for asphalt concrete mixtures. They formulated different laboratory tests to determine the properties and performances of the matrix in terms of dynamic shear modulus.

Even if the computational micromechanics model proposed by Aragão et al. (2010) was better than the semi-empirical models, it still did not address the issues of representative volumetric properties, such as compaction density and air void content. Thus, a computational micromechanics model was necessary which uses the properties of fine aggregate matrix mixtures with same proportion of binder and aggregates as in the matrix phase of asphalt concrete mixtures. In doing so, it was also necessary to compact the fine aggregate matrix mixtures with the same density of matrix phase in asphalt concrete

mixtures by using Superpave gyratory compactor. Thus, it was decided to fabricate the representative matrix mixtures and perform torsional shear tests to determine their viscoelastic properties as the input for the new model.

As the aggregate is typically stiffer than the matrix phase, previous studies did not determine the elastic properties of aggregates but instead relied on literature values. Recently, Aragão et al. (2010) showed that the predicted value of dynamic modulus varied significantly when three different values of aggregate elasticity were used (Figure 1.2).

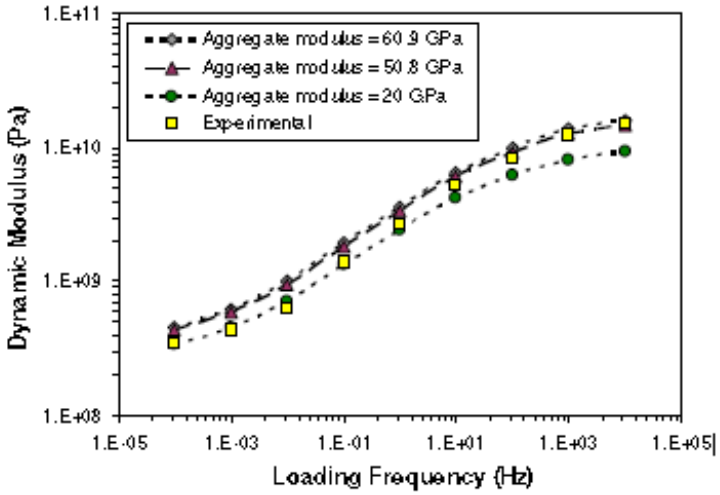

Figure 1.2 Parametric Analysis on Aggregate Stiffness (Aragão et al., 2010)

The researchers illustrated that the computationally predicted value of dynamic modulus can be misleading if inaccurate values of elastic modulus are used in model simulations. So, Aragão et al. (2010) performed nanoindentation tests of aggregates by using thin slices of asphalt concrete as an alternative for performing easier, faster and repeatable tests to determine aggregate properties. Earlier, Dai and You (2007) also performed conventional compressive tests of stone aggregates of larger size. Acknowledging the assessment of Aragão et al (2010) about the accuracy of their model with nanoindentation

test results, and the possibility of performing multiple tests of common aggregates in a shorter time, it was decided to perform nanoindentation tests of aggregates to get their elasticity as the input for the new model.

1.2 Research Objectives

The primary objective of this study was to propose a new computational micromechanics model to predict the dynamic modulus of bituminous composites by using the experimentally determined properties of their components.

This study also includes a protocol for designing the representative fine aggregate matrix mixtures of asphalt concrete mixtures and determining their viscoelastic properties along with a protocol for determining the elastic properties of aggregates.

1.3 Research Scope

As shown in Figure 1.3, three major research phases were formulated to accomplish the objectives mentioned above. The first phase experimentally characterized the asphalt concrete mixtures. The second phase experimentally characterized the fine aggregate matrixes and the aggregates, and established their use in a computational micromechanics model to predict the dynamic modulus of the mixtures based on the FEM. In the final phase, the dynamic modulus values of bituminous composites obtained from the experimental and simulation methods were compared to determine the better method.

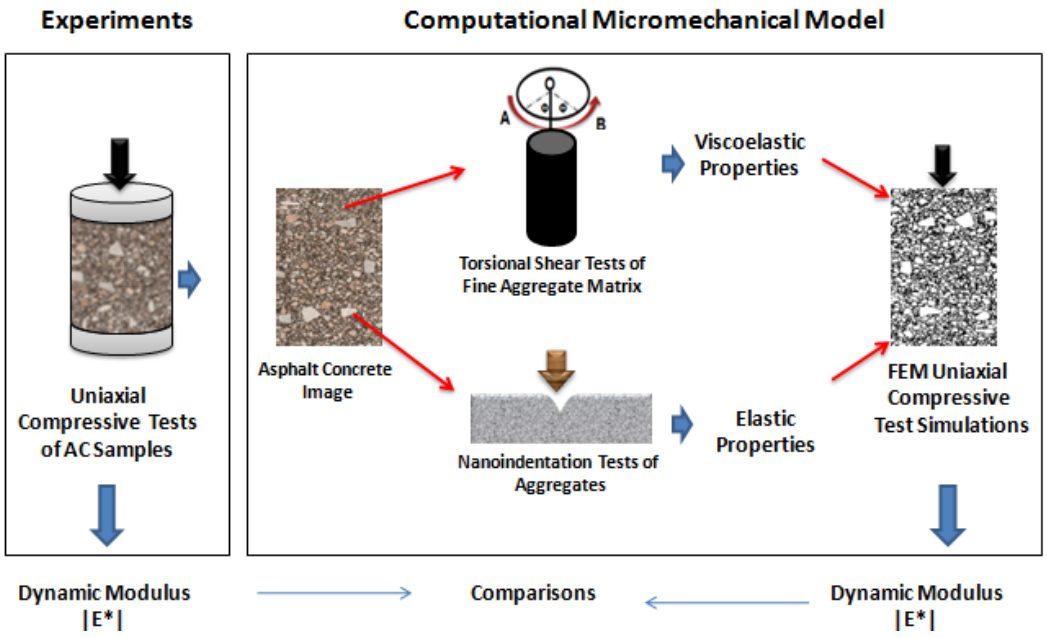

Figure 1.3 Flow Chart of Research Methodology

1.4 Thesis Organization

This thesis consists of eight chapters including this introduction. The second chapter includes the literature review, which prompted the need to propose the computational micromechanics model for predicting dynamic modulus. The third chapter describes the design, fabrication and experimental characterization of cylindrical specimens of asphalt concrete mixtures.

The mix design, test methodology and the characterization of fine aggregate matrix mixtures is discussed in chapter four. Unlike the conventional definition of asphalt concrete as a mixture of only aggregates and asphalt binder, the elastic phase of the aggregates retained on a 1.19 mm sieve and the viscoelastic phase of the fine aggregate matrix are described as the two distinct isotropic homogeneous phases of asphalt concrete mixtures. This chapter describes the mixing protocol for designing the fine aggregate

matrix mixture as a representative replicate of the fine aggregate matrix phase in asphalt concrete mixtures with respect to binder content, compaction method and density level.

Chapter five consists of the procedures of sample preparation, test methodology and data analysis of quasi-static nanoindentation tests of aggregates to determine their elastic modulus. These values were determined experimentally as there is a wide range of values reported in the literature.

Chapter six describes the steps related to image treatment, image analysis, finite element meshing and the test simulations for predicting the dynamic modulus of asphalt concrete mixtures. Unlike the three dimensional cylindrical samples used in the experimental characterization of asphalt concrete, two dimensional rectangular images of the vertical cross-section of cylindrical asphalt concrete samples were used to generate the microstructure required to predict the dynamic modulus computationally.

The viscoelastic properties of asphalt concrete mixtures provided in the form of master curves from experimental and finite element methods are compared in chapter seven. A comparison of typical properties of fine aggregate matrix mixtures, their compaction densities and air voids were also analyzed.

Finally in chapter eight, the suitability of using the computational micromechanics model as a substitute for the experimental method is reviewed and recommendations are provided.

CHAPTER TWO

LITERATURE REVIEW

2.1 Asphalt Binder

Asphalt binder is a cementitious material which is primarily composed of bitumen, which is available naturally or produced from petroleum refining. It is dark brown to black in color, highly viscoelastic in nature and composed of hydrocarbons that are chemically produced from petroleum distillation residues. Asphalt is separated from the other components in crude oil (such as naphtha, gasoline and diesel) by fractional distillation. It is sometimes confused with tar, which is an artificial material produced by the destructive distillation of organic matter. Both tar and asphalt are classified as bitumen, a classification that includes all materials entirely soluble in carbon disulphide. The main forms of asphalt used in pavement construction are asphalt binder itself, cutbacks, emulsifiers and foamed asphalts.

Determining a suitable type of bituminous binder for the specific purpose of a mixture has always been a crucial step of bituminous mixture design, which has been used graded according to the penetration, viscosity, aging and performance of binder. Originally developed by Bowen of Barber Asphalt Co. in 1888 and adopted officially by ASTM Committee D-4 in 1903, the penetration grading system measures the depth of penetration obtained by indenting a binder with a specially designed needle. In 1918, the Bureau of Public Roads (which is now the Federal Highway Administration, FHWA) developed different types of penetration grades with special suggestions for the northern and southern states, which are exposed to different climate conditions. AASHTO

published similar specifications in 1931, and added thin film oven tests in 1955. Citing the incapability of predicting complete behavior of binder based on tests at just 25^{o}C, the viscosity grading system was later introduced with provisions of tests at 60^{o}C, which is similar to the in-service pavement temperature during the summer season. The aged residue grading system was developed in the 1960s, which used rolling thin film oven tests of binders at 25^{o}C, 60^{o}C and 135^{o}C to account for the aging effect of a binder after being mixed as per ASTM D-3381.

The performance grading system is the latest grading system, which addresses the issues related to the construction and in-service temperatures, variable traffic volumes and speeds, short-term and long-term aging of binder. It was developed by the Strategic Highway Research Project (SHRP, 1987-1992) under the Superior Performing Asphalt Pavements (Superpave) system. In this new grading system, the fundamental properties of binders are related to the pavement performance in terms of the climate conditions experienced during the overall life of the pavement. Several tests to determine the properties of original and aged binders are conducted in this system, which are directly related to their performances against common distresses, such as rutting, fatigue, low temperature cracking and flow issues. Each binder in this system is represented by a simple notation PG XX-YY where PG refers to an abbreviation for Performance Grade, XX refers to the average seven day maximum pavement temperature (^{o}C) in a year and YY refers to the minimum temperature (^{o}C).

2.2 Aggregates

Aggregate is a collective term for sand, gravel and crushed stone mineral materials in their natural or processed state (NSSGA, 2010). By weight, 94 % of asphalt concrete

mixtures and 80 % of concrete mixtures are aggregates. According to NSSGA, nearly 1.9 billion metric tons of aggregates were produced in 2009 at an approximate cost of $17.2 billion. Every mile of interstate pavement contains 38,000 tons of aggregates. About 10 tons of aggregates are used per person annually in America. With more than 2 million miles of asphalt pavements, it is important to use the most efficient aggregate materials, design and construction methods to maximize pavement performance.

The sand, gravel, crushed stones, and recycled concretes are the main aggregates used in flexible pavements, which can vary in source, gradation and angularity. Usually, aggregates are obtained by crushing rocks in igneous, sedimentary and metamorphic rock quarries, and by collecting the sand and gravel obtained from continuous disintegration of natural rocks. 3ACR, 47B, 2A, 5/8" limestone, ¼" limestone, screenings, man sand, and fine sand are the common aggregates used in Nebraska roads. According to ASTM D692 and ASTM D1073, the coarse aggregates are separated from fine aggregates by retention on a 4.75 mm sieve. Also, ASTM D242 and AASHTO T11 identify the fillers as the aggregates, of which at least 70 % pass through a 0.075 mm sieve.

Druta (2006) reported that the increase of the amount of fine particles in asphalt binder decreases the stiffness of the mastic and increases the chances of rutting. Prowell et al. (2005) reported that the fine particles cover the aggregates and prevent the adherence of the asphalt to the surface, thus increasing the chances of damages related to moisture infiltration. A method to remove the excess amount of dust and fines from the aggregates is thus required.

2.3 Asphalt Concrete Mixtures

2.3.1 Background

Asphalt concretes are the primary mixtures used in the construction of flexible pavements. They are composed of heterogeneous mixtures of bituminous binder and aggregates with or without fillers such as hydrated lime, fly ash, and Portland cement. Bituminous mixtures were first produced and used in sidewalks, crosswalks, and even pavements in the United States in the late 1860s (Gillespie, 1992). Edmund J. DeSmedt mixed and laid the pavement in front of the City Hall in Newark, New Jersey with a mixture of sand and asphalt in 1870, marking the first use of asphalt mixtures in pavement construction in the United States. DeSmedt also paved 54000 square yards of road on Pennsylvania Avenue in Washington D.C. with the asphalt brought from Trinidad Lake.

Nathan B. Abbott filed the first U.S. patent for a hot mixed asphalt mixture in 1871. In 1900, Frederick J. Warren, from Warner Brothers Company, filed a patent for a "Bitulithic" mixture, which expired in 1920. Their mix protocol required sand, coarse sand, crushed gravel and penetration asphalt to be mixed in the proportion of 200 lb: 300 lb: 400 lb: 50 lb, respectively. Later, a number of innovative mixtures, such as Wilite, Romanite, National Pavement, Imperial, Indurite, and Macasphalt were patented, each with their own innovative recipe (Gillespie, 1992). Since then, asphalt concrete mixtures have been designed with more standard scientific methods following the guidelines from specialization agencies like Asphalt Institute, American Association of State Highway and Transportation Officials, and the state and federal transportation agencies.

2.3.2 Properties

2.3.2.1 Physical Properties

Specific Gravity

The specific gravity of mixtures is defined as the ratio of the weight of a unit volume of the mixture to the weight of unit volume of distilled water at the same temperature. Simply, it is the ratio of density of the mixture to the density of distilled water. Two kinds of specific gravities of aggregates are usually measured for mixtures – the bulk specific gravity of the compacted mixture and the theoretical maximum specific gravity of the mixture. The bulk specific gravity of a mixture is defined as the specific gravity of the compacted sample as determined by AASHTO T166. The theoretical maximum specific gravity of mixture is defined as the maximum specific gravity the asphalt mixture could possibly attain devoid of any air voids. It is determined by AASHTO T209 and called the rice test.

Volumetrics

McLeod (1956) proposed that asphalt concrete mixtures should be analyzed based on the volumetric criteria such as voids in mineral aggregates (VMA), which is based on the volume of specimen that is compacted by 75 blows on each side with a Marshall Compaction hammer. He recommended a minimum of 15 % for VMA, and an air void content of 3 % to 5 %, based on the bulk specific gravity of aggregates as 2.65 and that of asphalt cement as 1.01, without any consideration of absorbed binder. Later, McLeod (1959) included the binder absorption and recommended a minimum level of 4.5 % of asphalt binder to achieve satisfactory durability. The Asphalt Institute (AI) adopted the relationship between the voids in mineral aggregates (VMA) and the nominal maximum

particle size (NMAS), proposed by McLeod (1959) based on the bulk specific gravity of aggregates and an air void content of 5% for the compacted mix in 1984. It was not noticed until 1993 that McLeod (1959) recommendations were all based on an air void content of 5% but not the 4 % air voids used in design currently. The Asphalt Institute revised its mix design method of 1984 for the minimum VMA requirements based on 3%, 4% and 5% air voids in 1993. The Superpave mix design procedures used the similar volumetric requirements for VMA.

Kandhal et al. (1998) specified a minimum average film thickness of asphalt binder rather than specifying the minimum VMA requirement based on minimum asphalt content for the durability of asphalt mixtures. Campen et al. (1959) had earlier recommended an average film thickness ranging from 6 to 8 microns. Goode and Lufsey (1965) proposed to include a minimum value for the bitumen index as the criteria for mixing protocols. They defined the 'bitumen index' as the weight of asphalt cement in pounds per square foot of surface area, the minimum being 0.00123 which basically corresponds to an average film thickness of 6 microns.

Kumar and Goetz (1977) proposed that the ratio of film thickness factor to the permeability of HMA be used as the criterion for predicting the resistance of hardening of asphalt binder in a single-sized HMA mix. They defined the film thickness factor as the ratio of the percentage of asphalt cement content available for a thorough coating of the aggregates to the surface area of the aggregates. Kandhal and Chakraborty (1996) proposed that an optimum average film thickness of 4 to 13 microns be provided to asphalt mixtures, which was calculated by using a mathematical relation between the various asphalt film thickness and the aging characteristics of a dense-graded HMA mix.

In another study, Kandhal and Chakraborty (1996) found a strong relationship between asphalt binder film thickness, tensile strength and resilient modulus of HMA, and proposed film thickness of 9 to 10 microns for specimens compacted with 8 % air voids. Similarly, Hinrichsen and Heggen (1996), Roberts et al. (1996), Kandhal et al. (1998) discussed and recommended film thickness as one of the design criteria of asphalt mixtures.

Radovskiy (2003) derived an analytical formula for calculating film thickness in compacted samples of asphalt concrete. The researcher included the concept of degree of compaction and possible overlap between the film thicknesses, which yielded a value 40 % lower than the conventional method. Even if the researcher included the random geometric orientation of size-graded spheres, the researcher distributed the binder as spherical shells around the aggregate particles and used an average value of thickness. The previous studies consistently used the average film thickness, which is controversial because fine aggregates and coarse aggregates are coated with a different film thickness, and aggregates of the same type or size might have a different film thickness depending on their surface characteristics.

Film thickness is a proxy for the surface area of aggregates, unlike volumetric criteria, which are based on volume of the aggregates. The durability of asphalt mixtures is more related to a minimum film thickness of binder around the surface of aggregates to ensure better and stronger bonding. It is possible that a smaller thickness of binder around the coarser aggregates is preferable even when the VMA requirements are fulfilled. Eriksen and Wegan (1993) and Masad et al. (1999) studied film thickness using digital image analysis. Masad et al. (1999) characterized the internal structure of asphalt concrete

mixtures by quantifying the aggregate orientation, gradation, and aggregate segregation in HMA and studied the influence of compaction levels produced by a Superpave gyratory compactor.

Elseifi et al. (2008) studied the validity of asphalt film thickness in asphalt concrete by imaging the asphalt concrete mixtures with a live-feed camera that had a pixel to micron ratio of 0.008 and powerful software for the image processing and analysis. They studied the film thickness based on the measurements made by using the image analysis techniques, the reflective light microscope and the scanning electron microscopy (SEM), and concluded that films surrounding the large aggregates actually consisted of asphalt mastic films with irregular shape with varying thickness, ranging from 2 to 100 microns. Another important observation was that they did not detect any air voids in asphalt mastics, but only near the boundary between the large aggregates and asphalt mastic. They identified the asphalt mastics as mixtures of fine aggregates, mineral fillers and the asphalt cement. In this study, this kind of mixture was designed and studied as a fine aggregate matrix (FAM), an average uniform thickness of 12 microns was assumed based on the ranges provided by conventional methods and Elseifi et al. (2008), and by considering the workability during mixing and compaction.

2.3.2.2 Engineering Properties

The viscoelastic properties of asphalt concrete mixtures are characterized in terms of complex modulus obtained from the time-temperature dependent relationship of stress and strain. The complex modulus, E* is expressed in terms of two other modulus values, the storage modulus and the loss modulus; its absolute value is called the dynamic modulus. Mathematically, the storage modulus and loss modulus are the cosine and sine

values of dynamic modulus respectively. The storage modulus, E' represents the real part of the complex modulus, which describes the restoration of the shape of the body after being deformed by an applied load. Simply, it is the elastic part of the complex modulus and represents the elastic recovery property of the material. Similarly, the loss modulus, by name, is an imaginary modulus that describes the loss of the strength of viscoelastic materials with time, and hence represents their viscous property. Material property can also be characterized by using phase angle between the loss modulus and storage modulus. Phase angle refers to the lag between stress and strain signals. The phase angle of 0^0 refers to a purely elastic material while a phase angle of 90^0 refers to a purely viscous material. The relationships between the four moduli and the phase angle are expressed in the following equations and Figure 2.1:

$$E^* = E' + i\,E'' \tag{2.1}$$

$$E' = |E^*|\,cos(\Phi) \tag{2.2}$$

$$E'' = |E^*|\,sin(\Phi) \tag{2.3}$$

Where,

$$|E^*| = \sqrt{(E')^2 + (E'')^2} \tag{2.4}$$

$$\Phi = tan^{-1}\left(\frac{E''}{E'}\right) \tag{2.5}$$

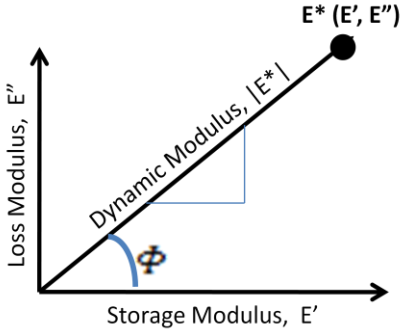

Figure 2.1 Components of the Complex Modulus

Experimentally, the loss or storage moduli of asphalt concrete are determined by conducting the dynamic modulus tests in the haversine loading model. The curves of dynamic modulus obtained for several frequencies at different temperatures are shifted horizontally in the frequency domain to a reference temperature to generate a master curve for a wide range of frequencies at that temperature. The lower and higher values of frequencies exhibited by the master curve are difficult to reproduce in the laboratory. This is one of the reasons for creating the master curves. Another benefit of creating a master curve is that with the shift factors, the master curve at a particular temperature can be shifted to any other temperature, which requires a long equilibrium time in the laboratory. The time-temperature shift factor can be defined as the horizontal shift that must be applied to the material properties at any temperature to determine the same properties at a reference temperature and is given by:

$$log(a_T) = log\,t(T) - log\,t(T_{ref}) \quad (2.6)$$

Where, t(T) and $t(T_{ref})$ refer to the loading time at the test temperature, T and reference temperature, T_{ref} respectively. The above equation shows that the shift factor is equal to one at the reference temperature and changes with change in temperature. Several models have been proposed to determine the shift factors of viscoelastic materials, the most common being the Arrhenius model and Williams- Landel-Ferry (WLF) model. In Arrhenius model, the shift factor is calculated by the following equation:

$$log(a_T) = \frac{\Delta F}{2.303R}\left(\frac{1}{T} - \frac{1}{T_{ref}}\right) \quad (2.7)$$

Where, R is 1.987 calories per gram mole per ^oK, ΔF is the activation energy (calories per gram mole), T is the measurement temperature (^oK) and T_{ref} is the reference temperature

(^{o}K). Similarly in Williams- Landel-Ferry (WLF) model, the shift factor is calculated by the following equation:

$$log(a_T) = \frac{-C_1(T-T_{ref})}{C_2+(T-T_{ref})} \quad (2.8)$$

Where, C_1 and C_2 are arbitrary material constants. An approximate method of master curve fitting is also available which uses a sigmoidal function of time with the maximum and minimum values of the dynamic modulus (α + δ) and δ and the curve fitting constants γ and β as shown below:

$$Log(|E^*|) = \delta + \frac{\alpha}{(1+e^{\beta+Y\ log\ (t_r)})} \quad (2.9)$$

The master curves of the storage modulus are similarly generated using the Prony series (Christensen, 2003). The Prony series represents the mechanical analogy of viscoelastic material behavior more rationally, where the linear elastic properties are represented by springs and the time-dependent viscous properties are represented by the dash pots.

$$E'(\omega) = E_\infty + \sum_{i=1}^{n} \frac{\omega^2\tau_i^2}{\omega^2\tau_i^2+1} E_i \quad (2.10)$$

$$E''(\omega) = \sum_{i=1}^{n} \frac{\omega\tau_i}{\omega^2\tau_i^2+1} E_i \quad (2.11)$$

Where, E_∞, E_i and τ_i represent the Prony series coefficients. The same coefficients are used to express the relaxation modulus of the material in time domain as follows:

$$E(t) = E_\infty + \sum_{i=1}^{n} E_i\ exp\left(-\frac{t}{\tau_i}\right) \quad (2.12)$$

Similar to the relaxation modulus, viscoelastic properties are expressed in terms of other moduli, namely the shear modulus and the bulk modulus. Given that Poisson's ratio, ν, does not change with time, these can be converted by using the following equations:

$$G(t) = \frac{E(t)}{2\,(1+\nu)} \tag{2.13}$$

$$K(t) = \frac{E(t)}{3\,(1-2\nu)} = \frac{2(1+\nu)}{3\,(1-2\nu)} G(t) \tag{2.14}$$

Similar to relaxation modulus, the shear and bulk moduli can be expressed in Prony series as follows.

$$G(t) = G_\infty + \sum_{i=1}^{n_G} G_i \, exp\left(-\frac{t}{\tau_i^G}\right) \tag{2.15}$$

$$K(t) = K_\infty + \sum_{i=1}^{n_k} K_i \, exp\left(-\frac{t}{\tau_i^k}\right) \tag{2.16}$$

Where, G_∞ and K_∞ represent the long-term values for shear and bulk modulus, respectively, τ_i^G and τ_i^k represent the relaxation times of shear and bulk modulus respectively, and n_G and n_K, are the number of Prony series terms.

2.3.3 Asphalt Concrete Characterization

2.3.3.1 Experimental Models

Hot mix asphalt (HMA) mixture is the most common composite that uses two distinct components with totally different behavior – elastic aggregates and viscoelastic binder. The overall behavior of the mixture depends on the properties of the individual components and how they react with each other. The behavior of viscoelastic mixtures is represented by a characteristic master curve which is generated simply by shifting the frequency sweep curves at several temperatures to one reference temperature until the resultant curve is smooth.

There are several standards in use for determining the dynamic modulus, which conduct frequency sweeps from 25 Hz to 0.01 Hz at -10^{o}C to 54.4^{o}C in sequence. The latest

design guide, the Mechanistic-Empirical Pavement Design Guide (MEPDG), which was developed by the American Association of State Highway and Transportation Officials (AASHTO) in 2004, incorporates different levels of analysis depending on the available input types. Level one of the MEPDG requires the experimental values of dynamic modulus, Poisson's ratio, loading frequencies and temperatures to generate the characteristic master curve. The other properties required for distress transfer functions and climatic modeling are tensile strength, creep compliance, coefficient of thermal expansion, surface shortwave absorptivity, thermal conductivity, heat capacity, asphalt binder viscosity, etc. Because it uses the experimental values, it is the most accurate method for predicting the property of mixtures.

The AASHTO provisional standard PP61 and AASHTO standard TP62 are the standard methods of determining the dynamic modulus of asphalt concrete mixtures experimentally. ASTM D3497 was also in use for determining dynamic modulus experimentally but was withdrawn in 2009. Kim et al. (2004) suggested of characterizing dynamic modulus as the most important property of hot mix asphalt mixtures by performing the indirect tensile (IDT). They recommended increasing the testing frequencies by two and decreasing the number of testing temperatures to three to decrease the total testing time without compromising the quality of the tests.

2.3.3.2 Empirical and Semi-empirical Models

The Shell Nomograph is a graphical model used to find the stiffness of asphalt concrete mixtures based on stiffness of binder, volumetric percentage of binder and aggregates. Similarly, Bonnaure et al. (1977) proposed an empirical model with the same variables used by the Shell Nomograph. Later, the Asphalt Institute (AI) incorporated material

properties, mix volumetrics, traffic loading and climate conditions by formulating an equation for dynamic modulus in terms of penetration depth of binder, percentage of aggregates less than 0.075 mm in size, volume content of binder, frequency of loading, air void content, and temperature.

Despite the available standards, the tests are still troublesome with respect to the time and money required for statistically agreeable results. In an attempt to reduce the cost and time required to fabricate and test the samples and obtain the characteristic master curves, researchers have suggested several semi-empirical predictive models to determine dynamic modulus (Bonnaure et al., 1977; Witczak et al., 1999, Christensen et al., 2003, Bari and Witczak, 2006). The properties of the individual components and the volumetrics of the mixtures are used as the inputs for these models, and a master curve is generated for any required temperature and reduced frequency. Christensen et al. (2003) proposed a semi-empirical model by modifying the Hirsch law of mixtures. The Hirsch model (1962) used the law of mixtures to determine the overall property of the composites in terms of properties of their components which Christensen et al. (2003) modified to derive the equation for predicting the stiffness of asphalt mixtures from inputs such as voids filled with asphalt (VFA), voids in mineral aggregates (VMA) of the mixture, dynamic shear modulus of the binder, $|G_b^*|$ and the contact volume of aggregate (P_c) as follows:

$$|E^*| = P_c\left(4200000\,x\,\left(1-\frac{VMA}{100}\right)+3\,|G_b^*|\,\left(\frac{VFA\,xVMA}{10000}\right)\right)+(1-P_c)\left(\frac{1-\frac{VMA}{100}}{4200000}+\right.$$

$$\left.\frac{VMA3x\,VFAx\,Gb*-1}{}\right)$$

(2.17)

Where,

$$P_c = \frac{\left(20+\frac{VFA\ x\ 3\ x\ |G_b^*|}{VMA}\right)^{0.58}}{650+\left(\frac{VFA\ x\ 3\ x\ |G_b^*|}{VMA}\right)^{0.58}} \quad (2.18)$$

Similarly, there are also methods to predict the dynamic modulus and constructing the master curves by using the volumetric and asphalt binder properties as inputs in second and third levels of MEPDG. These methods use a regression equation originally derived by Witczak in 1999 and modified by Bari and Witczak in 2006. The original Witczak's stiffness predictive model was developed by a multivariate regression analysis of 2,750 experimental data from more than 200 mixtures where the volumetric of mixtures, the viscosity of the binder η and the loading frequency f were used as the inputs to characterize the composites.

Bari and Witczak (2006) added 4650 experimental data from 346 mixtures to this original model (1999) and reran the multivariate regression analysis. Instead of using the viscosity and loading frequency to characterize the mechanical behavior of the binder phase, they introduced the dynamic shear modulus, |Gb*| and phase angle of the binder, δb as the material properties of binder in the revised equation. The percentage of aggregates passing through a No. 200 sieve by weight of total aggregates, ρ200, the cumulative percentages of aggregates retained on sieve number 4, sieve number 3/8" and sieve number 3/4", ρ4, ρ38, ρ34, respectively were the inputs for gradation. Similarly, the percentage of air voids by volume, Va and effective binder in the mixture by volume, Vbeff were the two inputs for the volumetric properties of the mixtures. The most recent equation is given below:

$$\log|E^*| = -0.349 + 0.754|G_b^*|^{-0.0052}\left(6.65 - 0.032\rho_{200} + 0.0027\rho_{200}^2 + 0.011\rho_4 - 0.0001\rho_4^2 + 0.006\rho_{38} - 0.00014\rho_{38}^2 - 0.08V_a - 1.06\left(\frac{V_{beff}}{V_{beff} + V_a}\right)\right) + \frac{2.56 + 0.03V_a + 0.71\left(\frac{V_{beff}}{V_{beff} + V_a}\right) + 0.012\rho_{38} - 0.0001\,\rho_{38}^2 - 0.01\,\rho_{34}}{1 + e^{(-0.7814 - 0.5785\,LOG\,(|G_b^*|) + 0.8834\,LOG\,(\delta_b))}}$$

(2.19)

The new version of predictive model from Bari and Witczak (2006) is better than the earlier version due to the use of more data and more representative properties of the binder. Some concerns still exist, including higher error percentage at extremely high and low temperature conditions, as discussed by Bari and Witczak (2006) themselves and Ceylan et al. (2009).

Ceylan et al. (2009) proposed to replace the regression analysis based-prediction models used in the dynamic modulus of asphalt concrete with one they developed based on artificial neural networks (ANNs). The researchers used the 7400 data points of dynamic modulus |E*| obtained from 346 HMA mixtures for the NCHRP Report 547 and concluded that the ANN |E*| models were more accurate than the existing regression models and could easily be incorporated into the MEPDG.

2.3.3.4 Analytical Micromechanics Model

There has been a keen interest in developing analytical micromechanics models to predict the properties and performance of polymer composites with time and temperature (Voigt,

1889; Hashin, 1962; Hirsch, 1962; Hashin and Shtrikman, 1963; Counto, 1964; Hashin, 1965; Mori and Tanaka, 1973; Christensen and Lo, 1979, Aboudi, 1991;, etc.). Similar interest has been seen in models of asphalt concrete composites by a micromechanics approach (Buttlar, 1996, 1999; Uddin, 2001; Shashidhar and Shenoy, 2002; Christensen et al., 2003). Buttlar and Roque (1996) found that the micromechanics models used for polymer composites were not suitable for asphalt concrete mixtures. Buttlar (1999) tried to use an equivalent rigid-layer modeling concept to understand the behavior of asphalt mastic. Shashidhar and Shenoy (2002) found deficiencies in the Buttlar model (1999) at higher volume fractions of fillers and derived a simplified equation to evaluate the efficiency of the model for correctly predicting the stiffness ratio of asphalt mastics in terms of merits and demerits.

Uddin (2001) proposed a micromechanics method to calculate the creep compliance of asphalt concrete mixtures by using the experimentally determined characteristics of binder as a viscoelastic material and that of aggregates as the elastic materials. Similarly, Shu and Huang (2008) studied dynamic modulus of the composites by embedding the mastic-coated aggregate particles into the equivalent medium of HMA mixtures and derived equations to predict their dynamic modulus, which accounted for the aggregate gradation and the air void size distribution. The researchers also conducted laboratory tests to determine the dynamic modulus of mastics and HMA mixtures, and incorporated these values into the analytical solutions. They obtained a good agreement between the predicted and experimentally obtained dynamic modulus values at high frequencies. However, there were several assumptions made to simplify and speed up the solutions derived by the analytical and semi-empirical models described above, which replaced the

conditions such as heterogeneity, cohesion, adhesion, anisotropy, etc. by homogeneity and isotropy.

2.3.3.5 Computational Micromechanics Model

The limitations of the models described above have been overcome in some of the computational micromechanics models based on the finite elements method (Masad and Niranjanan, 2002; Papagiannakis, 2002, Aragão et al. 2010, etc.) and the discrete element method (Abbas et al., 2005; You., 2003; Dai and You, 2007, 2008; You and Buttlar, 2006; You et al. 2008).

Masad and Niranjanan (2002) developed a finite element model to study the influence of localized strain distribution on HMA (hot mix asphalt) by using the microstructure obtained by image analysis, which identified particles greater than 0.3 mm as aggregates and others as mastics. Papagiannakis et al. (2002) used the two-phase microstructure of asphalt concrete mixtures to predict the dynamic shear modulus and phase angle using the finite element method (FEM) and verified by comparing the results to those from Superpave shear tester. Abbas et al. (2005) used the discrete element method (DEM) to predict the dynamic modulus of asphalt mastics made from different binders and minerals passing through 0.075 mm sieve in different volumetric proportions and compared them to other micromechanics models and the dynamic shear rheometer results. This model appeared to be more accurate than other models. Abbas et al. (2007) studied the two distinct aggregate and mastic components of the HMA microstructure, which were obtained by cutting the HMA and scanning them. They subjected the microstructure to oscillatory loads to simulate the simple performance tests (SPT) in two dimensions using

the DEM for analysis. They found that their results overestimated the dynamic modulus of mixtures with original binders but underestimated for modified binders.

Dai and You (2007) also presented micromechanics finite-element and discrete-element models to predict overall creep stiffness of asphalt mixtures by using the creep stiffness properties of the two distinct aggregate and mastic components. To determine the creep stiffness, they performed uniaxial compressive tests of aggregates and creep compliance tests of mastic samples fabricated by mixing binder and fine aggregates passing through 2.36 mm sieve. By comparing the results of the two models with the laboratory test results, they concluded that both methods were applicable for predicting the creep stiffness of the mixtures.

Recently, Aragão et al. (2010) predicted the dynamic modulus of asphalt mixtures by using two semi-empirical, models, one analytical model and one computational micromechanics model. The researchers obtained the properties of the fine aggregate matrix with hydrated lime by sweeping the oscillatory frequency at several temperatures and then obtained the characteristic Prony series coefficients from their master curves. Similarly, the researchers obtained the Young's modulus of elasticity of the aggregates by performing nanoindentation tests. Using the material properties of aggregates and fine aggregate matrix, the researchers predicted the stiffness of the asphalt concrete mixture in terms of dynamic modulus and compared these values to those derived from other semi-empirical and experimental models.

2.4 Fine Aggregate Matrix Mixtures

2.4.1 Background

Asphalt concrete mixtures are usually designed based on either volumetric properties such as, VMA, air voids or average film thickness, or properties of its distinct components – the elastic phase of aggregates and the viscoelastic phase of asphalt binder. This conventional method ignores the fact that there is a distinct matrix phase of fine aggregates and binder, rather than just binder. In addition to binder, the entire matrix phase is responsible for creating the more compliant phase in the asphalt concrete mixtures. This conventional method also ignores the fact that the fine aggregates and coarse aggregates have different film thicknesses.

Campen et al. (1959), Goode and Lufsey (1965), Kumar and Goetz (1977), Kandhal and Chakraborty (1996), Hinrichsen and Heggen (1996), Roberts et al. (1996), Kandhal et al. (1998) and Radovskiy (2003) specified a minimum average film thickness of asphalt binder around the aggregates to describe the durability of asphalt mixtures rather than specifying the minimum VMA requirement based on minimum asphalt content. In almost all of these conventional methods, binder was assumed to be coated as a spherical shell around the aggregate particles with a consistent average film thickness, which is in contrast to the fact that fine and coarse aggregates of same and different aggregates have different film thicknesses.

Eriksen and Wegan (1993), Masad et al. (1999), Masad and Niranjanan (2002), Kim et al. (2002, 2003, 2004 and 2007), Papagiannakis (2002), Dai and You (2007, 2008), Abbas et al. (2005, 2007), Elseifi et al. (2008), Aragão et al. (2010) defined asphalt matrix as the mixture of asphalt cement and fillers. Even though they used a different value for the

maximum size of fine aggregates, they all agreed in the viscoelastic behavior of the fine aggregate matrix.

Elseifi et al. (2008) studied the validity of asphalt film thickness in asphalt concrete by imaging the asphalt concrete mixtures with a live-feed camera that had a pixel to micron ratio of 0.008 and powerful software for the image processing and analysis. They measured the film thickness and concluded that the films surrounding the large aggregates actually consist of asphalt mastic films with irregular shape of varying thickness ranging from 2 microns to 100 microns. They identified the asphalt mastics as mixtures of fine aggregates, mineral fillers and the asphalt cement. Kim et al. (2002, 2003 and 2004) performed several kinds of tests using cylindrical torsional bars of a fine aggregate matrix made from Ottawa sand and binder, which defined the homogeneous phase of asphalt concrete mixtures. Kim et al. (2007) reiterated that the asphalt concrete can be modeled as a heterogeneous mixture with three characteristically different phases – coarse aggregates, fine aggregate matrix, and the cohesive zone within the asphalt matrix and along matrix and particle boundaries. Dai and You (2007) mixed the fine aggregates passing through a 2.36 mm sieve with binder and performed the creep compliance tests to determine the creep compliance and the creep stiffness.

Abbas et al. (2005) mixed binders and minerals passing through a 0.075 mm sieve in different volumetric proportions and performed dynamic shear modulus tests using a rheometer. Aragão et al. (2010) fabricated the fine aggregate matrix by blending aggregates in the same proportion as used in asphalt concrete mixtures and performed the frequency sweep tests of cylindrical torsional bars to characterize their viscoelastic properties. The researchers calculated the binder content by assessing the proportions of

binder associated with coarse aggregates and fine aggregates, which were defined on the basis of retention on a 0.6 mm sieve.

2.4.2 Properties

Relaxation modulus and creep compliance are basic viscoelastic properties of fine aggregate matrix as discussed by Kim et al. (2002, 2003, 2004 and 2007). These modulus values are obtained by browsing and converting the material constants determined from dynamic shear modulus of torsional bars of fine aggregate matrix. The dynamic shear modulus |G*| is the absolute value of complex shear modulus, G*, which consists of a real part and an imaginary part. The real part is called the storage shear modulus, which tends to recover the shear strength during a torsional loading. It thus signifies the elastic recovery tendency of the material, and is called the elastic part of complex shear modulus. Similarly, the imaginary part of the complex shear modulus is called the loss shear modulus due to its tendency to lose shear strength with time. The loss shear modulus, storage shear modulus, dynamic shear modulus, complex shear modulus and the phase angle are expressed in the following equations and Figure 2-2:

$$G^* = G' + i\,G'' \tag{2.20}$$

$$G' = |G^*| x\, cos(\Phi) \tag{2.21}$$

$$G'' = |G^*| x\, sin(\Phi) \tag{2.22}$$

Where,

$$|G^*| = \sqrt{(G')^2 + (G'')^2} \tag{2.23}$$

$$\Phi = tan^{-1}\left(\frac{G''}{G'}\right) \tag{2.24}$$

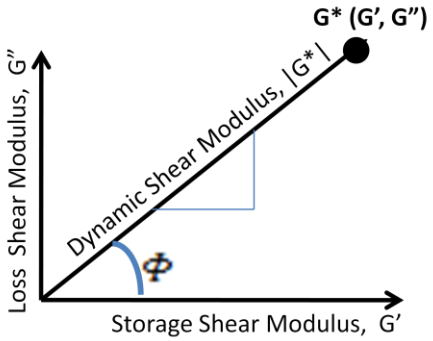

Figure 2.2 Components of the Complex Shear Modulus

Similar to asphalt concrete mixtures, the master curves of the loss shear modulus and the storage shear modulus in angular frequency domain are used to derive the Prony series coefficients which are the constants that can characterize the viscoelastic materials.

$$G'(\omega) = G_{\infty} + \sum_{i=1}^{n} \frac{\omega^2 \tau_i^2}{\omega^2 \tau_i^2 + 1} G_i \tag{2.25}$$

$$G''(\omega) = \sum_{i=1}^{n} \frac{\omega \tau_i}{\omega^2 \tau_i^2 + 1} G_i \tag{2.26}$$

Where, G_{∞}, G_i and τ_i respectively represent the long-term coefficient of the spring, the coefficients of the elastic constants and the relaxation times representing the time dependent viscous decay rates for n number of the dashpots. The same coefficients are valid for the shear modulus in the time domain as discussed with conversion factors in the property section of asphalt concrete mixtures above.

2.4.3 Fine Aggregate Matrix Characterization

Instead of predicting the total failures of pavement on a global scale, researchers assess the individual damages due to moisture, fatigue, rutting and low temperature effects by modeling the binders, aggregates and interfaces, and then superimposing those local damages into bulk samples to predict the cumulative failures. They have designated the aggregates and binder phases as the basic phases of the asphalt mixtures, which

correspond to the fact that asphalt concrete pavements are constructed using a heated mixture of aggregates and binder. However, experience has shown that fine aggregates and binder make a near homogeneous mixture when mixed at high temperature, covering and binding the coarse aggregates intact.

Goodrich (1988, 1991), Christensen and Anderson (1992) and some other researchers performed the torsional dynamic shear tests of rectangular bars of asphalt concrete mixtures to characterize their properties. Reese (1997) proposed to use torsional loading instead of bending citing the fact that torsional loading serves as a better simulation of damage due to traffic than bending. Kim et al. (2002, 2003 and 2004) developed a protocol to perform oscillatory torsional shear tests of cylindrical bars of asphalt binder and fine aggregates. Based on the 10 micron film thickness around the aggregates, the researchers derived a binder content of 8.23 % by weight of total mixture, and fabricated 50 mm long and 12 mm diameter cylindrical samples of fine aggregate mixtures by mixing the pure binders and Ottawa sand. The comparatively homogeneous test samples were able to maintain their shapes without plastic flow during testing. The researchers; however, compacted the samples in a specially fabricated mold applying impact loads without keeping a compaction consistent with the gyratory compaction in the laboratory. The researchers determined the linear viscoelastic limits from dynamic shear strain sweep tests, and the dynamic shear modulus and phase angle from dynamic frequency sweep tests, and major change in dynamic modulus, pseudo stiffness and strain energy from the time sweep tests. Similar studies by Kim et al. (2002, 2003 and 2004) have also used the fine aggregate matrix as the more homogeneous phase of asphalt concrete mixtures.

Kim et al. (2007) reiterated that asphalt concrete can be modeled as a heterogeneous mixture with three characteristically different phases (i.e., coarse aggregates, surrounding black phase or asphalt matrix, and the cohesive zone phase within the asphalt matrix and along matrix/particle boundaries) to signify the damage evolution due to crack growth. They modeled the coarse aggregates as isotropic elastic materials with an elastic modulus of 55.2 G Pa and a Poisson's ratio of 0.15. They characterized fine aggregates matrix by performing dynamic frequency sweep tests of cylindrical matrix bars of 50 mm length and 12 mm diameter from 0.01 Hz to 10 Hz at 10^{o}C, 25^{o}C and 40^{o}C.

Abbas et al. (2005) performed dynamic shear tests in a rheometer to predict the dynamic shear modulus of the mastics made of binders and aggregates passing through a 0.075 mm sieve in different volumetric proportions. Dai and You (2007, 2008) described aggregates and mastic as the components of asphalt concrete mixtures, defining mastic as a fine mixture composed of asphalt binder mixed with fine particles and fine aggregates. They fabricated the sand mastic mixture using binder and aggregates passing through a 2.36 mm sieve, and performed creep compliance tests to determine creep compliance and creep stiffness.

Aragão et al. (2010) evaluated the oscillatory frequency sweep tests and oscillatory time sweep tests to determine the properties and performance of lime mixed fine aggregate matrix in displacement controlled and force controlled modes. In another study, Aragão et al. (2010) predicted the dynamic modulus of asphalt concrete mixtures from different models and methods by using the dynamic shear modulus of the fine aggregate matrix. The researchers obtained the properties of fine aggregate matrix with hydrated lime by sweeping the oscillatory frequency from 25 Hz to 0.01 Hz at 5^{o}C, 20^{o}C and 40^{o}C and

then constructed their master curves to obtain the characteristic Prony series coefficients. Kim et al. (2002, 2003 and 2004) and Aragão et al. (2010) fabricated the fine aggregate matrix mixtures in a specially designed mold by compacting them with impact load from with a hammer without considering the gyratory compaction.

2.5 Nanoindentation Tests for Elastic Modulus of Aggregates

Nanoindentation, essentially, is a simple test of material in which a hard indenter of known geometry and properties is pushed into the surface of a material of unknown properties at a nano-scale of depth. Values of the elastic modulus and hardness are then derived from the load and indentation depth profile.

Federick Mohs was the first person to document the semi-quantitative hardness test. In the scale proposed by Mohs (1822), hardness was defined by how well a substance of unknown hardness resisted from being scratched by another substance of known hardness. The size of the imprint left by scratching a material of interest with another material of known hardness was used to infer the hardness of the material. This method had no consideration of surface roughness and had no theory to support the rank order. Typically, a wooden testing kit is used for these tests, which contains low cost specimens of the ten minerals in the Moh's scale with a label of their hardness number. However, Hertz (1881) was the first person to propose the theory behind the deformation created due to the application of a contact load by a material of known properties into a material of unknown property. Hertz (1881) derived an equation for the indentation of a sphere into a lens when a pressure is exerted on the lens which became the basis for the field of contact mechanics. His theory explains the behavior of two purely elastic axisymmetric

curved bodies placed in contact with an externally applied load, where adhesion between the bodies in contact is neglected.

Using the classical theory of elasticity and continuum mechanics, Boussinesq (1885) later derived solutions for the stress distribution within an isotropic elastic half space when it is deformed by the normal pressure against its boundary of a rigid punch. These solutions still had limitations for practical computations. Love (1929, 1939) worked on solving the same problems. Sneddon used a cylindrical indenter (1946) and conical indenter (1948) as well as a semi-infinite half plane by using the theory suggested by Boussinesq (1885). Sneddon later (1965) solved the contact problem for any arbitrary axisymmetric indenter and a semi-infinite half plane. His derivations for determining the depth of penetration of the tip of a punch of arbitrary profile and for the total load which must be applied to the punch to achieve this penetration as:

$$D = \int_0^1 \frac{f'(x)dx}{\sqrt{1-x^2}} \tag{2.27}$$

$$P = \frac{4\mu a}{1-\eta}\int_0^1 \frac{x^2 f'(x)dx}{\sqrt{1-x^2}} \tag{2.28}$$

Where D, P, a, μ, η and f represent the depth of penetration, the total load on the punch, the radius of circle of contact, the rigidity modulus of material of half space, Poisson's ratio of the same material of half space and arbitrary axisymmetric indenter profile function f, respectively. Included in the study were the illustrations of how these derivations led to the formulae for indentation depth and total load when the indenter is a flat-ended cylindrical punch, a conical punch, spherical punch, a punch in the form of a paraboloid of revolution and a punch in the form of an ellipsoid of revolution. The same theory was used to determine the radius of deformation on a semi-infinite surface when a pressure was exerted by a sphere (Figure 2.3) as shown below:

$$a = \left\{\frac{3}{4} Wgr\left(\frac{1-\nu_1^2}{E_1} + \frac{1-\nu_2^2}{E_2}\right)\right\}^{1/3} \quad (2.29)$$

Where W is the load applied, E1 and E2 are Young's Modulus values, ν1 and ν2 are the corresponding values of Poisson's ratio, r is the radius of the sphere, a is the radius of curvature of deformation on the flat surface. This derivation was modified by scientists in later studies by including the concept of adhesion between the two bodies in contact.

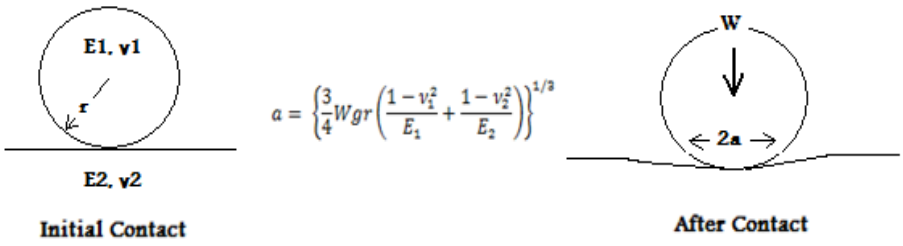

Figure 2.3 Sphere Indenting on a Semi-Infinite Substratum

Sneddon's equation for the effective modulus of the material of half-space when an axisymmetric indenter exerts pressure was as follows:

$$E_r = \frac{E}{(1-\nu^2)} = \sqrt{\frac{\pi}{A}} x \frac{S}{2} \quad (2.30)$$

Where E r is the effective elastic modulus defined in terms of Young's modulus E and Poisson's ratio ν, S is the contact stiffness, and A is the projected contact area. This equation has been the fundamental for subsequent research, hence still serving as the corner stone in nanoindentation today. Brinell (1901) introduced a new test in which the imprint, h, made on a flat plate by applying a fixed load, P, of a hard spherical steel indenter of diameter, D, was used to derive the hardness number, HB, using the chordal diameter of the residual impression, d, as in equation below:

$$H_B = \frac{2P}{\pi D^2\left(1-\sqrt{1-\left(\frac{d}{D}\right)^2}\right.} \quad (2.31)$$

Later, Meyer (1908) defined hardness as the ratio of the load to the projected area of indentation; this is the most common definition of hardness in use today. The applied load, P, that produces an impression of diameter, d, is more than the elastic limit. Hence, Meyer's hardness is also called the plastic pressure, and is given by:

$$H_M = \frac{4P}{\pi d^2} \quad (2.32)$$

Ludwik (1908) and Vickers (1925) replaced the spherical indenters with pyramidal and conical indenters. Berkovich (1951) came up with the three-faceted pyramidal diamond for micro hardness testing. With the development of several types of indenters and elastic solutions by the mid-twentieth century, scientists started looking into various aspects of indentation tests, like adhesion, plasticity, frictional effects, viscoelasticity, nonlinear elasticity and adhesion.

During the 1970s and 1980s, depth sensing indentation tests were developed. Bulychev et al. (1975, 1976) introduced a new method to determine the Young's modulus of elasticity using the indentation tests. These researchers developed the depth-sensing indentation tests with reduced sized indenter tips and increased accuracy and resolution of the depth and load measurements. Newey et al. (1982) and Loubet et al. (1984) modified a micro-hardness testing machine to instantaneously record the indentation load and depth during an indentation test. Loubet et al. (1984) adopted the solution of Sneddon (1965) for the elastic deformation of an isotropic elastic material with a flat-ended cylindrical punch. They proposed that the area of the punch made by indenting the semi-infinite plane material of interest by a harder indenter, with the same projected area of contact, and derived a relation for Vickers indenter as follows:

$$\frac{dP}{dh} = D \times E_r \times \sqrt{\frac{2}{\pi}} \quad (2.33)$$

Where, the reduced modulus is given by the following equation:

$$\frac{1}{E_r} = \frac{1-\nu_s^2}{E_s} + \frac{1-\nu_i^2}{E_i} \quad (2.34)$$

And where dP/ dh is the slope of the load –displacement curve, D is the Vickers diagonal length, E and ν are the Young's modulus and Poisson's ratio where subscripts, s and i refer to the material of the test sample and the indenter, respectively. Other studies worked on improving, defining and simplifying the indentation tests and data analysis in several ways (e.g., Ternovskii et al., 1973; Pethica et al., 1983; Loubet et al., 1986).

With the development of depth-sensing indentation machines and the solutions for various types of indenters for load and displacement profile, the focus shifted to determining the elastic properties directly from these test data. Ternovskii et al. (1973) introduced the stiffness equation for the reduced modulus of the material of interest by using the instrument measured load –displacement data as follows:

$$\frac{dP}{dh} = \frac{2}{\sqrt{\pi}} x\, E_r x \sqrt{A} \quad (2.35)$$

Where dP/dh, E r and A are the slope of the load –displacement curve, the reduced modulus for the material and the projected contact area of the indent .The most popular methods of analysis of instrumented indentation are those of Doerner and Nix (1986) and Oliver and Pharr (1992), the latter been used as the default in most commercial indentation instruments. Doerner and Nix (1986) modified the Loubet et al. (1984) equations for elastic properties of indentation samples by assuming an indenter with an ideal pyramidal geometry and a plastic depth hp as follows:

$$\frac{dh}{dP} = \frac{1}{2h_p} x \sqrt{\frac{\pi}{24.5}}\ x\ \frac{1}{E_r} \quad (2.36)$$

Doerner and Nix (1986) also found that the hardness value was dependent on the strain rate of indentation, and eliminated the effect of elastic properties of the substrate on the indentation tests involving the thin films as follows:

$$\frac{1}{E_r} = \frac{1-\nu_s^2}{E_s}\left(e^{-\frac{\alpha t}{h_{eff}}}\right) + \frac{1-\nu_{sub}^2}{E_{sub}}\left(1 - e^{-\frac{\alpha t}{h_{eff}}}\right) + \frac{1-\nu_i^2}{E_i} \quad (2.37)$$

$$h_{eff} = \sqrt{\frac{Area}{24.5}} \quad (2.38)$$

Where the notation dh/dP is the reciprocal of the unloading slope, or the compliance, α is the empirically determined constant, h eff. is the effective depth of indentation, sub refers to the substratum, "i" refers to indenter material and s refers to the material of the thin film. The equation transforms into the one given by Sneddon (1948) when the substrate effect is ignored. They obtained a relationship between the contact depths, where the contact areas in the acetate replicates of indentations in soft brass were measured with the help of the Transmission Electron Microscope (TEM). They proposed a method to interpret the data obtained from depth-sensing hardness to get the elastic and plastic properties of thin films. They illustrated the method to determine hardness values by using the load-displacement data after subtracting the elastic displacements from the total depth and Young's modulus from the slope of the linear portion of the unloading curve. This study also suggested that the unloading stiffness can be computed from a linear fit of the upper one-third of the unloading curve, which Oliver and Pharr (1992) improved by suggesting to fit the unloading curve with a power law.

Oliver and Pharr (1992) proposed an improved technique to determine hardness and elastic modulus using load and displacement sensing indentation experiments. Using a Berkovich indenter, they indented six materials, which included fused silica, soda-lime

glass, and single crystals of aluminum, tungsten, quartz, and sapphire and analyzed the load-displacement data using a technique derived by improving the Doerner and Nix (1986) model and the Sneddon (1965) stiffness equation. They proved that their load – displacement model works for all the axisymmetric indenters that have any infinitely smooth profile. Unlike the linear unloading curve proposed by Doerner and Mix (1986), Oliver and Pharr (1992) proposed a nonlinear power law relation of load and displacement during the unloading as follows:

$$P = \alpha (h - h_f)^{m} \tag{2.39}$$

Where P, h, hf, represent the applied load, instantaneous indentation displacement at any time during unloading and residual depth of indentation, respectively and α & m are the material constants obtained by curve fitting the unloading curve by power law, respectively. Physically, hf is the final value of depth of indentation just before the indenter leaves the specimen during unloading. Similarly, h-hf is the elastic displacement, the value of α and that of m are obtained by fitting the unloading curve by a power law. The effective or reduced modulus of material of the indented sample is given as function of contact stiffness S, contact area A:

$$E_r = \frac{\sqrt{\pi}}{2} \text{ x } \frac{S}{\sqrt{A}} \tag{2.40}$$

Where, contact stiffness is calculated as the slope of the unloading curve at the beginning as follows:

$$S = \frac{dP}{dh} = m \alpha (h - h_f)^{m-1} \tag{2.41}$$

Oliver and Pharr (1992) also proposed an analytical solution for contact area as a function of contact depth and the indenter shape function as follows:

$$A_{(h_c)} = \sum_{n=0}^{8} C_n \text{ x } h_c^{2-n} \tag{2.42}$$

The calibration constants C0, C 1, C i and C n are obtained by indenting standard samples of known material properties (e.g. quartz) before performing the indentation tests on experimental samples. Oliver and Pharr (1992) found that the area determined by this analytical procedure was a good measure of the residual contact impression because the modulus values predicted by this method were within a 4 % of the values reported in the literature for the materials with isotropic elastic properties. The procedure for determining the area function gave an attractive alternative to the process of determining the projected area by image analysis. With the known values of elastic modulus, Poisson's ratio of the indenter material, and Poisson's ratio of the material in the specimen and the calculated value of effective modulus, the Young's modulus of elasticity for the material in the specimen can be calculated by following the original relation by Sneddon as follows:

$$E_s = \frac{1-\nu_s^2}{\frac{1}{E_r}-\frac{1-\nu_i^2}{E_i}} \tag{2.43}$$

Similarly, dividing the maximum applied load by the area of contact at that instantaneous moment represents the hardness of the material of test specimen.

$$H = \frac{P_{max}}{A} \tag{2.44}$$

Since the inception of this method to determine material properties, such as hardness and elastic modulus, by instrumented indentation techniques, there have been several studies that addressed the associated intricacies and numerical simulations. The effective indenter shape concept was modified by Pharr and Bolshakov (2002) to give a more representative value for the indenter as follows:

$$\varepsilon = m\left(1 - \frac{2\Gamma\left(\frac{m}{2(m-1)}\right)}{\sqrt{2}\Gamma\left(\frac{1}{2(m-1)}\right)}(m-1)\right) \quad (2.45)$$

Similarly, some studies (e.g., Bolskashov and Pharr, 2002 and Oliver and Pharr, 2004) proposed a correction factor, β, to account for the inaccuracies in the stiffness equation obtained by Sneddon (1965). The corrected stiffness equation is given below:

$$S = \beta \text{ x } \frac{2}{\sqrt{\pi}} \text{ x } E_r \text{ x } \frac{\sqrt{A}}{2} \quad (2.46)$$

The correction factor β depends on the included angle of the indenter and the Poisson's ratio of the sample. Oliver and Pharr (2004) stated that the value of β should be always greater than unity and lie inside the range of $1.0226 \leq \beta \leq 1.085$; it was typically 1.05 for Berkovich with approximate error of ± 0.05. For the conical type of indenter, β equals to one. But because this error of ± 0.05 is too small in the case of aggregates, which have varying modulus with respect to the type of mineral and the indentation location, a unity value is used in this study hereafter. In summary, the nanoindentation tests are governed by the assumptions: (1) the specimen is an infinite half-space, (2) the indenter has an ideal geometry, (3) the material is linearly elastic and incompressible, and (4) there is no interaction surface force during the contact e.g., frictional forces. Nanoindentation test was used for determining the elastic modulus of aggregates most recently by Aragão et al. (2010). For this study, the Berkovich type of diamond indenter will be used to determine the elastic modulus of aggregates used in asphalt concrete specimens.

CHAPTER THREE

EXPERIMENTAL CHARACTERIZATION OF ASPHALT CONCRETE MIXTURES

3.1 Material Selection

3.1.1 Aggregates

The main aggregates used in the fabrication of asphalt concrete samples were 5/8" limestone, ¼" limestone, Screenings, 2A, 47B and 3ACR. The aggregate types, 5/8" limestone, screenings and ¼" limestone were from same mineral of limestone while others were obtained as mixtures of several types of aggregates of different mineralogical origin. Based on the sieve analysis of the aggregates, the nominal maximum aggregate size (NMAS) was 12.5 mm and the maximum aggregates size (MAS) was 19.5 mm. The proportions of aggregates by type and size are listed in Table 3.1.

Table 3.1 Aggregate Proportions in Asphalt Concrete Mixtures

All Aggregate % in AC														
Sieve Size (mm)	19.0	12.5	9.50	4.75	2.36	1.18	0.6	0.3	0.15	0.075	0	Ret. %	Cum. Ret. %	
Sieve Number (#)	3/4"	1/2"	3/8"	#4	#8	#16	#30	#50	#100	#200	-200			
5/8" LS		5.0	5.4									10.4	10.4	
2A			0.6	2.6								3.2	13.6	
SCREENINGS					14.0	15.0	4.2	1.2	1.1		1.8	37.3	50.9	
47B					4.0		0.7	1.2	1.3			7.2	58.0	
3ACR				6.8	18.0		2.1	1.6	0.6	3.5	1.8	34.4	92.4	
1/4" LS				7.7								7.7	100.0	
AC Retained %	0.0	5.0	6.0	17.0	36.0	15.0	7.0	4.0	3.0	3.5	3.5	100.0		
AC Cum. Ret. %	0.0	5.0	11.0	28.0	64.0	79.0	86.0	90.0	93.0	96.5	100.0	100.0		SP4 - Special AC
AC Cum. Passing %	100.0	95.0	89.0	72.0	36.0	21.0	14.0	10.0	7.0	3.5	0.0	100.0		
AC Sieve Size$^{0.45}$ (mm)	3.8	3.1	2.8	2.0	1.5	1.1	0.8	0.6	0.4	0.3	0.0	-		
AC Max. Den. Line	100.0	82.8	73.2	53.6	39.1	28.6	21.1	15.5	11.3	8.3	0.0	100.0		

11.0 % of the total aggregates were retained in a 4.75 mm sieve, and were called coarse aggregates according to ASTM D692. Only aggregates from 4/8" limestone and 2A

belonged to this group. According to ASTM D1073, the remaining 89% of the aggregates were called fine aggregates which contain aggregates from all six types. However, only 3.6 % aggregates were identified as fillers according to AASHTO T11 and ASTM C117 and contained the aggregates from screenings and 3ACR only. The screenings passing 1.19 mm sieve were washed before blending them with other aggregates to remove the dusty particles in them.

3.1.2 Binder

The asphalt binder used in this study was a Superpave performance graded binder PG 64-28 obtained from Jebro Inc. This kind of binder can perform well from a minimum daily temperature of -28^{o}C to the average seven-day maximum temperature of 64^{o}C.

3.2 Mix Design

The hot mix asphalt (HMA) mixtures were designed according to the SP4-Special mix design used in low traffic highways of Nebraska. The binder content was decided as per the volumetric requirements of mixtures, which were set by Nebraska Department of Roads (NDOR). The AASHTO PP60 was used to fabricate the cylindrical specimens of HMA mixtures using the Superpave gyratory compactor (SGC). Their volumetric design was based on the AASHTO R35. The HMA mixtures in this study required a 6 % binder content by weight of total mixture to achieve a 4 % target air voids.

3.3 Sample Fabrication

The six types of aggregates were sieved and then preheated to a mixing temperature of 318^{o}F for couple of hours. The binder was also preheated to the same mixing temperature of 318^{o}F and mixed thoroughly using the mixer in the laboratory as per AASHTO R30. A

portion of the mixture was used to determine the theoretical maximum specific gravity, G_{mm} according to AASHTO T209. 6900 grams of asphalt concrete mixtures were compacted by applying compaction pressure of 600.00 K Pa at 271^{o} F using Superpave gyratory compactor (SGC) to produce cylindrical samples of 150.00 mm diameter and 170.00 mm height. The bulk specific gravities, G_{mb} of the samples were determined according to AASHTO T166.

The Superpave gyratory compacted hot mix samples were then cored into 100 mm diameter using a diamond bit in a water-cooled coring machine to remove the outer surfaces with higher air void contents. 10 mm thick slices were peeled off from the two faces of the cored cylindrical samples using a diamond saw machine to obtain a final height of 150 mm. Three replicates samples were fabricated using the same procedure (Figure 3.1).

Figure 3.1 Sample Fabrication of Asphalt Concrete Mixtures

3.4 Dynamic Modulus Tests

3.4.1 Test Sample Preparation

Three pairs of gage points were glued to the sample at a horizontal angle of 120 ^{o} from each other in each sample. The two gage points in each pair were kept at 101 mm in the direction parallel to the central axis of the sample (Figure 3.2).

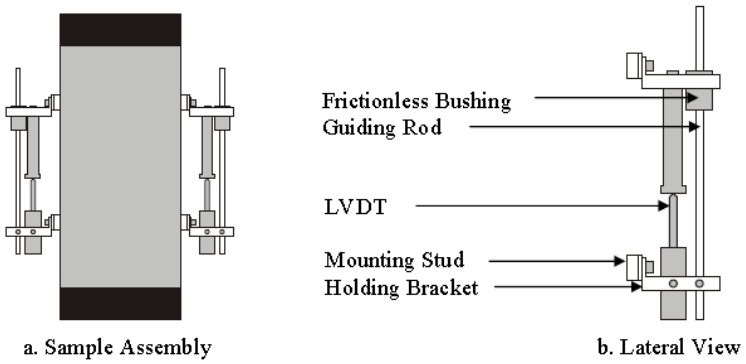

Figure 3.2 Gages in Asphalt Concrete Samples (AASHTO TP 62)

Then the jigs to hold the linear variable differential transformers (LVDTs) were screwed at those gage points such that each pair held one LVDT. There were all together three LVDTs in each sample to measure the displacement of gage points. The change in distance between the gages in each pair was required to calculate the strain with respect to their original distance. The test samples were then put in the working stage inside the environmental chamber of the universal testing machine, UTM-25. Hardened steel disks were placed on the top and the bottom faces of the specimens for transferring the load uniformly (Figure 3.3).

Figure 3.3 Installing the Asphalt Concrete Samples for Tests

3.4.2 Temperature Equilibrium

Three test temperatures of 4^{o}C, 20^{o}C and 40^{o}C were selected on the basis of PG 64-28 binder as per the provisional standard AASHTO PP61 instead of the five temperatures prescribed in standard AASHTO TP62. The objective of using only three test temperatures was to perform the dynamic modulus tests at the least possible time without compromising the quality of master curves.

Before starting the tests, the samples were conditioned at testing temperature in the environmental chamber to guarantee the same temperatures at every local coordinates of it. A dummy sample with a thermocouple inside it was used to monitor the temperature of the sample continuously. The tests were conducted only when the temperature was steady at the required test temperature.

3.4.3 Load Profile

Once the temperature was verified, the tests were then performed at several frequencies by applying a cyclic uniaxial compressive force on the top face of the cylindrical sample. The frequencies for this study were decided as 10, 1 and 0.1 at all three temperatures mentioned earlier, including an extra test at 0.01 Hz at 40^{o}C as per AASHTO PP61. In each dynamic modulus tests, different values of the amplitude of force were assigned to limit the amplitude of strain within the range of 50 - 75 microns. The force F was assigned as a haversine function of instantaneous time t, loading frequency f and input amplitude of force, F_o. The displacement signal would react with a lag in its phase angle. Both input and output are expressed as:

$$F = \frac{F_o\left(1-\cos\left(2\pi f t\right)\right)}{2} \quad (3.1)$$

$$\Delta = \Delta_o \frac{1-sin(2\pi ft-ø)}{2} \quad (3.2)$$

Where, $f = \frac{2\pi}{\omega}$

In terms of stress and strain, they can be expressed as:

$$\sigma = \frac{\sigma_o(1-sin\ (2\pi ft))}{2} \quad (3.3)$$

$$\varepsilon = \varepsilon_o \frac{1-sin(2\pi ft-ø)}{2} \quad (3.4)$$

Where, F_o, Δ_o, σ_o, ε_o, ø, ω, t and f respectively refer to force amplitude, displacement amplitude, stress amplitude, strain amplitude, phase angle, angular frequency, instantaneous time and loading frequency in a complete cycle of loading.

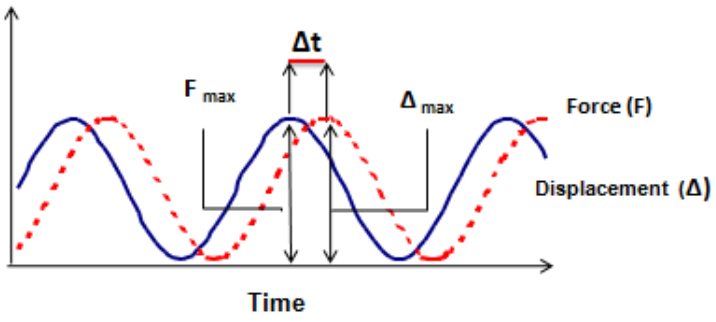

Figure 3.4 Input and Output Signals of Dynamic Modulus Tests

3.4.4 Cyclic Uniaxial Compressive Tests

The cyclic uniaxial compressive tests were performed by changing the loading frequency at three different temperatures and controlling the force by a haversine function. In this study, unique amplitude of force was selected for each frequency and temperature such that the overall strain was within the range of 50-75 microns. The tests were conducted by decreasing the loading frequencies through 10 Hz, 1 Hz and 0.1 Hz, and increasing the temperatures through 4°C, 20°C and 40°C. The temperature of 40°C also included the

frequency of 0.01 Hz. The high temperature of 40^{o}C and the low temperature of 4^{o}C were selected for observing the responses to the common distresses such as like rutting and fatigue.

3.4.5 Test Execution and Data Acquisition

The fully computerized measuring system of the UTM -25 was used to measure and record the time history of force and displacement due to the load applied through a hydraulically controlled load cell. The built-in system of force sensor was used to capture the instantaneous force. The linear variable differential transformers (LVDTs) were used to record the instantaneous change in the distance between two gage points in the same vertical alignment.

3.5 Data Analysis

3.5.1 Dynamic Modulus Tests

The instantaneous displacement of each gage points and the instantaneous force applied from the load cell were measured using the LVDTs and the load sensor of the universal testing machine. The amplitudes of force and displacement were then converted into amplitudes of stress, σ_o and amplitude of strain, ε_o from the following equations:

$$\sigma_0 = \frac{4F_o}{\pi D^2} \tag{3.5}$$

$$\varepsilon_0 = \frac{\Delta}{GL} = \frac{\Delta_{max} - \Delta_{min}}{GL} \tag{3.6}$$

Where,

GL = Gage Length or Distance between the two gauge points in a LVDT (mm), here 101 mm

D = Diameter of the sample (mm), here 100 mm

F_o = Amplitude of input forces in last five cycles (KN)

Δ_{max} = Average of maximum displacements of all 3 LVDTs in last five cycles (mm)

Δ_{min} = Average of minimum displacements of all 3 LVDTs in last five cycles (mm)

The dynamic modulus and phase angle were then determined from the amplitude of compressive stress, σ_o, which corresponded the time of maximum force t_{F_o} and the amplitude of strain ε_o, which corresponded to the time of the maximum elongation of the gage length, t_{Δ_0}:

$$|E^*| = \frac{\sigma_0}{\varepsilon_0} \quad (3.7)$$

$$ø = 2\pi\, x\, f\ x\, \Delta t = 360^0 x\, f\, x\, \Delta t \quad (3.8)$$

Where, the time delay between the stress and strain cycles was determined by:

$$\Delta t = t_{F_o} - t_{\Delta_o} \quad (3.9)$$

3.5.2 Master Curve Development

Then a master curve was constructed by shifting the frequency sweep curves at 4°C and 40°C towards the frequency sweep curve at 20°C until a single smooth curve was obtained. While shifting the curves from the lower and the higher temperatures to the reference temperature, shift factors were also obtained for each temperature, 4°C, 20°C

and 40°C, which were curve fitted by a quadratic function of temperature. From the master curve at 20°C, another master curve at 23°C was developed by multiplying the frequencies at reference temperature 20°C by a shift factor calculated from the quadratic equation of shift factor. It is very important to know that the same procedure can be applied for constructing the master curves of other viscoelastic materials such as, fine aggregate matrix, and asphalt binder.

3.6 Results

3.6.1 Sieve Analysis

The mix design resulted in 10.4%, 3.2%, 37.3%, 7.2%, 34.4% and 7.7 % of 5/8" limestone, 2A, screenings, 47B, 3ACR and ¼" limestone by weight of total aggregates (Figure 3.5.a). The sieve analysis of aggregates (Figure 3.5.b) shows 11 % of total aggregates were retained on 4.75 mm sieve and rest 89 % passed through it, representing the coarse and fine aggregate proportions.

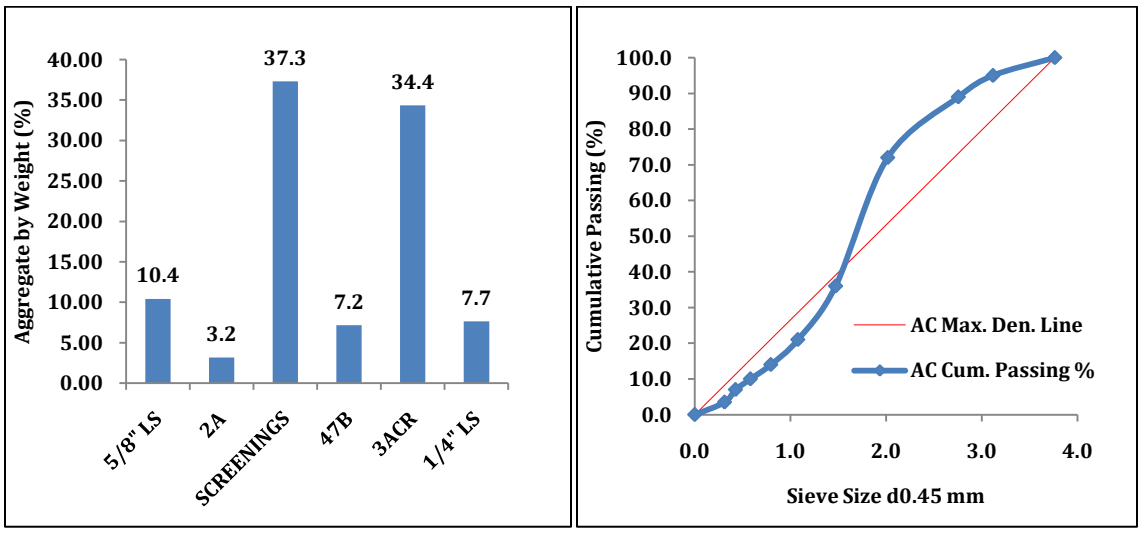

Figure 3.5 Aggregate Proportions in AC Mixtures by (a) Type (b) Size

3.6.2 Volumetric Analysis

The theoretical maximum specific gravity, G_{mm} of the asphalt concrete mixtures was determined as 2.426 ± 0.006 following AASHTO T209. The bulk specific gravities, G_{mb} of the Superpave gyratory compacted samples with 170 mm height and 150 mm diameter was determined as 2.336 ± 0.001 following AASHTO T166. The bulk specific gravities, G_{mb} of the Superpave gyratory compacted and cored samples with 150 mm height and 100 mm diameter was determined as 2.357 ± 0.003 following AASHTO T166. The cored samples had a higher value of G_{mb} due to the decreased level of air voids in the cored samples because of the removal of the outer surface of higher air void content. Similarly, other volumetric calculations were also carried out with the results from above two test standards and tabulated below in Table 3.2.

Table 3.2 Volumetric Properties of Asphalt Concrete Mixtures

Details	Uncored Sample (H170 mm x 150 mm)		Cored Sample (150 mm x 100 mm)	
	Avg.	S.D.	Avg.	S.D.
G_{mm}	2.426	0.006	2.426	0.006
G_{mb}	2.336	0.001	2.357	0.003
G_{sb}	2.577	0.000	2.577	0.000
G_{se}	2.664	0.008	2.664	0.008
$\%V_a$	3.7	0.3	2.8	0.2
%VMA	14.8	0.0	14.0	0.1
%VFA	74.9	1.7	79.7	1.6
$\%P_b$	6.0	0.0	6.0	0.0
$\%P_{ba}$	1.3	0.1	1.3	0.1
$\%P_{be}$	4.8	0.1	4.8	0.1
$\%V_{beff}$	11.1	0.2	11.2	0.2

3.6.3 Dynamic Modulus Tests

Each of the three samples obtained by cutting and coring from the central region of the Superpave gyratory compacted HMA mixtures were placed in the environmental chamber of universal testing machine (UTM-25) where they were subjected to a temperature of 4^{o}C until the thermocouple put in the dummy sample kept along with the test sample showed a steady temperature. The uniaxial haversine compressive tests were conducted respectively at 10 Hz, 1 Hz and 0.1 Hz such that the strains did not exceed the limits 75 microns. Similar tests were conducted at 20^{o}C and 40^{o}C, including an extra test at 0.01 Hz of frequency at 40^{o}C. The results of dynamic modulus tests of three cylindrical samples of asphalt concrete samples are given in Table 3.3.

Table 3.3 Dynamic Modulus of Asphalt Concrete Mixtures

Temperature (oC)	Frequency (Hz)	Dynamic Modulus |E*| (MPa)	
		Average	Std. Dev.
4.0	10	1.26E+10	1.70E+09
	1	8.81E+09	1.60E+08
	0.1	5.51E+09	5.25E+07
20.0	10	4.85E+09	6.54E+08
	1	2.41E+09	6.45E+08
	0.1	1.32E+09	3.56E+08
40.0	10	1.20E+09	3.93E+08
	1	6.77E+08	2.55E+08
	0.1	5.00E+08	1.90E+08
	0.01	5.26E+08	2.83E+08

As seen in Table 3.3, the dynamic modulus values increased with the increase of loading frequency at a constant temperature and vice versa. This fact illustrated the time dependency of viscoelastic material which states that the viscoelastic materials like asphalt concrete mixtures behave strongly against the slower loading rate than they do

against the faster loading rate. Similarly, the dynamic modulus of asphalt concrete samples increased with the increase of test temperature and vice versa. This fact illustrated the temperature dependency of viscoelastic materials which states that the viscoelastic materials behave strongly at low temperature but strongly at high temperature. The reason behind the temperature dependency of viscoelastic materials is the dominance of viscous properties at high temperature and that of elastic properties at low temperature. The frequency sweep curves of dynamic modulus of cylindrical samples of asphalt concrete mixtures are given below (Figure 3.6).

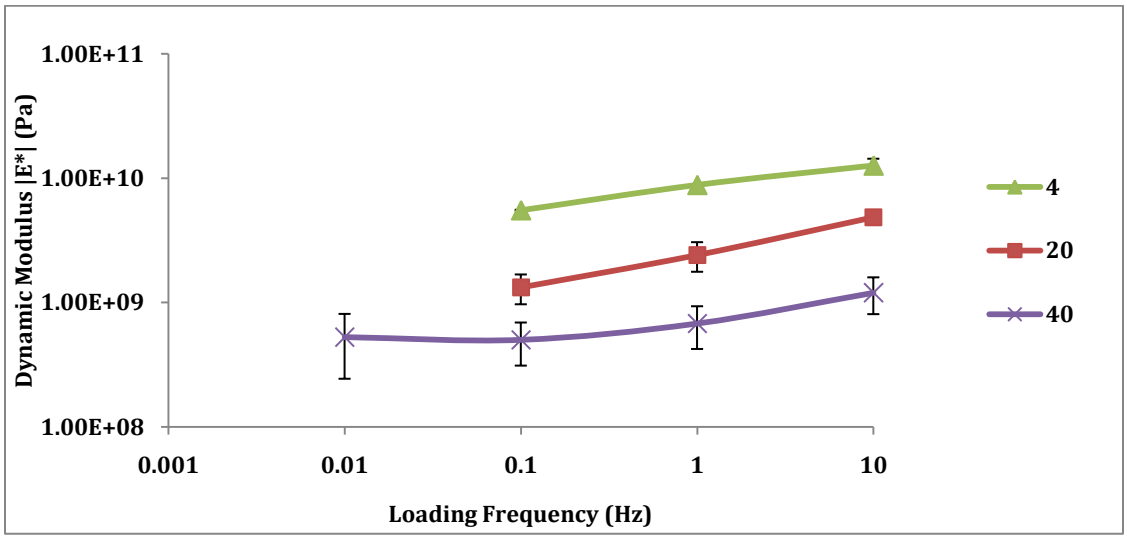

Figure 3.6 Dynamic Modulus Tests of Asphalt Concrete Mixtures

3.5.4 Master Curve Generation

The frequency sweep test curves at 4^{o}C and 40^{o}C were then shifted horizontally toward the curve at reference temperature, 20^{o}C until the curves produced a single smooth master curve by the process of time temperature superposition.

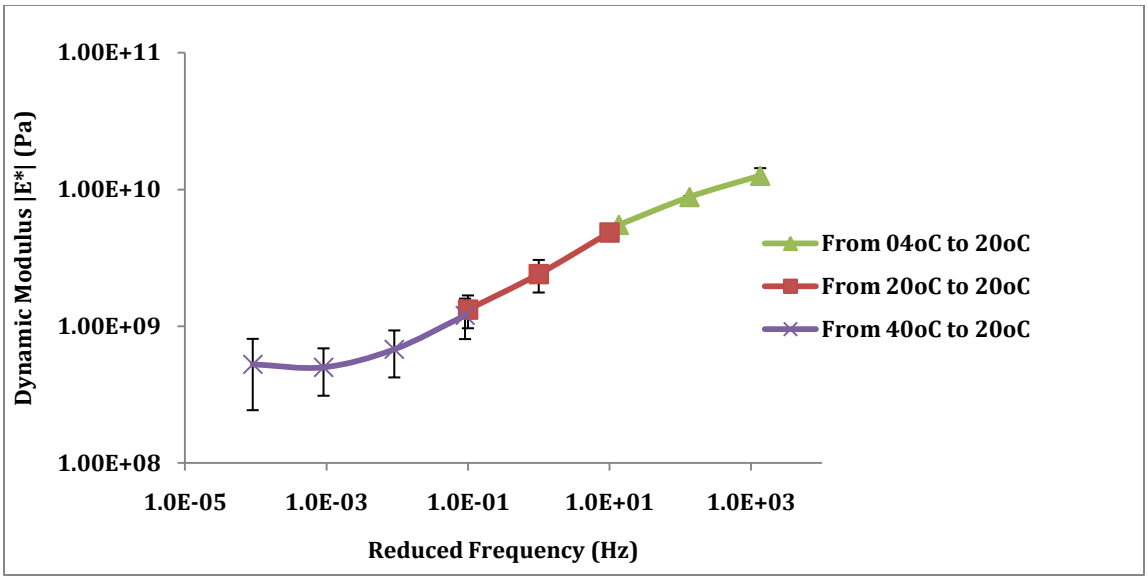

Figure 3.7 Dynamic Modulus Master Curve of Asphalt Mixtures

The range of frequency in the master curve (Figure 3.7) increased significantly in comparison to the range of frequency applied in the laboratory tests (Figure 3.6). The frequency of master curve obtained by shifting the original dynamic modulus test curves is defined as the reduced frequency. In the case of this study, the reduced frequency ranged from 0.0001 Hz to 10000 Hz in contrast to the shorter experimental frequency range from 0.01 to 10 Hz. There are few testing machines which are capable of performing and recording the extreme frequencies that were obtained during the master curve generation.

When the dynamic modulus test curves conducted at 4^{o}C and 40^{o}C were shifted towards the dynamic modulus test curve at 20^{o}C, a single smooth curve was formed with the logarithmic values of shift factors as 2.13 and -2.03 respectively and with value of 0.00 for the reference temperature 20^{o}C. The curve of shift factors at different temperatures was fitted with a simple quadratic equation (Figure 3.8).

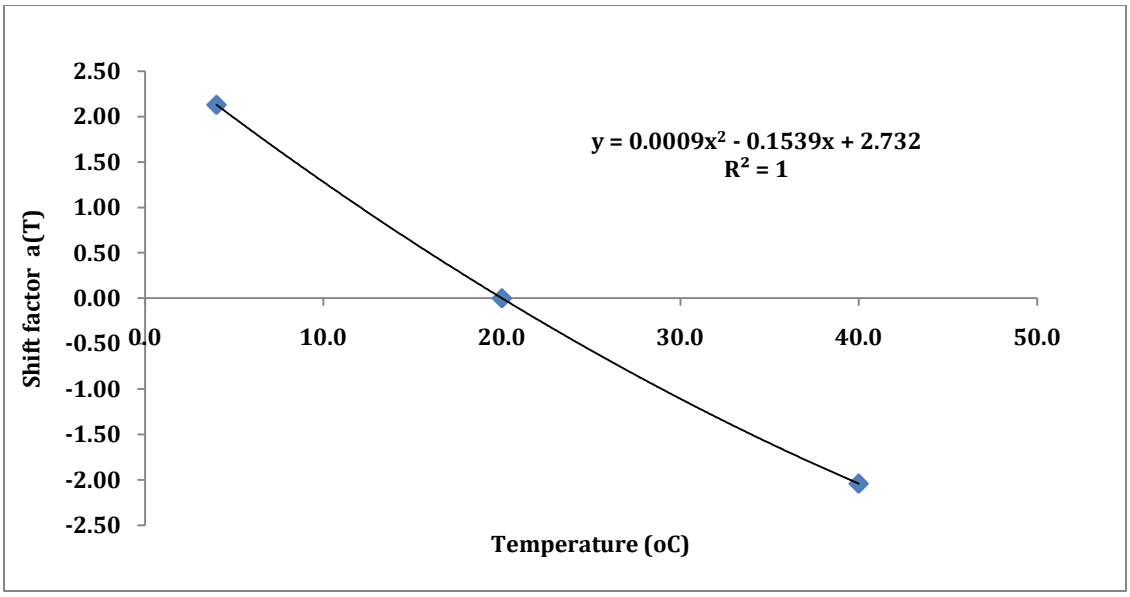

Figure 3.8 Shift Factors for Asphalt Concrete Mixtures

The shift factors at different temperatures and the master curve at the reference temperature are very useful in constructing the master curve of same material at any temperature without doing any more tests. The master curve for a viscoelastic material at any temperature can be simply constructed by multiplying the reduced frequency of the master curve at a reference temperature by a shift factor calculated from the shift factor function.

CHAPTER FOUR

EXPERIMENTAL CHARACTERIZATION OF FINE AGGREGATE MATRIX

4.1 Material Selection

4.1.1 Aggregates

Depending up the digital image analysis of the aggregates sizes captured by the two dimensional images of the vertical cross-section of cylindrical asphalt concrete mixtures, 1.19 mm was decided as the maximum aggregate size (MAS) in fine aggregate matrix. The 1.19 mm refers to the sieve number 16 in the 0.45 power FHWA gradation chart. All the aggregate types passed through 1.19 mm sieve were selected as the constituent aggregates of fine aggregate matrix mixtures. Out of the six different types of aggregate used in SP4 –Special mixtures, only 3ACR, screenings and 47B (Figure 4.1) fell in this category. Similar to asphalt concrete mixtures, the screenings were washed and dried before blending with other aggregates to avoid excess amount of fines in the binder.

Table 4.1 Aggregate Proportions in Fine Aggregate Matrix

All Aggregate % in FAM								
Sieve Size (mm)	1.18	0.6	0.3	0.15	0.075	0	Ret. %	Cum. Ret. %
Sieve Number (#)	#16	#30	#50	#100	#200	-200		
SCREENINGS		20.0	5.7	5.3		8.3	39.3	39.3
47B		3.3	5.7	6.1			15.2	54.5
3ACR		10.0	7.6	2.9	16.7	8.3	45.5	100.0
FAM Retained %	0.0	33.3	19.0	14.3	16.7	16.7	100.0	
FAM Cum. Ret. %	0.0	33.3	52.4	66.7	83.3	100.0	100.0	SP4 - Special FAM
FAM Cum. Passing %	100.0	66.7	47.6	33.3	16.7	0.0	100.0	
FAM Sieve Size$^{0.45}$ (mm)	1.1	0.8	0.6	0.4	0.3	0.0	-	
FAM Max. Den. Line	100.0	73.8	54.0	39.5	28.9	0.0	100.0	

The percentages of 47B, screenings and 3ACR in fine aggregate matrix were decided as 39.3 %, 15.2% and 45.5% in consistence with the proportion of 8.3%, 3.2% and 9.6% in

fine aggregate matrix phase which accounted for 21 % of total weight of aggregates in asphalt concrete mixtures (Table 4.1, Figure 4.1 and Figure 4.2).

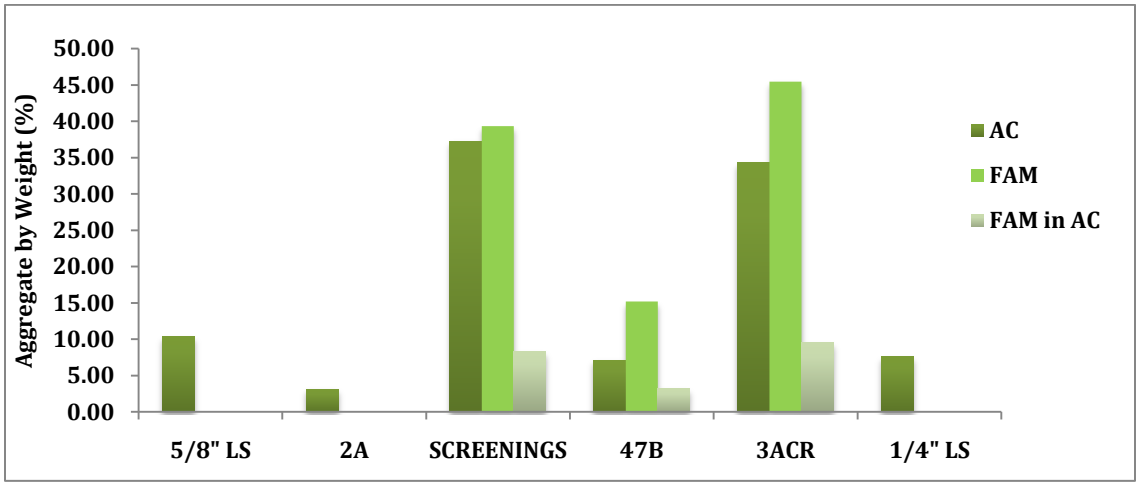

Figure 4.1 Aggregate Proportions in AC and FAM by Type

The proportion of the aggregates was kept the same as they had in the fine aggregate matrix phase of the asphalt concrete mixtures with respect to size and types of aggregates (Figure 4.1 and Figure 4.2).

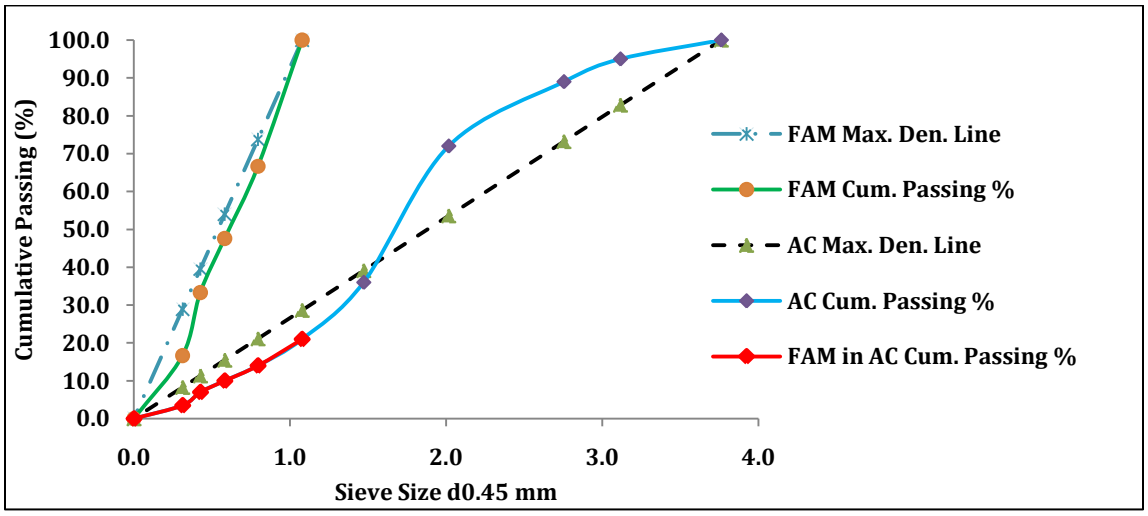

Figure 4.2 Sieve Analysis of Aggregates in AC and FAM

4.1.2 Binder

The asphalt binder used in this study was a Superpave performance graded binder PG 64-28 from Jebro Inc. which was also used in fabricating the asphalt concrete samples.

4.2 Mix Design

The mix design of fine aggregate matrix was conducted by keeping the same proportions of aggregates in SP4-Special asphalt concrete mixtures and calculating the binder content based on its sharing by coarse and fine aggregates.

4.2.1 Binder Content

The first task of the mix design was to determine the appropriate percentage of binder in the fine aggregate matrix. It was assumed that the coarse aggregates in asphalt concrete mixtures could be separated from the fine aggregate matrix by virtually picking them from the compacted samples. While picking the coarse aggregates out of the asphalt concrete mixtures, it was also assumed that they would be still coated with a thin film of binder around them and would contain binder in their surface voids. Finally, the amount of binder left after picking all coarse aggregates from asphalt concrete mixtures along with the binder in its surface and voids was assumed as the binder content of the fine aggregate matrix phase.

So the first step in finding the binder content was the calculation of weight of binder used by the coarse aggregates. The weight and percentage of asphalt binder film on the surface of coarse aggregates was determined by the following simple relation:

$$W_{bf,Ret16} = SA_{Ret16} x\, W_{s,Ret16} x\, T_{f,Ret16} x\, G_b x\, \gamma_w \quad (4.1)$$

$$\%P_{bf,Ret\,16} = \%P_b \; x \frac{W_{bf,Ret\,16}}{W_b} \quad (4.2)$$

Where, $T_{f,\,Ret16}$ refers to the film thickness surrounding the aggregates, here retained in a 1.19 mm sieve, $W_{s,Ret16}$ refers to the weight of coarse aggregate in entire AC mixtures, G_b is the specific gravity of binder and ρ_w is the density of water. Similarly, SA_{Ret16} refers to the total surface area of the coarse aggregates retained in the 1.19 mm sieve as determined by using the following formula:

$$SA_{Ret\,16} = \sum_{i=1}^{n} \frac{PP_{i,Ret\,16} \; x \; CP_{i,Ret\,16}}{100} \quad (4.3)$$

Where, $PP_{i,\,Ret.16}$ is the percentage of aggregate passing a particular sieve, $CP_{i,\,Ret16}$ is the surface area factor (m^2/kg or ft^2/lb) for that sieve as outlined in the Asphalt Institute MS-2 and n is the total number of sieves used for coarse aggregates.

The next step was to determine the weight and percentage of asphalt binder absorbed by coarse aggregates by using the following relation:

$$W_{ba,Ret\,16} = \frac{W_b}{\%P_b} \; x G_b x \left(\frac{1}{G_{sb,Ret\,16}} - \frac{1}{G_{se,Ret\,16}} \right) x \; 100 \quad (4.4)$$

$$\%P_{ba,Ret\,16} = \%P_b \; x \frac{W_{ba,Ret\,16}}{W_b} \quad (4.5)$$

Where, bulk specific gravity and effective specific gravities of coarse aggregates retained in the 1.19 mm sieve were determined by:

$$G_{sb,Ret\,16} = \frac{\sum_{i=1}^{n} \%P_{s,i} \; x \; G_{sb,Ret\,16,i}}{\sum_{i=1}^{n} \%P_{s,i}} \quad (4.6)$$

$$G_{se,Ret\,16} = \frac{100 - \%P_{b.Ret\,16}}{\frac{100}{G_{mm,Ret\,16}} - \frac{\%P_{b,Ret\,16}}{G_b}} \quad (4.7)$$

Where,

$\%P_{s,\,i}$ = Percent of aggregates retained in sieves above and in sieve # 16

$G_{sb,\,Ret16,\,i}$ = Specific gravity of aggregates retained in sieves above and in sieve # 16

$\%P_{b,Ret16}$ = Percent of binder used in rice tests of aggregates retained in Sieve #16

Then the weight of binder in fine aggregate, $W_{b,FAM}$ was determined as the weight of binder left after subtracting the weight of binder used by coarse aggregates, $W_{ba,CA}$ and $W_{bf,CA}$, from the total weight of binder in asphalt concrete mixture, W_b. Similarly, the weight of fine aggregates was calculated by subtracting the weight of coarse aggregates retained in 1.19 mm sieve, $W_{b,Ret16}$ from the total weight of aggregates in asphalt concrete mixture, W_s. The relations between the different weights of aggregates and binders in asphalt concrete and fine aggregate matrix mixtures are given below:

$$W_{b,FAM} = W_b - W_{ba,Ret16} - W_{bf,Ret16} \quad (4.8)$$

$$W_{s,FAM} = W_s - W_{s,Ret16} \quad (4.9)$$

The percentage of binder and aggregates in fine aggregate matrix mixture was finally calculated using the equations below:

$$\%P_{b,FAM} = \frac{W_{b,FAM}}{W_{b,FAM} + W_{s,FAM}} x\ 100 \quad (4.10)$$

$$\%P_{s,FAM} = \frac{W_{s,FAM}}{W_{b,FAM} + W_{s,FAM}} x\ 100 \quad (4.11)$$

For the determination of binder content of the fine aggregate matrix phase of the asphalt concrete mixtures in this study, a 12 micron film of binder was assumed to surround the coarse aggregates within the range prescribed by several researchers as discussed in the chapter two. For the asphalt concrete mixtures containing 6.0 % binder by total weight of mix, the binder content in the fine aggregate matrix was determined as 8.23 % by total weight of fine aggregates.

4.2.2 Compaction Density

After determining the binder content in fine aggregate matrix, the next step was to find the compaction density of the samples with air voids in them. The compaction density of the fine aggregate matrix was determined by dividing the total weight of the fine aggregate matrix mixture by its total volume as shown below:

$$\gamma_{FAM} = \frac{W_{FAM}}{V_{FAM}} \quad (4.12)$$

The weight of fine aggregate matrix, W_{FAM} in the compacted samples of asphalt concrete mixtures was calculated by subtracting the weight of coarse aggregates and the weight of binder on its surface and voids, $W_{non\text{-}FAM}$ from the total weight of the compacted samples of asphalt concrete mixtures, W_{mb}.

$$W_{FAM} = W_{mb} - W_{non-FAM} \quad (4.13)$$

Where,

$$W_{mb} = V_{mb}\, x\, \gamma_{mix} \quad (4.14)$$

$$W_{non-FAM} = \frac{(\%P_{s,Ret\,16} + \%P_{ba,Ret\,16} + \%P_{bf,Ret\,16})\, x\, \gamma_{mix}}{100} \quad (4.15)$$

Where,

$$\gamma_{mix} = G_{mb}\, x\, \gamma_w \quad (4.16)$$

Where, G_{mb} is the bulk specific gravity of the AC sample, V_{mb} is its volume and γ_w is the specific density of water.

Similarly, the volume of fine aggregate matrix in the compacted samples of asphalt concrete mixtures was calculated by subtracting the volume of coarse aggregates and the weight of binder on its surface and voids, $V_{non\text{-}FAM}$ from the compacted maximum

volume of the compacted samples of asphalt concrete mixtures V_{mm}. The relations of volume follow as:

$$V_{FAM} = V_{mm} - V_{non-FAM} \quad (4.17)$$

Where,

$$V_{mm} = 1 - V_a \quad (4.18)$$

$$V_{non-FAM} = \frac{(\%P_{s,Ret\,16} + \%P_{bf,Ret\,16})\ x\ G_{mb}}{100\ x\ G_{sb}} + \frac{\%P_{ba,Ret\,16}\ x\ G_{mb}}{100\ x\ G_b} \quad (4.19)$$

Where, the percentage of coarse aggregates in compacted samples of asphalt concrete mixtures is given by:

$$\%P_{s,Ret\,16} = 100\ x \left(\frac{W_s - W_{s-FAM}}{W_s + W_b}\right) \quad (4.20)$$

The above calculation of compacted density can be possible only if the value of air void content in fine aggregate matrix is known which is determined from its relationship with bulk specific gravity and theoretical maximum specific gravity of fine aggregate matrix mixtures. But the determination of air void content in FAM could not be conducted experimentally because of unavailability of the standards, and literature for performing the theoretical maximum specific gravity tests with the mixtures containing aggregates less than 1.19 mm only. So air voids were assumed from 0 % to 4 % and used to back-calculate the compaction density by the series of calculations as shown in above relations. The fine aggregate matrix mixtures with ideal value of 0% air voids had the highest density level whereas the fine aggregate matrix with 4 % air voids had the least density level.

4.3 Sample Fabrication

Similar to the asphalt concrete mixtures, the aggregates and the binder were both preheated to the mixing temperature of 318^{o}C and thoroughly mixed with each other following AASHTO R30. The mixture was then compacted to a controlled height of 80.00 mm and a diameter of 150.00 mm by applying compaction pressure of 600.00 KPa with a Superpave gyratory compactor at a speed of 30 gyrations per minute to obtain the compacted samples with different air void contents.

Out of the samples with different densities, only the samples with air void content of 1.75%, 1.50 %, 1.00%, 0.50 % and 0.00 % were compacted. The samples with more than 1.75 % air voids collapsed while compacting. The 80 mm thick and 150 mm diameter bulk matrix samples were then sliced with the help of a diamond saw machine into three parts; the middle parts were 45.00 mm height and 150.00 mm diameter. The entire process involved in preparing the samples is shown in Figure 4.3.

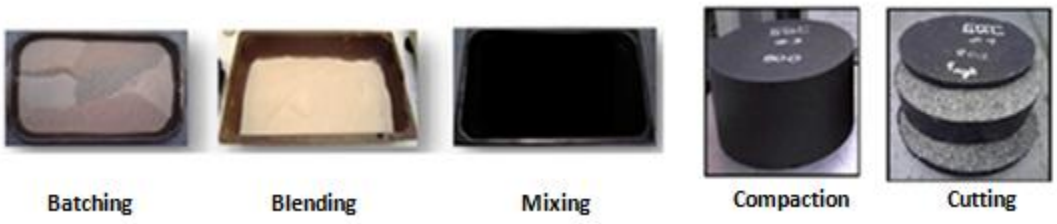

Figure 4.3 Superpave Gyratory Compaction of Fine Aggregate Matrix

The volumetric properties of the fine aggregate matrix which could be compacted are listed below in Table 4.2.

Table 4.2 Volumetric Properties of Fine Aggregate Matrix

Design Air Voids (%)	Density (g/cm3)	Gyrations
0.00%	2.152	16
0.50%	2.097	10
1.00%	2.054	8
1.50%	2.012	6
1.75%	1.973	3

Keeping the three parts intact in a 150 mm diameter cylindrical case open at both ends, the 45.00 mm long and 12.25 mm diameter torsional bars were cored out of the SGC samples using the water-cooled diamond coring machine. The top and bottom slices of the matrix, and the cylindrical case were used to produce the torsional bars of matrix samples without any problems at their two ends during the coring. Since there are no standard methods to compact the fine aggregate matrix with Superpave gyratory compactor, it was felt necessary to monitor the difference, if any, in the properties of the matrixes at different locations of SGC sample. So a total of ten cylindrical torsional bars were extracted by coring the SGC samples; the first five were extracted from the central region and other five from the circumferential region (Figure 4.4).

Figure 4.4 Torsional Bars Extraction SGC Fine Aggregate Matrix

4.4 Oscillatory Frequency Sweep Tests

4.4.1 Test Sample Preparation

A total of 50 samples were used in the whole testing procedure at all temperatures and loadings. For identifying the samples, each sample was given a unique name as either as Matrix_ X_ Side or as Matrix_ X_ Centre which meant the torsional bar extracted either from the circumferential or the central region of Superpave gyratory compacted puck samples with X % of air voids. Then the samples were glued with the specially designed geometry heads to attach them to the torsional kits of dynamic shear rheometer, AR2000ex.

4.4.2 Temperature Equilibrium

The matrix samples were conditioned for 20 minutes in the environmental chamber of AR2000ex rheometer at each temperature before conducting the tests to guarantee that the samples had same temperature at all its coordinates. Due to small size of torsional bar samples and efficient temperature controlling system of the machine, 20 minutes of temperature conditioning was enough for matrix samples. Along with the isothermal condition, equilibrium of normal force was also maintained before starting the test so that there would not be any stresses or strains due to excess normal forces other than contact force.

4.4.3 Load Profile

The cylindrical samples were then tested in pure torsion at several frequencies at three different temperatures by controlling their rotational twist with a sinusoidal function (Figure 4.6). The shear strain was assigned as a function of instantaneous time t, loading

frequency f and input amplitude of shear strain γ_o. The shear stress also followed a similar sinusoidal function of time, frequency and the shear stress obtained from the torque which was required to obtain the corresponding strain. The input shear strain and output shear stress followed the following relations:

$$\gamma = \gamma_o \sin(2\pi f t) \quad (4.21)$$

$$\tau = \tau_o \sin(2\pi f t - \delta) \quad (4.22)$$

Where, τ_o, γ_o, δ, ω, t and f respectively refer to the shear stress amplitude, the shear strain amplitude, phase angle, angular velocity, instantaneous time, loading frequency and time period for a complete cycle of stress and strain (Figure 4.5).

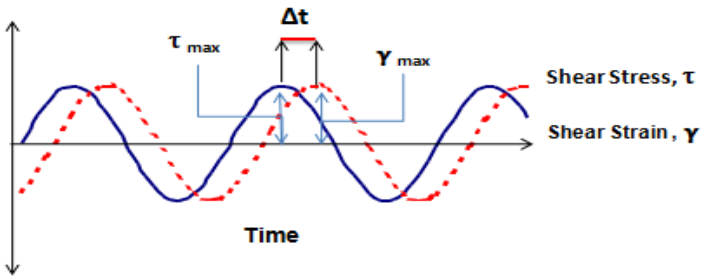

Figure 4.5 Input and Output Signals of Torsional Shear Tests

4.4.4 Oscillatory Torsional Shear Tests

The torsional shear tests were performed by changing the loading frequency at a given temperature by keeping the maximum shear strain constant inside the linear viscoelastic range in each cycle. In this study, amplitude of 0.006 % strain was kept constant in each cycle of loading while the frequency was changed from 25Hz to 0.01 Hz in decreasing order to monitor the effect of loading time in the stiffness of fine aggregate matrix mixtures (Figure 4.6). The samples were tested at three different temperatures, 5^{o}C, 20^{o}C and 40^{o}C in increasing order to monitor the effect of temperature in their stiffness.

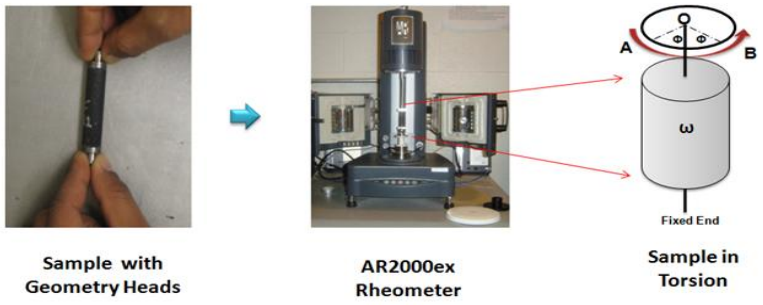

Figure 4.6 FAM Sample Installation and Test Methodology

4.4.5 Data Acquisition

The torque required to reach the assigned value of controlled strain was recorded using the Rheology Advantage software of dynamic shear rheometer, AR2000ex (Figure 4.6). The calibration constants, frequency, angular twist, oscillatory stress, temperature, the length of the sample as the gap length, etc. were also recorded at each instantaneous time for facilitating the calculation of dynamic modulus values and phase angles.

4.5 Data Analysis

4.5.1 Oscillatory Torsional Shear Tests

Dynamic shear modulus of the fine aggregate matrix |G*| was calculated by dividing the amplitude of sinusoidal shear stress τ_0 at a given loading frequency and temperature by the amplitude of sinusoidal shear strain γ_0 in the corresponding cycle as follows:

$$|G^*| = \frac{\tau_0}{\gamma_0} \tag{4.23}$$

The amplitudes of the shear stress and the shear strain were directly determined from the amplitude of torque T_o required to obtain the amplitude of rotational displacement Φ_o in each cycle:

$$\tau_0 = \frac{2\ x\ T_0}{\pi\ x\ R^3} = \frac{16\ x\ T_0}{\pi\ x\ D^3} \tag{4.24}$$

$$\gamma_0 = \Phi_o x \frac{R}{L} \quad (4.25)$$

Where, R and L denote the radius and the length of the torsional bar of matrix. Similarly, the phase angle was calculated from the dynamic modulus test curves as follows:

$$\delta = 2\pi x f x \Delta t = 360^0 x f x \Delta t \quad (4.26)$$

Where, the time delay between the stress and strain cycles was given by the following relation:

$$\Delta t = t_{T_o} - t_{\Phi_o} \quad (4.27)$$

4.5.2 Master Curve Generation

A master curve was constructed by shifting the frequency sweep test curves of fine aggregate matrix by the same procedure used for constructing the master curve of dynamic modulus tests of asphalt concrete mixtures. The curves of dynamic shear modulus values at 5^{o}C and 40^{o}C in the frequency range of 0.01 Hz to 25 Hz were horizontally shifted towards the curve of dynamic shear modulus at 20^{o}C by applying the time and temperature superposition principle until they superimposed into a single smooth curve. While shifting the curves to a reference temperature, shift factors for the horizontal transposition of the curves at each temperature were also determined and curve fitted by quadratic function of temperature. Using the shift factor interpolated by using the function, the master curve at 20^{o}C was shifted to a temperature of 23^{o}C. The master curve of storage shear modulus was also constructed at 20^{o}C and 23^{o}C to obtain the Prony series coefficients.

4.5.3 Prony Series Coefficients

The master curves constructed for storage shear modulus at 23^{o}C in angular frequency domain were curve fitted by Prony series to obtain the constants G_o, G_∞, G_i and τ_i. The constants obtained from Prony series curve fitting of master curves are used to characterize the viscoelastic materials such as fine aggregate matrix in this study:

$$G'(\omega) = G_\infty + \sum_{i=1}^{n} \frac{\omega^2 \tau_i^2}{\omega^2 \tau_i^2 + 1} G_i \quad (4.28)$$

$$G''(\omega) = \sum_{i=1}^{n} \frac{\omega \tau_i}{\omega^2 \tau_i^2 + 1} G_i \quad (4.29)$$

Where,

G_∞ = Long term Prony series coefficient representing the spring

G_i = Prony series coefficients representing the linear spring constants

τ_i = Prony series coefficients representing the time dependent decay of dashpots

n = Number of the dashpots

The values of constants in the Prony series were determined by collocation method until the master curve from the analytical solution converged with the master curve constructed from the experimentally determined storage shear modulus in angular frequency domain. Then the material constants were normalized using the following relations:

$$g_i = \frac{G_i}{G_0} \quad (4.30)$$

Where,

G_0 = Short term Prony series coefficient representing the spring

g_i = Normalized Prony series coefficients representing the linear spring constants

The short term Prony series coefficient was obtained by calculating the relaxation shear modulus at zero value of time as follows:

$$G_0 = \lim_{t = 0} G(t) = G_\infty + \sum_{i=1}^{n} G_i \quad (4.31)$$

Where,

$$G(t) = G_\infty + \sum_{i=1}^{n} G_i \; x \; e^{-t/\tau_i} \quad (4.32)$$

4.6 Results

4.6.1 Sieve Analysis of Aggregates

Out of the six types of aggregates used in asphalt concrete mixtures, only those aggregates passing through 1.19 mm sieve were used to fabricate the fine aggregate matrix. The only three aggregate types in this category were the aggregates from screenings, 47B and 3ACR, totaling a 21 % by weight of total aggregates used in asphalt concrete.

Out of these three aggregates, screenings weighed 39.3 %, 47B weighed 15.2 % and 3ACR weighed 45.5 % by weight of total aggregates in fine aggregate matrix mixtures keeping the proportion of 8.3: 3.2: 9.6 constant same as it was in the matrix phase of asphalt concrete mixtures. The sieve analysis results are listed in Table 4.3 in terms of cumulative passing percentage.

Table 4.3 Sieve Analysis of Aggregates in Fine Aggregate Matrix

Sieve			Cumulative Passing %	
Size (in.)	Size (mm)	Size $^{0.45}$	Mix Design Density Line	Max. Density Line
No. 16	1.19	1.08	100.0	100.0
No. 30	0.6	0.79	66.7	73.5
No. 50	0.3	0.58	47.6	53.8
No. 100	0.15	0.43	33.3	39.4
No. 200	0.08	0.32	16.7	29.7

Similarly, the values of cumulative passing percentage of aggregates through different sieve sizes is illustarted in Figure 4.7.

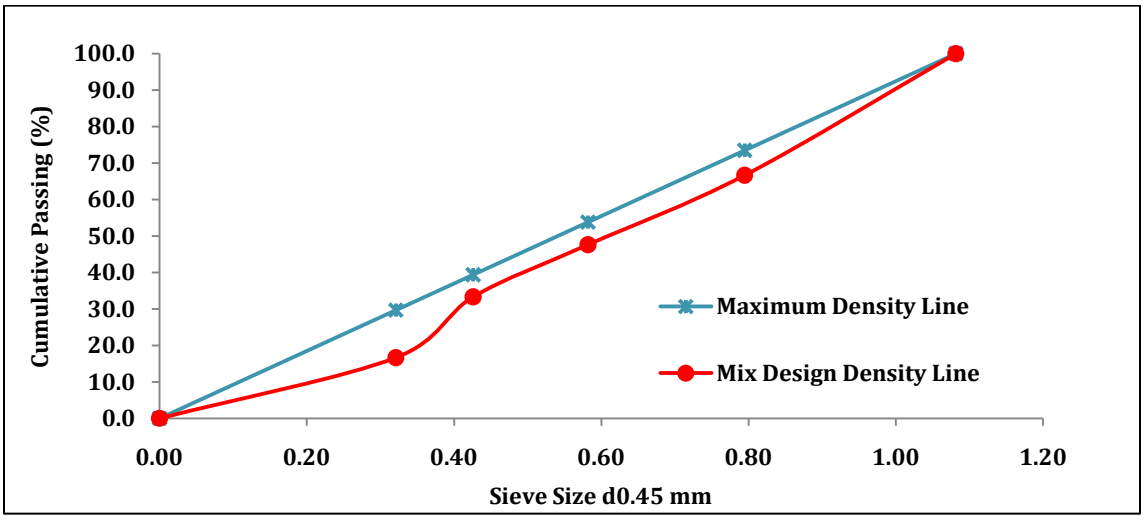

Figure 4.7 Sieve Analyses of Aggregates in Fine Aggregate Matrix

4.6.2 Volumetric Analysis of Mixtures

A total of five different types of Superpave gyratory compacted hot mixed FAM samples were prepared in the laboratory with the height of 80 mm and diameter of 150 mm, and air voids of 0.0%, 0.5%, 1.0%, 1.5% and 1.75%. Depending on the compaction effort required for different air voids and densities, it was expected that the stiffness of the matrix would decrease with the increase of air voids. The volumetric information of

different types of the SGC matrixes showed an increasing trend of number of gyrations with the decrease in air void content and increase in density as expected.

4.6.3 Oscillatory Torsional Shear Tests

Then oscillatory torsional shear tests were conducted at 5^{o}C by sweeping the frequency from 25 Hz to 0.01 Hz at constant strain amplitude of 0.006% in each cycle. Similar tests were conducted for all the samples at 20^{o}C and 40^{o}C too (Figure 4.8).

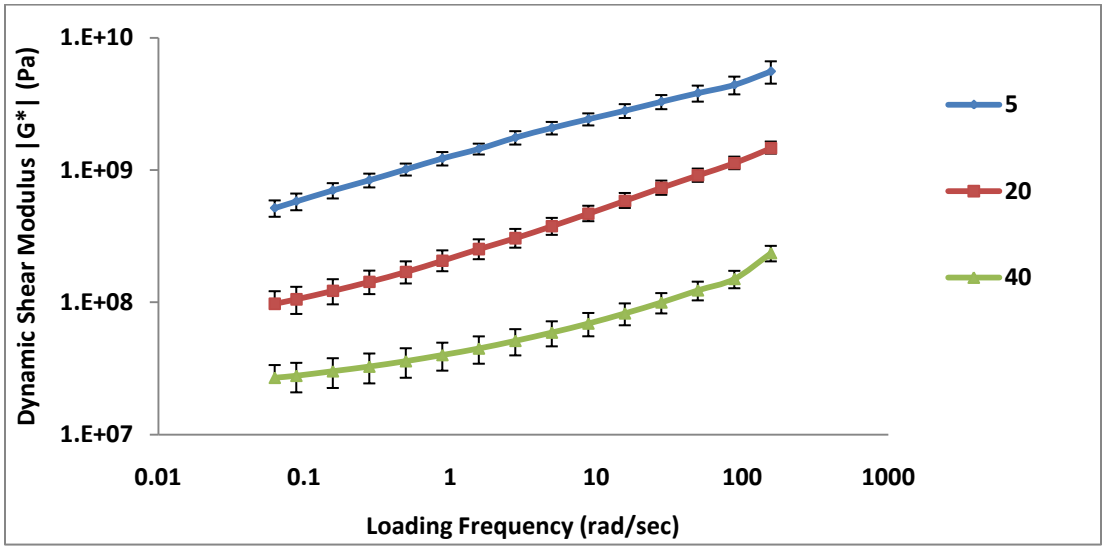

Figure 4.8 Frequency Sweep Tests of Fine Aggregate Matrix Bars

The dynamic shear modulus increased with the increase in loading frequency at a constant temperature and vice versa, which illustrated the time dependency of FAM mixtures. Another clear tendency observed from the frequency sweep tests is that they resisted the shear stresses and the shear strains weakly in high temperature conditions but strongly in low temperature conditions. The behavior of temperature dependency is attributed to the fact that fine aggregate matrix behaves like viscous fluids at higher temperature and elastic solids in lower temperature. These two facts of time and

temperature dependency of FAM mixtures prove them to be thermo-rheological materials.

4.6.4 Master Curve Development

Since the mixtures of asphalt binder and fine aggregates are thermo-rheological simple materials as discussed above, the curves obtained by conducting the oscillatory frequency sweep tests of torsional bar samples at 5°C and 20°C were horizontally shifted to the curve obtained for the reference temperature of 20°C to generate the master curve. The master curves were constructed for average values of dynamic shear modulus and storage shear modulus for five torsional samples extracted from the circumferential region and for other five samples from central region, and also for the average of all ten samples. The process was repeated for all the five types of FAM mixtures with example in Figure 4.9.

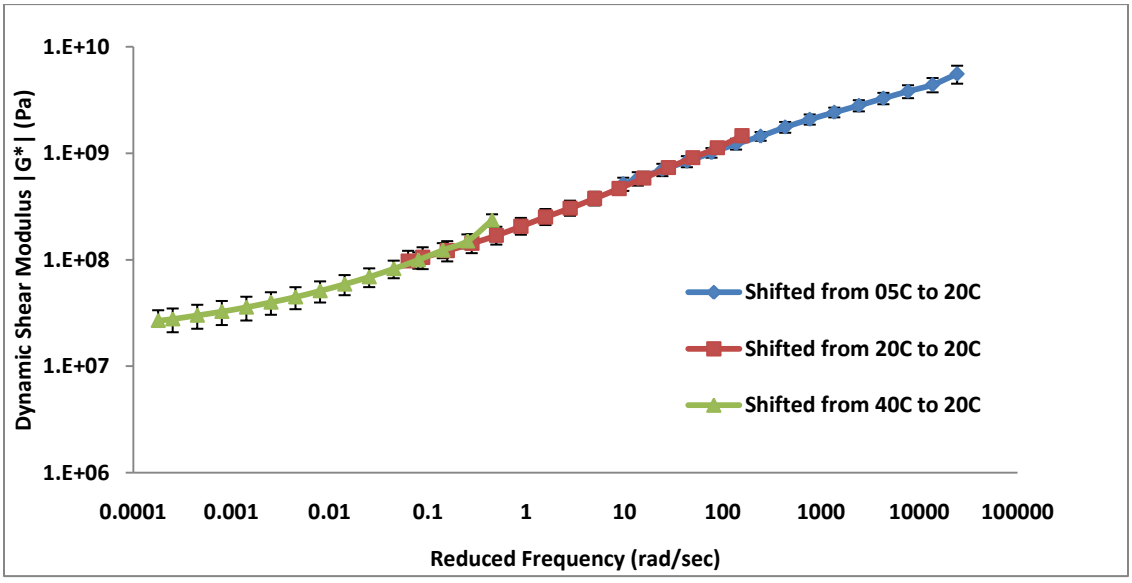

Figure 4.9 Master Curve of Dynamic Shear Modulus of FAM Bars

While shifting the frequency sweep curves at different temperatures, one shift factor was obtained for each of 5°C, 20°C and 40°C which were fitted with quadratic function of temperature. The function was used to determine the horizontal shift required to transpose the master curve at 20°C to 23°C. The shift factors for the dynamic modulus curves of the fine aggregate matrix mixtures with 0% air voids are fitted in Figure 4.10.

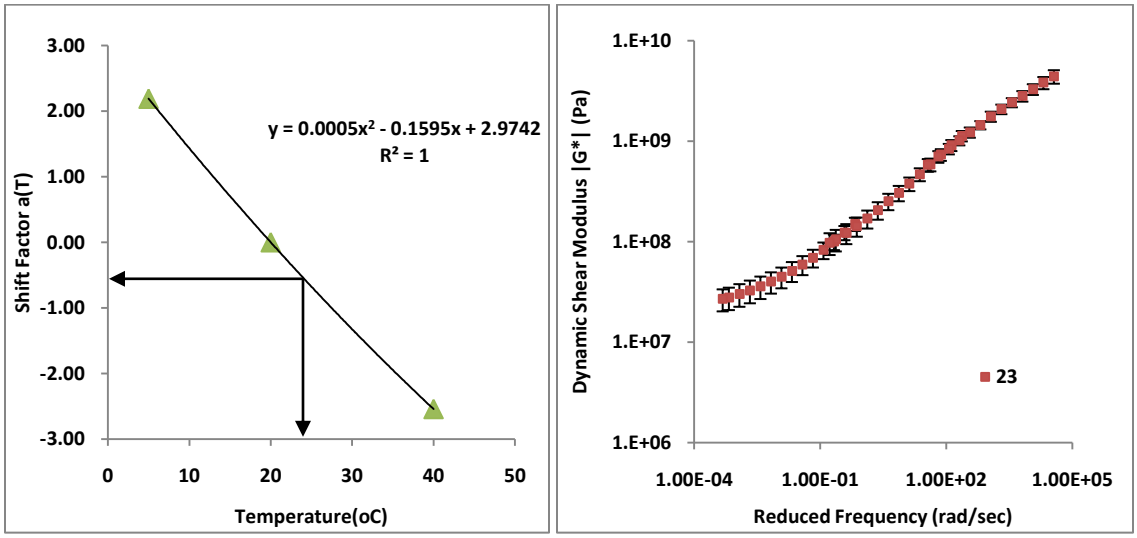

Figure 4.10 FAM Master Curves (a) Shift Factors (b) Shift at 23°C

Shift factors were determined for each type of matrix mixtures and curve fitted by corresponding quadratic functions. By the principle of time-temperature superposition, a wider range of frequencies in master curves was obtained for the matrix samples too. The fact illustrated the benefit of using the thermo-rheological behavior of fine aggregate matrix to determine the dynamic shear modulus at the extreme frequencies at which laboratory tests are almost not possible. With the shift factors determined from their quadratic functions, the master curve was constructed for different types and locations of SGC FAM samples for 23°C by shifting the master curves at 20°C.

4.6.5 Prony Series Coefficients

The master curves of storage shear modulus of the fine aggregate matrix mixtures at 23^{o}C in angular frequency domain were curve fitted by Prony series using the collocation method to get the material constants, namely the normalized storage modulus coefficients, g_i, relaxation times, τ_i and the long term shear modulus of the materials G_∞. The shear modulus in time domain was then constructed by using the coefficients obtained for the shear modulus in angular frequency domain and just changing the loading time. The shear modulus values were converted into bulk and relaxation modulus values to get the Prony series coefficients for each of them. All the coefficients obtained for the Prony series of shear, relaxation and bulk moduli were later used for the finite element computations, as discussed in chapter six. The master curves of storage shear modulus of FAM mixtures with different air void contents in frequency domain are given in Figure 4.11.

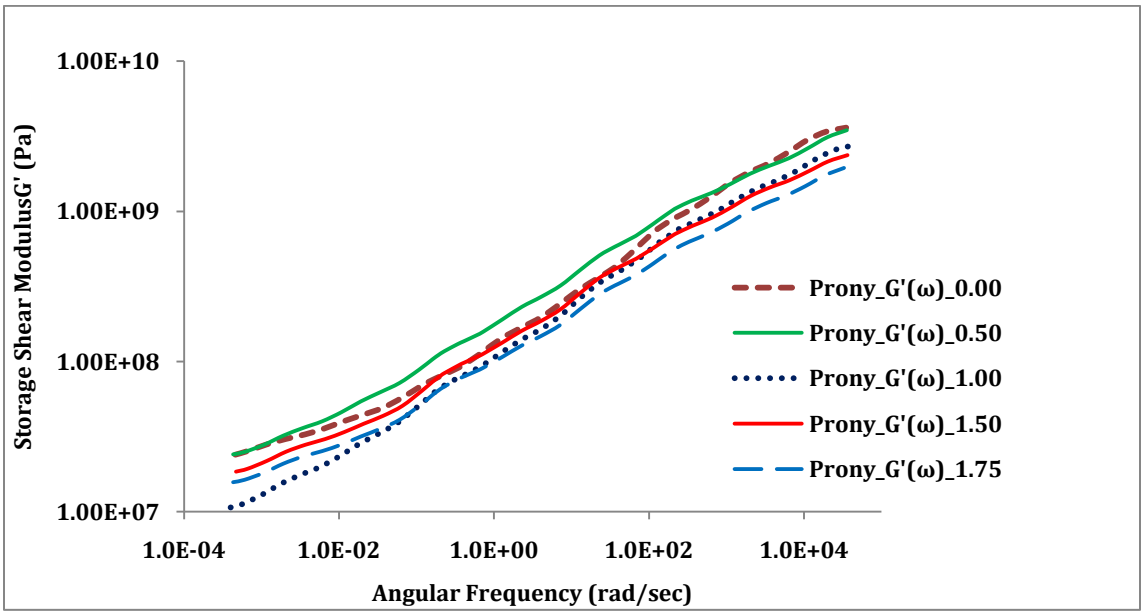

Figure 4.11 Storage Shear Modulus of Fine Aggregate Matrix

The master curves obtained by plotting the analytically calculated values of relaxation shear modulus in time domain are shown in figure 4.12 below:

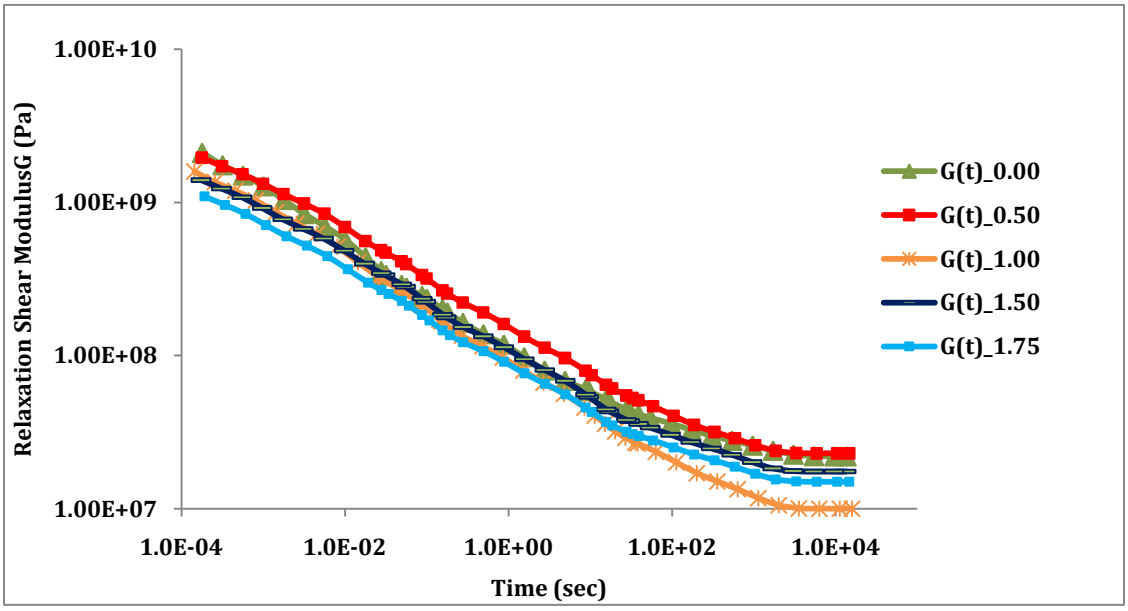

Figure 4.12 Relaxation Shear Modulus of Fine Aggregate Matrix

CHAPTER FIVE

EXPERIMENTAL CHARACTERIZATION OF AGGREGATES

5.1 Material/ Sample Selection

One sample of limestone and two samples of asphalt concrete mixtures were selected for nanoindentation tests to obtain their elastic modulus values. The sample of limestone was selected to study the workability and consistency of nanoindentation tests in aggregates with respect to indentation numbers and load. The samples of asphalt concrete mixtures were selected to determine the elastic moduli of the aggregates used their fabrication by indenting them at random locations of aggregate phase. The asphalt concrete samples were obtained from SP4-Special mixtures of aggregates like 5/8" limestone, 3ACR, 47B, Screenings, 2A and ¼" limestone and the PG 64-28 binder. The limestone sample was prepared by cutting the coarse aggregate of limestone while the asphalt concrete samples were prepared by cutting the Superpave gyratory compacted cylindrical samples.

The size of the sample was decided based on different factors such as objective of selecting the sample, number of required indentations, degree of heterogeneity, degree of surface roughness, etc, and also workability for coring, cutting, grinding, polishing and indenting the samples.

For the asphalt concrete samples, the thickness was primarily governed by the maximum thickness allowed in the nanoindenter and the degree of absorption of deformation by the binder around the aggregates of interest. Secondly, it was limited by the maximum depth of indentation which, in no case, was allowed more than one tenth of the total thickness for the safety of the indenter. The least thickness that the diamond cutter could deliver

was inside the range and, so it was decided as the thickness of both asphalt concrete samples and the limestone sample as well.

Similar to the thickness, the x-y size of the asphalt concrete samples was also governed by the dimensions of the working stage, the efficiency and perfections required in surface polishing. So the dimensions of the samples were taken as small as possible to avoid extra work of polishing by avoiding voids, valleys and elevations. It was also verified that they contained different types of aggregates and binder (Figure 5.1).

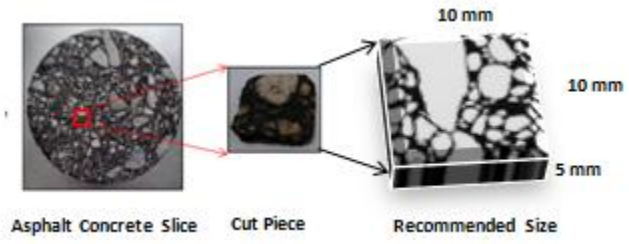

Figure 5.1 Sampling of AC Mixtures for Nanoindentation

The cylindrical samples of asphalt concrete mixtures, 170 mm in length and 150 mm in diameter, were cored and cut into almost 5 mm height and 150 mm diameter slices, which were cut with a marble cutting machine into rectangular pieces with sides averaging around 10 mm. The limestone sample was obtained by cutting the coarse limestone aggregate into a thickness of 5 mm and side length of close to 10 mm.

5.2 Sample Preparation

Since nanoindentation is in nano scale, even a small irregularity in gradient or depth at any point inside the samples can make the indenter collide with the surface and give misleading results. Thus, the surfaces of asphalt concrete and limestone samples were smoothened to give flat and parallel surface before performing the indentations. For smoothing, the samples were first glued to the closed end of cylindrical metal piece with

a base plate in between them by using a heat sensitive adhesive bond, Crystalbond™ 509. Then the assembly was inserted into a circumferential ring with corrugations in one side (Figure 5.2).

Figure 5.2 Assembly for Holding the Sample During, Grinding and Polishing

Buehler ECOMET® 3 and its accessories (Figure 5.2 and Figure 5.3) were used for making the samples smooth by grinding the surface of interest with several grades of abrasive papers and grinders in the presence of water. The abrasive papers and grinders were continuously rotated to make the extra materials on the surface of the sample wear out and wash away with the water through the corrugations of the circumferential ring. Three levels of sandpapers were used for grinding the test surface until the surfaces were uniformly smooth.

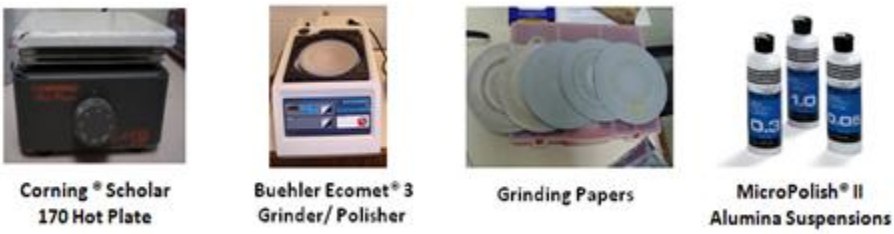

Figure 5.3 Accessories for Gluing, Grinding and Polishing

After removing the larger extra materials, the samples were polished using the Aluminum suspensions on special polishing cloths in the presence of water to remove the smaller

materials which were not removed by the grinders. Three different levels of MicroPolish® II Alumina suspensions, 1.0 micron, 0.3 microns and 0.05 microns were used in sequence. Each suspension was used with different polishing cloth to remove the wear and tear particles larger than the size of the Aluminum suspensions. For example, the 0.05 micron Aluminum suspensions removed the particles greater than 0.05 microns from the surface. The entire process of grinding and polishing the samples was conducted with the least force required to hold the samples and corrugations in contact while touching the rotating grinders and polishers without causing breakage or surface disruption (Figure 5.3 and Figure 5.4).

Figure 5.4 Grinding and Polishing for Nanoindentation

5.3 Nanoindentation Tests

Since the objective of the nanoindentation tests of asphalt concrete and limestone was to determine only the elastic properties of aggregates in them, only quasi-static tests were conducted by using a Berkovich diamond indenter attached in Hysitron Bio Ubi VII Nanoindenter. Berkovich indenter is a three sided probe with a total included angle of 142.35^{o} plane to edge, half angle of 65.35^{o}, an aspect ratio of 1:8 and an average radius of curvature of about 150 nm. It is usually used to indent samples with thickness greater than 100 nm. The instrumentation of the nanoindentation test is shown in Figure 5.5.

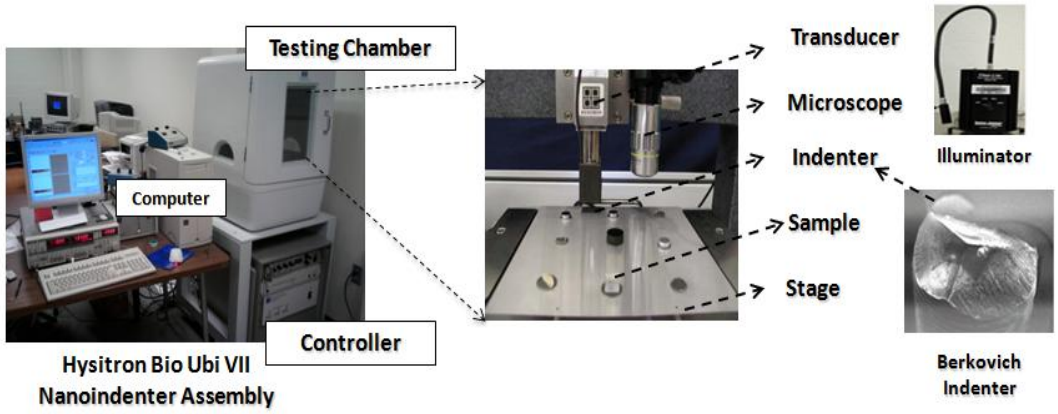

Figure 5.5 Nanoindentation Test Equipments and Indenter

5.3.1 Calibration

Before testing the samples of interest, a fused silica quartz sample was indented with a Berkovich indenter in quasi-static condition. The elastic modulus of quartz obtained from the nanoindentation test was same as the elastic modulus obtained from standard literature, signifying the fact that the elastic modulus of any other samples would be accurate if the same testing conditions of indenter, temperature, machine, etc. were maintained. By back calculating the projected area from elastic modulus, six coefficients were obtained for curve fitting the projected area and the indentation depth in the quartz sample. Since these coefficients were related to the machine compliance and the Berkovich indenter geometry, they were used for determining the projected areas at different contact depths for all samples in this study.

5.3.2 Selection of Points of Interest

The samples were placed in the central region of the magnetic stage inside the environmental chamber of the indenter machine such that the metallic base of the test sample assembly was attached on the stage as a substratum, hence creating a support and

ensuring no movements of sample during the indentation process. The samples were then viewed through the powerful microscope attached inside the environmental chamber with an appropriate zoom level to identify the aggregates and the matrix. The regions with distinct phase of aggregates with one or more types were selected by assigning the control points. The area within the boundary along the control points was used to make the indentation. The areas of interest were selected randomly for the limestone sample due to their homogeneity. The points of interest were manually selected by looking on the surface of the sample with a microscope.

Nine points of interest were assigned for the first set of tests in limestone sample and thirty more in the second set. One extra point was also assigned for the indentation test at a higher peak load. Thirteen points of interest in two different regions were assigned in each of the two asphalt concrete samples such that some of them would lie in aggregates and others outside them (Figure 5.6)

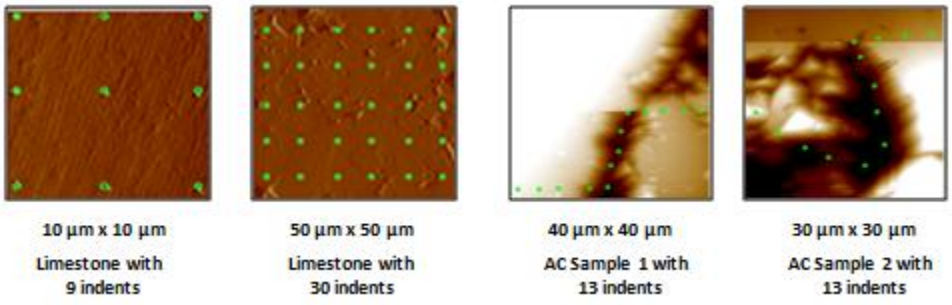

Figure 5.6 Points of Interest for Nanoindentation Tests

All together forty indents were assigned in limestone sample to capture the consistency of the tests and fifty two in asphalt concrete samples to check the heterogeneity of the asphalt concrete samples respectively. The indents only in aggregate phase of asphalt concrete would be used for simulation purposes described in chapter six.

5.3.3 Load Profile

There are multiple numbers of quasi-static and oscillatory loading schemes which can be implemented separately or in combinations. In this study, a trapezoidal loading profile (Figure 5.7 and Figure 5.8) and a triangular loading profile (Figure 5.9) were implemented. For the first set of nine tests in limestone sample and all four sets of thirteen tests in asphalt concrete samples, a trapezoidal loading profile was constituted with three steps in it – loading, holding and unloading. All indentation tests in asphalt concrete samples were carried out with this loading profile. The trapezoidal loading profile was used for indenting the asphalt concrete samples to allow them to relax the effect of viscoelasticity of binder, if any, during the holding period so that only elastic property of aggregate could be captured.

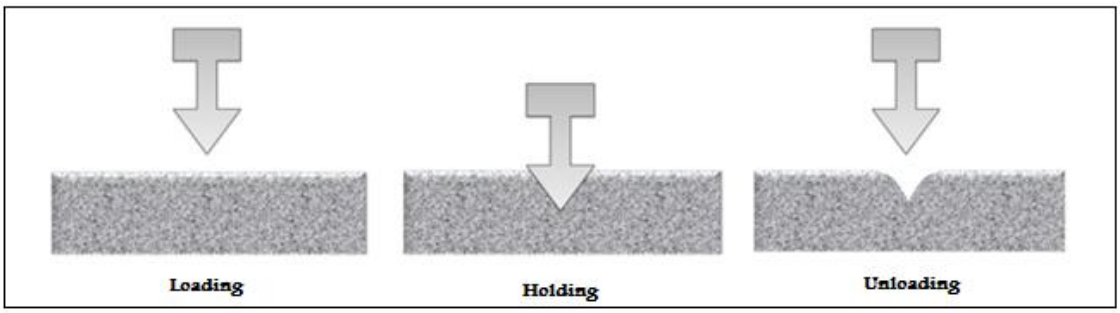

Figure 5.7 Visualization of Trapezoidal Loading Profile

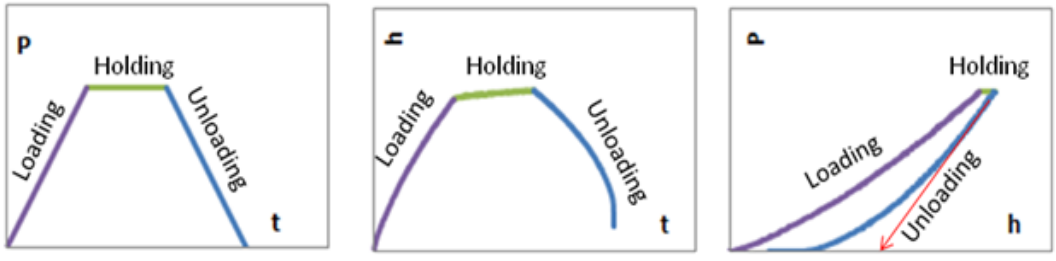

Figure 5.8 Indentation Curves from Trapezoidal Loading Profile

The triangular loading profile (Figure 5.9) was constituted with one loading step and one unloading step without any holding step. The holding period was decided to be omitted because the creep in the limestone was very small and could be ignored. This profile was applied for limestone sample only for the second set of nine indents with same peak loads and one single test with a higher peak load.

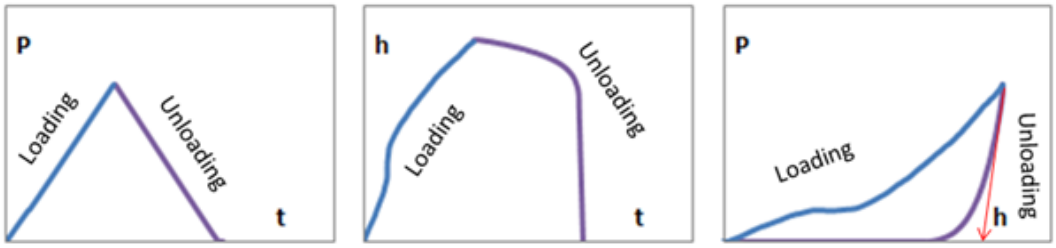

Figure 5.9 Indentation Curves from Triangular Loading Profile

For the limestone, each three steps of trapezoidal loading profile (Figure 5.10) were assigned with a peak load of 2000 μN for 10 seconds. Similarly, the another thirty indentations in limestone sample were assigned with a triangular load profile which contained only loading and unloading steps of 10 seconds each and same peak load of 2000 μN (Figure 5.10). One single indent in it was assigned with a peak load of 5000 μN to monitor the change in modulus, if any, with the change in load (Figure 5.10).

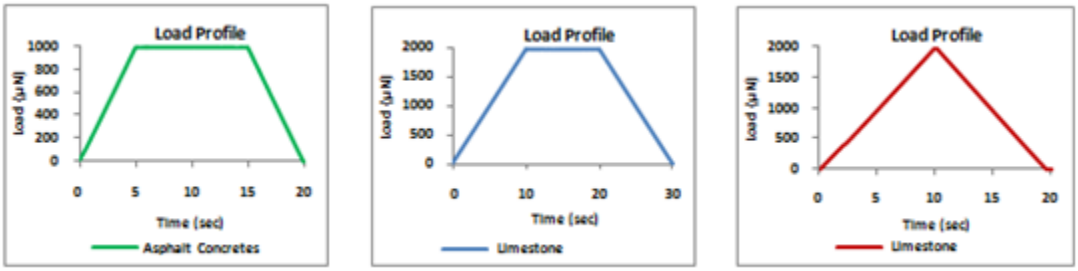

Figure 5.10 Loading Profiles for Nanoindentation Samples

The trapezoidal load function in asphalt concrete samples were designed with 5 seconds of loading, 10 seconds of holding and 5 seconds of unloading with a peak force of 1000 μN.

5.3.4 Quasi Static Tests

The nanoidentation tests were then executed with the help of TriboScan® software. The indentation were done at a constant rate of indentation, creating a quasi-static conditon of loading and unloading. The indentations were conducted with a time gap in between each indents to allow the material of indenter to recover from the any effects from consecutive indentations.

5.3.5 Data Acquisition

Every data of instantaneous time, indentaion loads and indentaion depths were recorded starting from the time when the indenter first touched the smooth surface of the samples until the last second when it completely left the samples with the dents behind.

5.4 Data Analysis

The instantaneous data of indentation force and depth were extracted and plotted out of which one–fourth portion of the unloading data was curve fitted with a power law (Figure 5.11). The slope of the curve at the start of unloading was calculated as the contact stiffness of the specimen materials by taking the first order derivative of load function obtained for unloading curve with respect to the indentation depth:

$$S = \frac{dP}{dh}_{h=h_{max}} = m\,\alpha\,(h_{max} - h_f)^{\,m-1} \qquad (5.1)$$

Where, h_{max} represents the depth of indentaion at the start of unloading process, and h_f represents the depth of indentaion still left after the elastic recovery of the specimen.

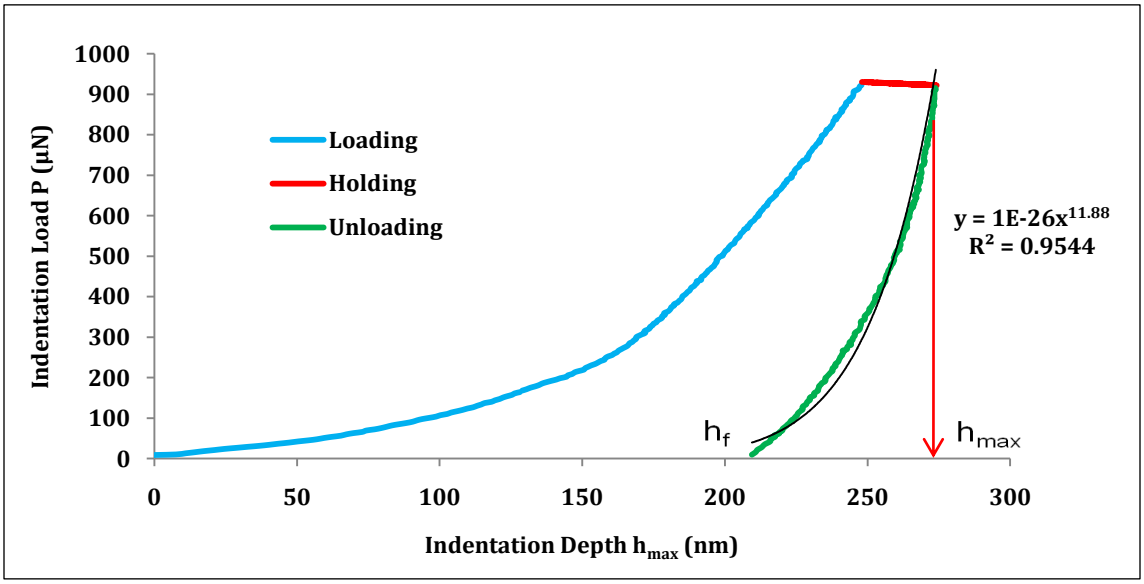

Figure 5.11 Load-Indentation Depth Profile in Nanoindentation

The projected area of indentation was calculated from the function of the contact depth h_c and the six coefficients obtained during the calibration as follows:

$$A_{(h_c)} = \sum_{n=0}^{6} C_n \, x \, h_c^{\,2-n} \qquad (5.2)$$

The contact depth was determined from its relation with the maximum indentation depth, h_{max}, the sink-in depth h_s, contact stiffness S, indenter constant, ε and the maximum force applied at the start of unloading curve, P_{max} as follows:

$$h_c = h_{max} - h_s \qquad (5.3)$$

$$h_s = \varepsilon \, x \, \frac{P_{max}}{S} \qquad (5.4)$$

Where, the geometric constant, ε is equal to 0.75 for a Berkovich indenter. The effective modulus of the material due to the deformation in the indenter and the specimen was then calculated by the following relation where the correction factor β was taken as 1.05:

$$E_r = \frac{1}{\beta} x \frac{\sqrt{\pi}}{2} x \frac{S}{\sqrt{A}} \quad (5.5)$$

With the known values of Young's modulus of elasticity, E_i and Poisson's ratio, ν_i of indenter material and the effective modulus of elasticity, E_r and Poisson's ratio, ν_s of specimen material, the elastic modulus of specimen material was calculated from the equation (5.6) derived by assuming the indenter and the specimen in series combination without any adhesion and slippage in between them.

$$E_s = \frac{1-\nu_s^2}{\frac{1}{E_r} - \frac{1-\nu_i^2}{E_i}} \quad (5.6)$$

In this study, the elastic modulus of 1141 G Pa and Poisson's ratio of 0.07 were used for the Berkovich indenter made of diamond as per the literature (Bei et al., 2004; Shen and Tang, 2009). Similarly, the Poisson's ratio of aggregates in asphalt concrete mixtures was assumed as 0.15. The same process of data analysis was followed for each indentation to determine the elastic modulus of limestone sample and the aggregates in asphalt concrete samples.

5.5 Results

When the deformation of the indenter is small enough, the reduced modulus of elasticity can be taken as the elastic modulus of the sample. Considering that there was no deformation in the diamond indenter, the nine nanoindentation tests of limestone sample under the trapezoidal loading sequence of loading, holding and unloading with peak value of 2000 μN gave an average value of 68.0 G Pa ± 10.3 G Pa with an standard error of 15.1%.

Similarly, out of the thirty indents performed again in the same sample of limestone, the modulus values from three of them were too low. These values can be attributed to the surface imperfections of limestone at local points. Excluding these outliers, the remaining values gave an average elastic modulus of 65.3 G Pa ± 7.0 G Pa with standard error of 10.7 %. The single indentation done in the same sample with a peak load of 5000 μN gave 67.0 G Pa as its elastic modulus. When all these values were considered, the modulus values averaged to 66.0 G Pa ± 7.9 G Pa with standard error of 12.0%. The residual impressions in the limestone sample are shown below in Figure 5.12 at different levels of magnifications.

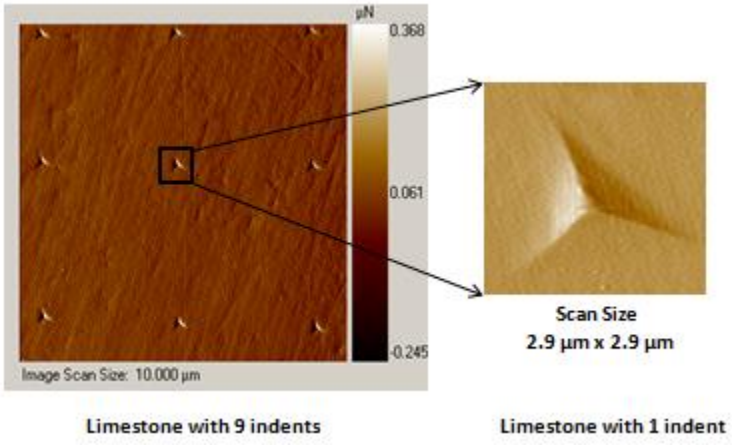

Figure 5.12 Images of Residual Indentations

When the deformation of diamond indenter was taken into consideration, the elastic modulus of limestone increased to 70.6 G Pa ± 11.4 G Pa with standard error of 16.1% for the set of nine indents, 67.6 G Pa ± 7.6 G Pa with standard error of 11.3% for the set of twenty nine indents, 69.4 G Pa for the single indent, and 68.4 G Pa ± 8.7 G Pa with standard error of 12.7% for all the forty indents (Figure 5.13).

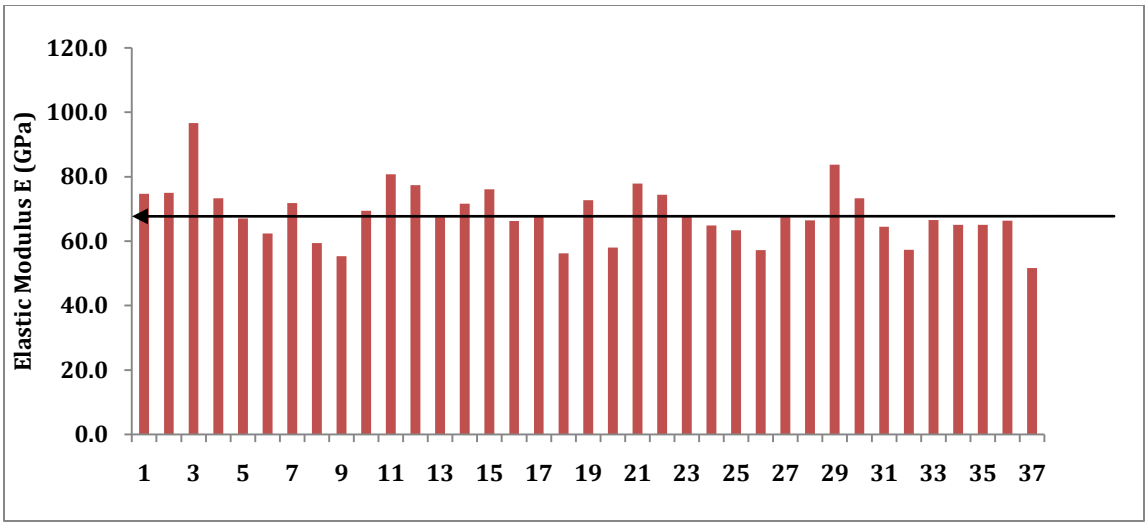

Figure 5.13 Results of Nanoindentation Tests in Limestone

The nanoindentation tests thus gave consistent values of elastic modulus for a number of indentations within a short period of time, clearly signifying that the test method can be applied in determining the elasticity of aggregates of unknown mineralogy like those used in asphalt concrete mixtures.

Out of the fifty two indentations assigned in asphalt concrete samples, only forty three tests were successfully completed. The other nine indents could not be completed because of the excessive values of indentation depths that were not allowed by the machine for safety reasons. The successful forty three indentations were still statistically significant to conclude that the nanoindentation tests can be conducted in asphalt concrete samples and that there is a high degree of heterogeneity in them which should be dealt with while deciding the elastic properties of aggregates and fine aggregate matrix.

A simple illustration of the heterogeneity is provided by Figure 5.14.

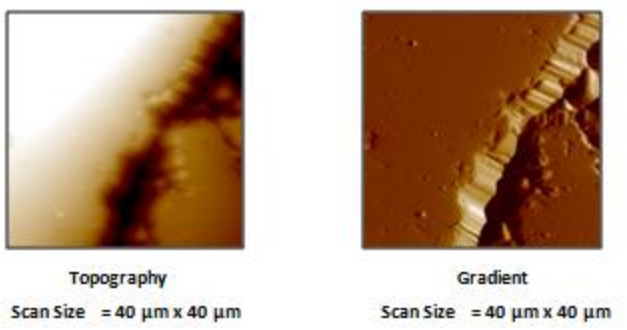

Figure 5.14 Topography and Gradients of AC Samples

It was also observed that some values of elastic modulus were as low as 0.4 G Pa and some were as high as 84 G Pa (Figure 5.15).

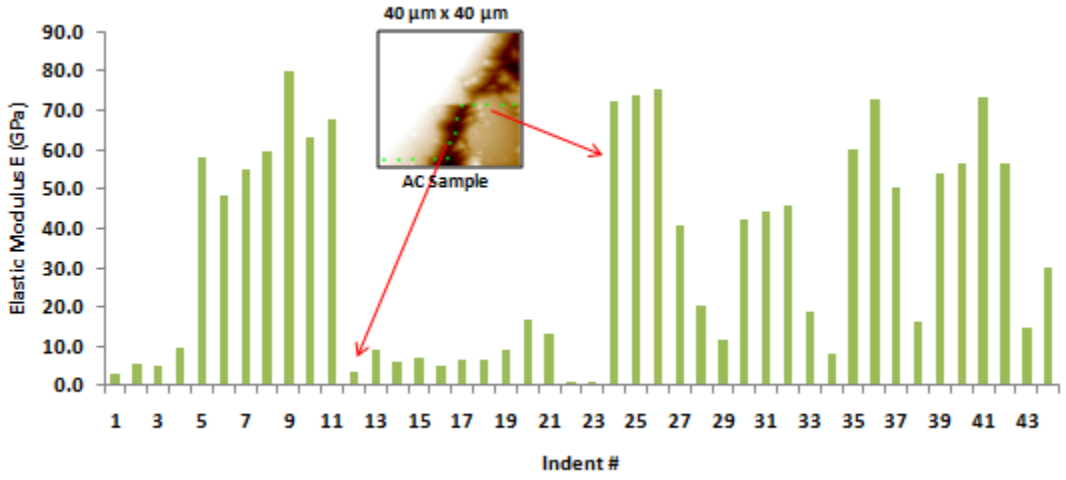

Figure 5.15 Results of Nanoindentation Tests in AC Samples

Based on the properties of fine aggregate matrix and the location of indentations, the lower values were close to the short term relaxation modulus values of fine aggregate matrix mixtures of binder and fine aggregates. This can be explained by the fact that when the indenter was loading or unloading in a fine aggregate floating on binder substrate, there was a combined effect and a resultant modulus which refers to the property of fine aggregate matrix, but not merely of the aggregates. Similarly, when the indenter pushes a very fine aggregate floating on binder, there are chances of the indenter

either reaching the binder by piercing through it or pushing the aggregate down into the binder with very small dents in them. There are also chances of aggregates being toppled in the binder due to some cantilever effect or chances of obliquely indenting some part in binder and some part in aggregates. All of these cases can give the combined effect of binder and fine aggregates which ultimately refer to the property of fine aggregate matrix discussed in chapter four. In these cases, massive sink-ins and pile-ups are possible while loading and unloading the indenter. So the indents that were targeted only in the aggregates were chosen for determining the average value of elastic modulus for the aggregates. The calculation gave an average value of 60.9 G Pa whose details are discussed in chapter seven.

CHAPTER SIX

COMPUTATIONAL CHARACTERIZATION OF ASPHALT CONCRETE MIXTURES

6.1 Sampling

The same asphalt concrete samples which were used in the laboratory tests of dynamic modulus were selected for determining the dynamic modulus using the computational micromechanics model based on finite element method in commercially available software, Abaqus 2008. The 150 mm long and 100 mm diameter cylindrical samples of asphalt concrete mixtures were cut into two halves along the diametric plane with a diamond saw machine in order to expose two 150 mm x 100 mm rectangular surfaces.

6.2 Sample Preparation

6.2.1 Digital Scanning

The clean and dry 150 mm x 100 mm rectangular surfaces of the asphalt concrete samples were digitally scanned at a resolution of 100 pixels per inch with the help of a regular scanner. A pixel is defined as the smallest unit of square shape with same lengths in each edge. With 100 DPI, each dot or pixel measured 0.25 mm x 0.25 mm in size.

6.2.2 Image Treatment

The scanned images of the asphalt concrete specimens also captured some air voids along the edges while cutting the samples. To avoid these voids, the images were cropped to a length of 135 mm and a breadth of 90 mm from their sides (Figure 6.1.a). The resultant size was larger than the minimum size of representative volume element (RVE) which Kim et al. (2010) defined to be at least 60 mm x 60 mm.

The two dimensional original gray images of asphalt concrete samples were then converted into black and white images by defining a threshold to identify aggregates and fine aggregate matrix (Figure 6.1.b). Each aggregate area was converted into elements with a number of white pixels. Likewise, the fine aggregate matrix phase was converted into black pixels. When the scanned and cropped gray images were compared with the black and white images one to one, a number of aggregate areas were found undistinguishable because of their merger, which was not the case in real samples.

Also contrary to the real samples, a number of white and black dots were observed inside the regions of fine aggregate matrix and aggregates respectively. Thin black lines were drawn between the aggregate areas to separate them. Similarly, the white or black dots which did not represent any aggregates or binder in asphalt concrete mixtures were treated with opposite colors correspondingly. The black and white boundary treatment was done keeping in mind not to violate the gradation, orientation, location, and the volume fraction of aggregates (Figure 6.1.c)

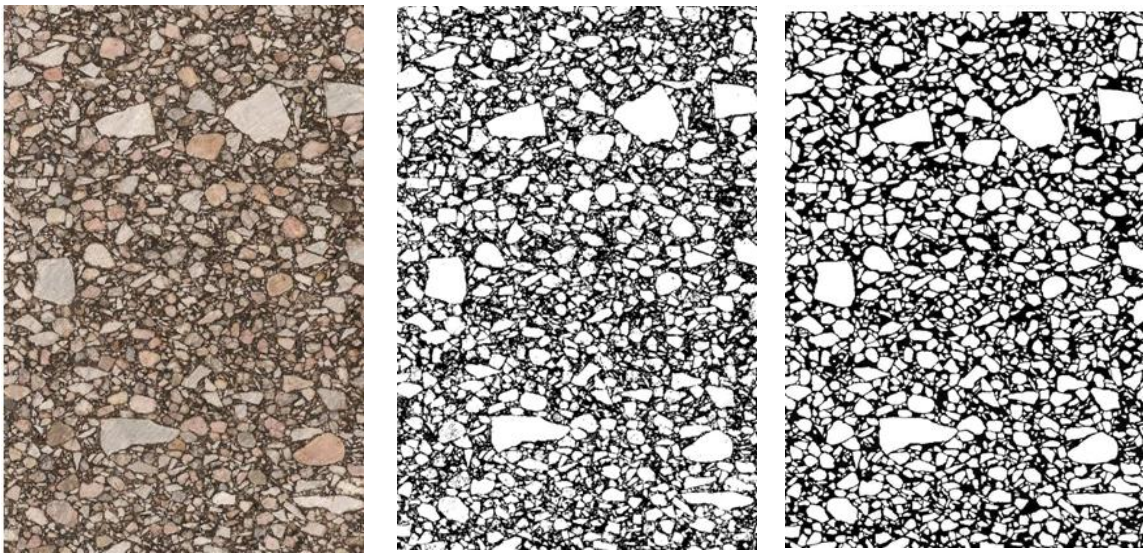

Figure 6.1 Image Treatment for (a) Scanning (b) Black and White (c) Boundary

6.2.3 Image Analysis

Finally, the boundary treated images were analyzed for their gradation in terms of area using the same process of gradation analysis as done in terms of weight. The sieve size to which a particular aggregate belonged to was determined based on the length of minor axis of that aggregate, and its area was used for determining the percentage passing or retained on that particular sieve. Along with the length of the minor axis and area of each aggregate, other geometric parameters like coordinate locations, angles of major and minor axes, length of major axis, etc. were also determined to account for other properties like orientation, percentage of flat and elongation, etc.

Sieve analysis was carried out using a 0.45 power FHWA graph in which the cumulative passing percentage in each sieve by total area of aggregates was X-axis and the 0.45 power of corresponding sieve size was plotted in Y-axis. The gradation analysis showed negligible amount of aggregates passed though sieve number 16. It referred to the fact that the black phase in asphalt mixture microstructure constituted binder and fine aggregates less than 1.19 mm in size and represented the fine aggregate matrix phase of asphalt mixtures. Along with the gradation, the area fraction of aggregates and fine aggregate matrix was also determined to check whether they were in par with the volume fraction as used in the volumetric design of the three dimensional samples. However, the gradation and weight fraction of the two dimensional images were not expected to be the same as the cylindrical samples of asphalt concrete mixtures.

6.2.4 Finite Element Mesh Generation

The image files were then converted into text files which converted pixels into the numbers 0 and 255; the number 0 represented the black phase of fine aggregate matrix and the number 255 represented the white phase of aggregate. With 0s and 255s, the input files were created for the computational finite element software Abaqus 2008 using the node configuration code. The code assigned a node number to each of the 0s and 255s keeping them at a distance of 0.25 mm from each other, hence creating a 90 mm x 135 mm two-dimensional two-phase geometry. The geometry comprised of the elements of fine aggregate matrix phase with nodes from 0s and the aggregate phase with nodes from 255s. For one of the samples, all together 195301 nodes were created by using triangular elements for the meshing. The total number of triangular elements in the final mesh of the FAM phase was 141710 which was 36.4 % by total area of the sample; the rest 63.4 % was occupied by 247090 elements of coarse aggregates.

6.3. FEM Simulations of Dynamic Modulus Tests

6.3.1 Material Properties

The two dimensional digital image of asphalt concrete illustrated a heterogeneous mixture of two distinct materials – the coarse aggregate phase and the FAM phase. The aggregate phase was considered isotropic, homogeneous and elastic, and assigned with an average elastic modulus value of 60.9 G Pa obtained from their nanoindentation tests and a Poisson's ratio of 0.15 obtained from literature (Barksdale, 1993).

Similarly, the fine aggregate matrix phase was considered isotropic, homogeneous and viscoelastic and assigned with the normalized Prony series coefficients obtained from

oscillatory torsional shear tests at 23^{o}C. There were eight values of the coefficients g_i and τ_i in Prony Series function of shear modulus and same number of k_i in bulk modulus along with the short term and long term relaxation modulus E_o, E_∞. A Poisson's ratio of 0.35 was assumed for asphalt concrete mixtures to account for the lateral strains assuming the ratio between lateral and axial strains does not change with time. Considering no influence of bulk moduli in two dimensional simulations, they were taken as zeros.

6.3.2 Boundary Conditions

Both displacement (U) and traction (T) boundary conditions were applied. The top boundary was loaded with haversine traction in vertical direction without any traction in horizontal direction. The bottom boundary was fixed against any displacement in vertical direction and without any traction in horizontal direction. The left and right boundaries were allowed to move in both vertical and horizontal directions without any traction.

Top Boundary ($0 \leq x \leq 90$, $y = 135$);

$$T_x = 0 \tag{6.1}$$

$$T_y = -0.05(1 - \mathrm{Cos}(2\pi ft)) \tag{6.2}$$

Bottom Boundary ($0 \leq x \leq 90$, $y = 0$);

$$T_x = 0 \tag{6.3}$$

$$U_y = 0 \tag{6.4}$$

Left Boundary ($0 \leq y \leq 135$, $x = 0$) and Right Boundary ($0 \leq y \leq 135$, $x = 90$);

$$T_x = 0 \tag{6.5}$$

$$T_y = 0 \tag{6.6}$$

The traction and displacement boundary conditions are illustrated in Figure 6.2.

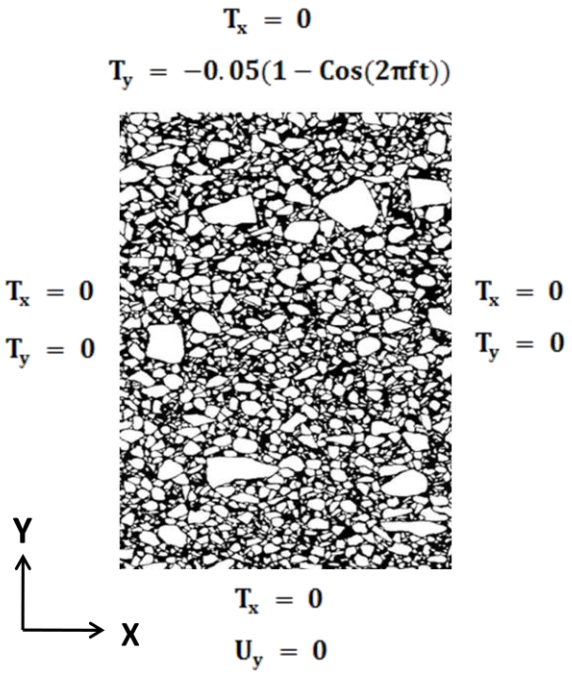

Figure 6.2 Boundary Conditions for FEM Test Simulations

6.3.3 Load Profile

A haversine uniaxial compressive force with amplitude of 1 N was assigned at each element of top boundary of the samples in par with the uniform load applied on the top of asphalt concrete samples in experimental dynamic modulus tests. A total of five cycles were run for each of the nine frequencies 0.0001, 0.001, 0.01, 0.1, 1.0, 10, 100, 1000, 10000. The input and the output signal are illustrated in Figure 6.3.

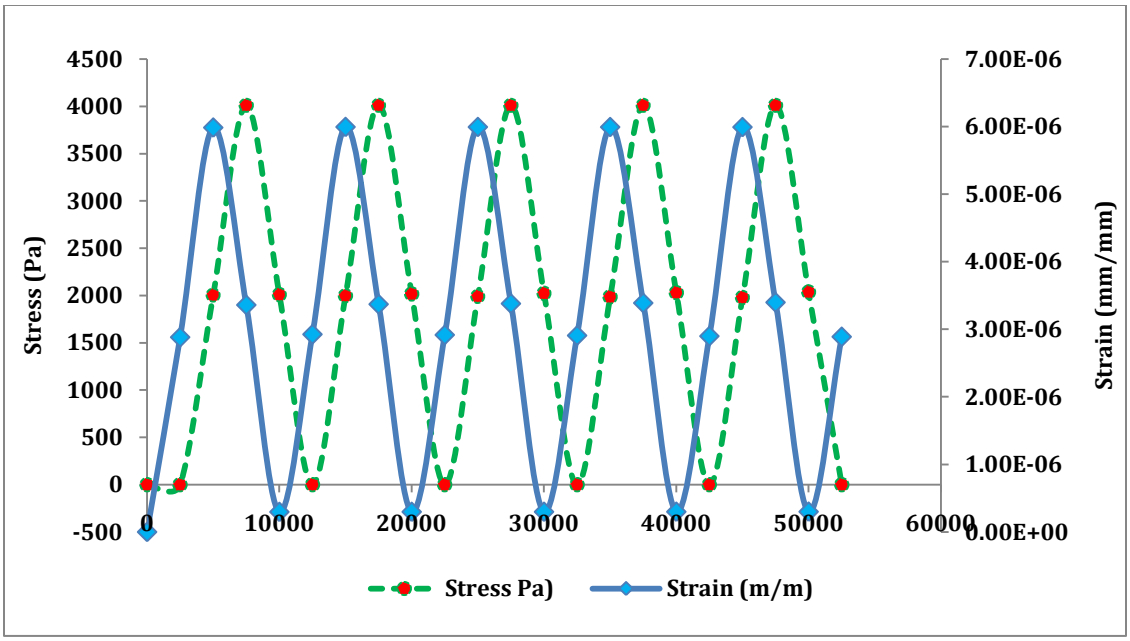

Figure 6.3 Input and Output Signals of FEM Test Simulations

6.3.4 Test Execution

Then the tests were conducted at nine different frequencies each of which took around forty minutes. The tests were repeated for all five types of fine aggregate matrix without changing the aggregate property.

6.3.5 Data Acquisition

Four replicate gage points 9 mm x 9 mm were virtually installed in the finite element mesh at four locations, each with 1389 nodes (Figure 6.4). The centre to centre distance of gage points were kept 100 mm in the vertical and 33 mm in the horizontal. The areas of the gage points were also kept as same as that of the real gage points used in laboratory tests. A total number of four data points were assigned to be extracted for each cycle along with one extra in the initial condition and one more after the fifth cycle, hence totaling a set of 22 data points.

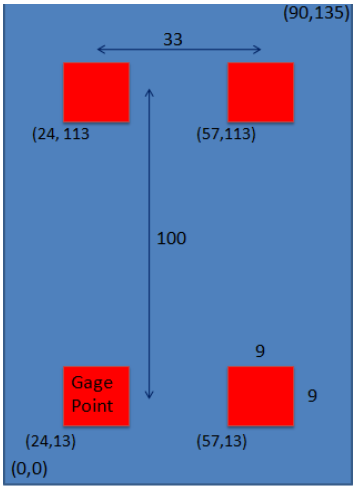

Figure 6.4 Virtual Measuring Gages in FEM Test Sample

For each element on the top boundary, instantaneous vertical stress values were requested over the total test period from the Abaqus 2008 software. Similarly, for each node in the virtually installed four gage points, the displacements in vertical direction were requested over the total test period.

6.4 Data Analysis

The stresses at each element on the top boundary and the displacements of each node of the gage points were averaged separately to determine average stress at the top surface and displacement of each gage point as follows:

$$\sigma = \sum_{i=1}^{m} S22_i \tag{6.7}$$

$$U2_{Gage} = \sum_{i=1}^{n} U2_i \tag{6.8}$$

Where, $S22_i$ represents the vertical stress for i^{th} element out of m elements in the top surface, and $U2_i$ represents the vertical stress for i^{th} node out of n nodes in the gage points. The changes in distance between the top and the bottom gages were then

calculated by subtracting the average vertical displacement of bottom gage from that of top gage as in equation 6.9.

$$\Delta U2 = U2_{Top} - U2_{Bottom} \quad (6.9)$$

The average change in distances between top left and bottom left and between top right and bottom right gage points was converted into strain by dividing it by the initial distance L of 100 mm as given by equation 6.10.

$$\varepsilon = \frac{\Delta U2}{L} \quad (6.10)$$

The dynamic modulus was finally determined by dividing the amplitude of stress by the amplitude of strain observed in the five cycles of loading at each frequency as shown in equation 6.11.

$$|E^*| = \frac{\sigma_0}{\varepsilon_0} \quad (6.11)$$

The dynamic modulus values for each frequency were then plotted in angular frequency domain to give a characteristic master curve.

6.5 Results

6.5.1 Characteristics of AC Microstructure

The areas occupied by aggregates of each sieve sizes were calculated and analyzed for their percentage in the total mixtures. The sieve analysis of aggregates was conducted using the same procedure as used in sieve analysis of aggregates by percent weight. The sieve analysis results are tabulated in Table 6.1 for comparison purposes.

Table 6.1 Sieve Analysis of Aggregate by Area and Weight

Sieve			Cumulative Passing %			
			Two Dimensions	Three Dimensions		
Size #	Size (mm)	Sieve$^{0.45}$	AC w/o FAM - by Imaging	AC w/o FAM by Weight	Maximum Density Line	AC with FAM - by Weight
3/4"	19.00	3.76	98.1	100.0	100.0	100.0
1/2"	12.70	3.14	95.7	83.4	93.7	95.0
3/8"	9.51	2.76	82.9	73.2	86.1	89.0
4	4.76	2.02	45.7	53.6	64.6	72.0
8	2.38	1.48	15.5	39.3	19.0	36.0
16	1.19	1.08	5.8	28.7	0.0	21.0
30	0.60	0.79	1.2	21.0	0.0	14.0
50	0.30	0.58	0.1	15.4	0.0	10.0
100	0.15	0.43	0.1	11.3	0.0	7.0
200	0.08	0.31	0.0	8.3	0.0	3.5

Since these calculations were based on two dimensional image of the sample, it was well understood that there should not be one to one comparison of gradation of the three dimensional sample. Having said that, there should still be a correlation between the area fractions of fine aggregate matrix and the coarse aggregate phases similar to, but might not be equal to, their volume fraction in three dimensional samples.

It is obvious from Table 6.1 and Figure 6.5 that the percentage of aggregates passing through 1.19 mm sieve were captured the least. This signifies that 1.19 mm was the maximum size of aggregates in fine aggregate matrix phase of asphalt concrete mixtures.

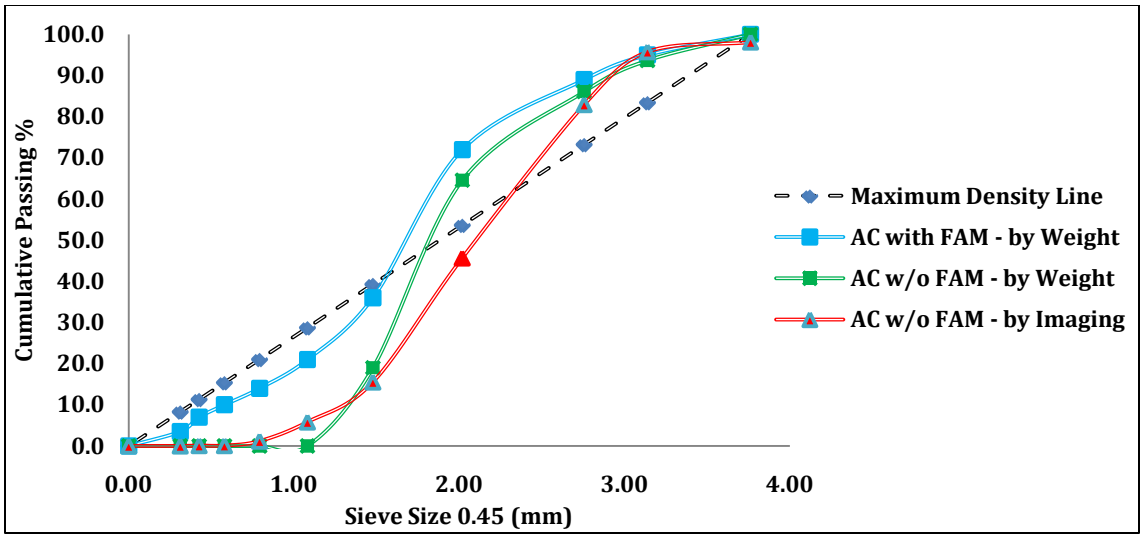

Figure 6.5 Sieve Analysis by Aggregates by Areas and Weights

6.5.2 Dynamic Modulus Tests

The dynamic moduli of the asphalt concrete samples at 23°C were determined as described above and the results were plotted. The master curves obtained for the asphalt concrete mixtures containing the fine aggregate matrix with different density levels are shown in Figure 6.6.

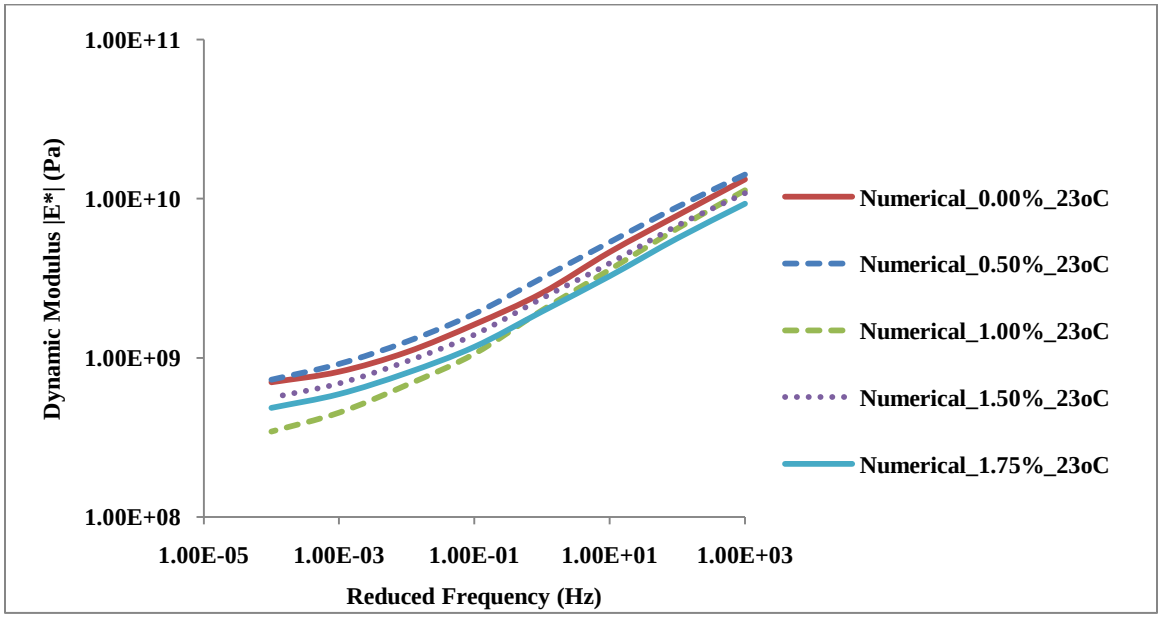

Figure 6.6 Master Curves of Dynamic Modulus from Simulations

As shown in Figure 6.6, the dynamic modulus values increased with the increase in loading frequency at a constant temperature and vice versa, illustrating the rate dependency of asphalt concrete mixtures. The figure also illustrates that stiffness of asphalt concrete increases with the decrease in air voids signifying the sensitivity of stiffness with volumetric and parametric properties of its components.

It is also obvious that FEM simulations can be used to construct a master curve of dynamic modulus of bituminous composites over a wide range of frequency including very fast and very slow loading rates.

CHAPTER SEVEN

RESULTS AND DISCUSSIONS

7.1 Results from Experimental Characterization of Asphalt Concrete Mixtures

In spite of the same mix design, fabrication and test procedures, there were still some deviations in dynamic modulus values of asphalt concrete mixtures (Figure7.1). These deviations were the results of accumulation of small but unavoidable errors in each steps of sample fabrication, testing and as well as sample to sample variations such as the orientations of the aggregates, the distributions of fine aggregate matrix mixtures, heterogeneity, etc. This is one of the reasons why the laboratory tests should be replaced with more repeatable, cheaper and faster method of predicting dynamic modulus.

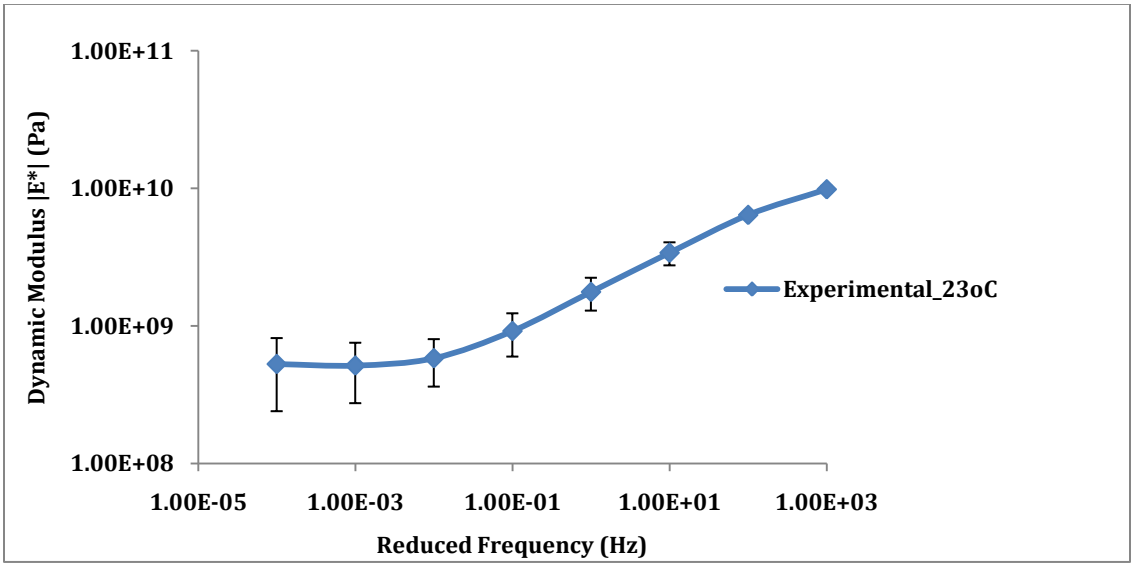

Figure 7.1 Master Curve of Dynamic Modulus of Mixtures from Tests

The lower part of the master curve related to the higher standard deviations was obtained by shifting the dynamic modulus test curves at high temperatures towards the curve at

reference temperature. At high temperatures, such tendency of sample to sample variations is usual for heterogeneous samples of asphalt concrete.

7.2 Results from Experimental Characterization of Fine Aggregate Matrix Mixtures

7.2.1 Properties at the Different Locations of SGC Matrix Samples

The dynamic modulus of fine aggregate matrix torsional bars extracted from different locations of the Superpave gyratory compacted FAM mixtures were compared with each other to determine whether there was different level of air voids at different locations of SGC samples. This check was also conducted to decide whether fine aggregate matrix was compacted uniformly. For this check, the master curves of dynamic shear modulus for the five FAM torsional bars from the circumferential region and those for other five from central region were compared one to one. Figure 7.2 illustrates a comparison of master curve of dynamic modulus of the fine aggregate matrix samples extracted from different locations of SGC matrix sample with same air void content of 0.00 % by volume.

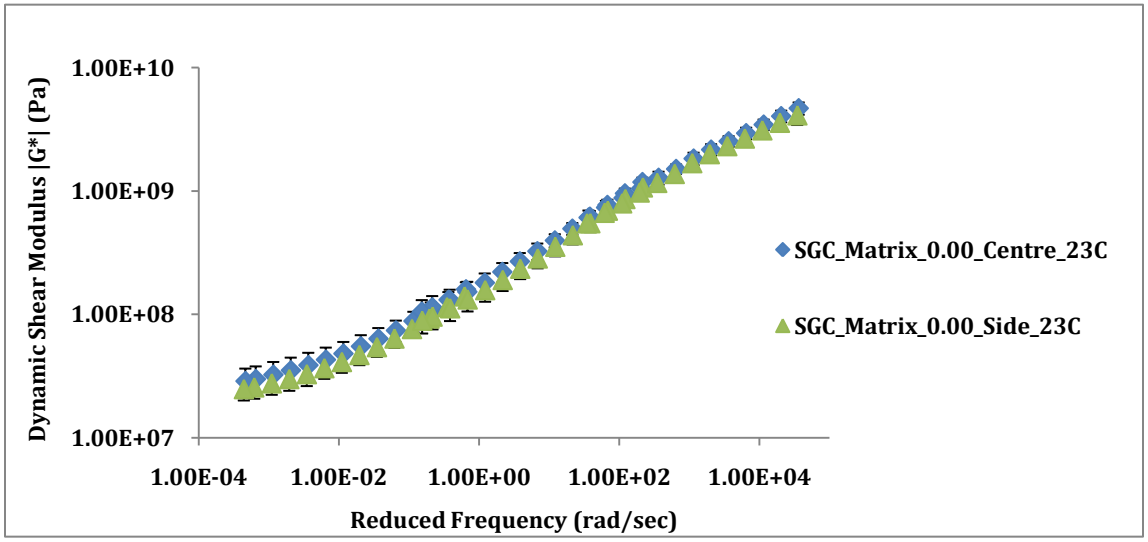

Figure 7.2 Comparison of Compaction of FAM with 0.00 % Air Voids

A small discrepancy was found in between the dynamic modulus of torsional bars extracted from the central and the circumferential regions of SGC FAM samples. This difference was less than standard deviations of the samples a particular region, and thus ignored, which signified the same level of compaction in all locations of the SGC samples. Similar observation could be made with the master curves of SGC FAM samples with 1.75 % air voids (Figure 7.3).

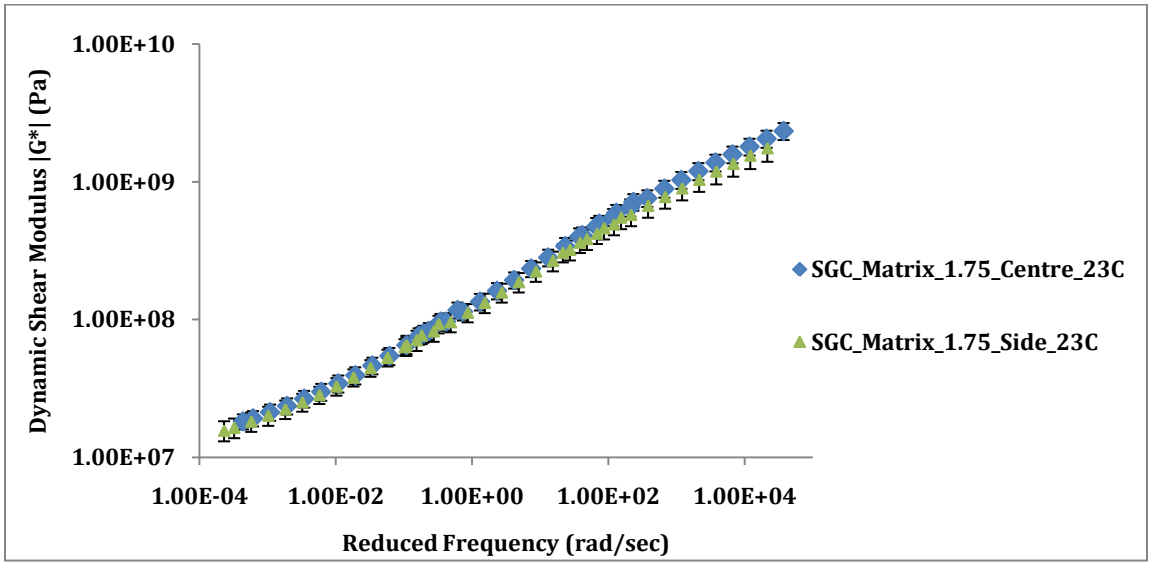

Figure 7.3 Comparison of Compaction of FAM with 1.75 % Air Voids

Because of the same compaction level of FAM mixtures with Superpave gyratory compactor, all the torsional bars extracted from the two regions of SGC FAM specimens were tested and averaged for the representative properties.

7.2.2 Properties of Different Types of SGC Matrix Samples

Based on earlier discussion, the discrepancy between the properties of the central and the circumferential region of Superpave gyratory compacted samples were ignored and average of dynamic shear modulus of all ten samples were selected for comparison. It

was expected that the samples with lower air void content would be stiffer than the samples with higher air void content. The master curves of dynamic modulus of the five different types of fine aggregate matrix exhibit the same trend as expected. The master curves of average dynamic shear modulus of ten samples of each type of SGC fine aggregate matrix mixtures at 23^{o}C are shown in Figure 7.4.

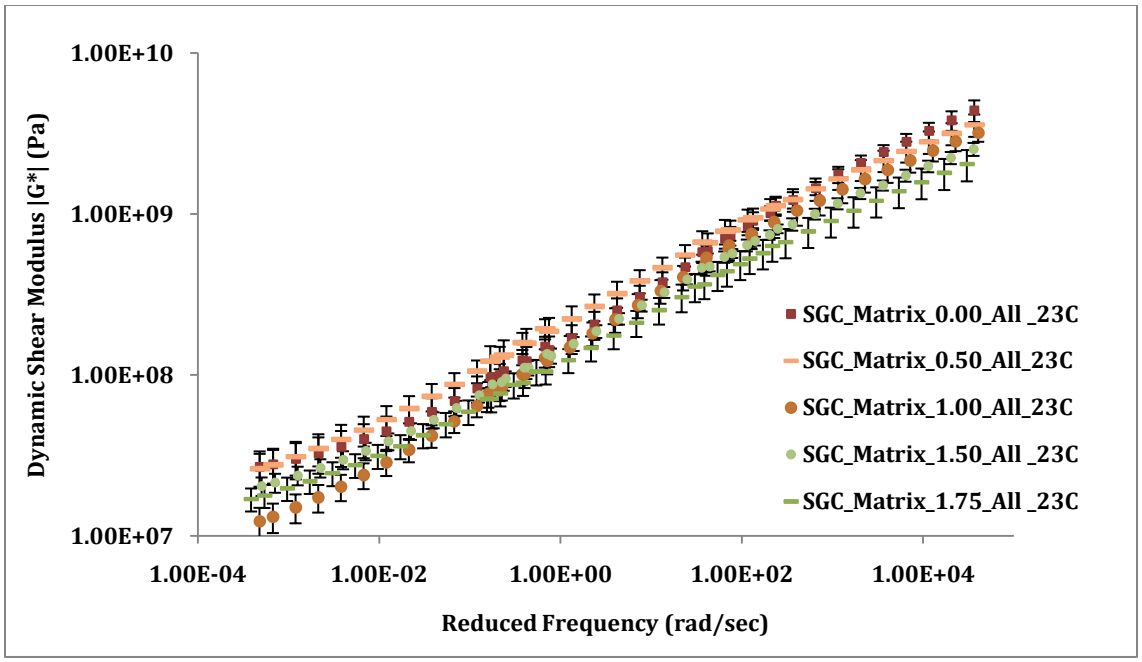

Figure 7.4 Comparison of Dynamic Modulus of Different Types of Matrix

Figure 7.4 shows that the stiffness of the FAM mixtures increased with the decrease in air voids and decreased with the increase in air void content. In other words, the denser the material, the higher was the stiffness. The Superpave gyratory compacted FAM mixtures with 1.75 % air voids had the lowest stiffness and those with 0.00 % had the highest stiffness; the stiffnesses of other three types were inside this range.

Again, the average values of the dynamic modulus at 50 radians per second and 23^{o}C were extracted from the master curves of the torsional samples of all five types of SGC FAM samples extracted from two regions. Figure 7.5 illustrates the difference between

the properties the samples from circumferential and central regions of the SGC samples at 50 rad. / seconds at 23^{o}C and also exhibits the change when all samples were considered.

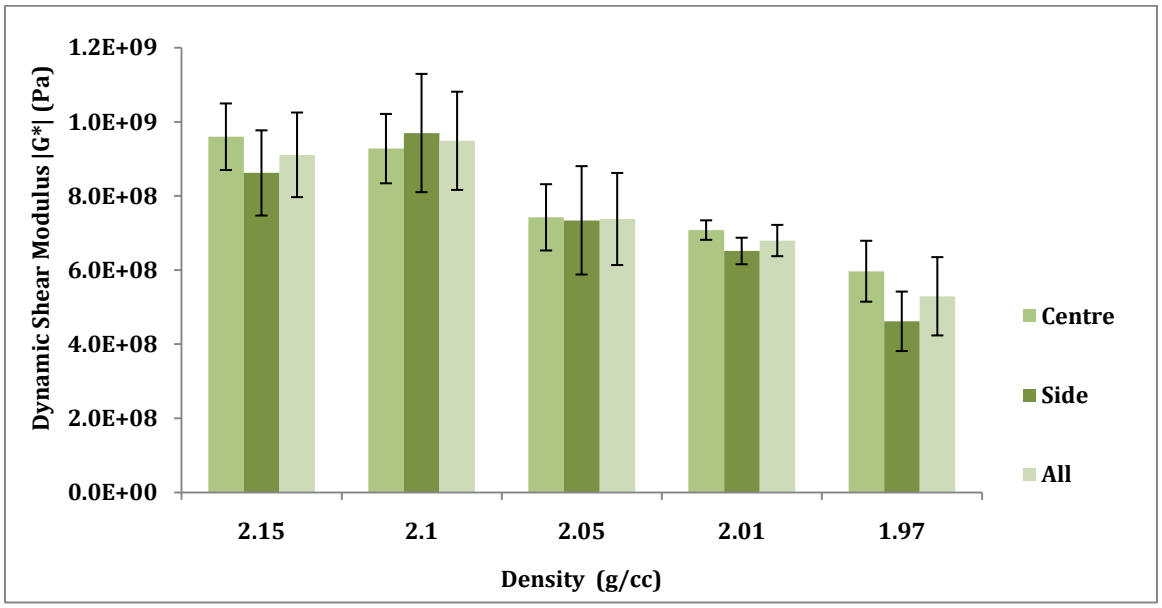

Figure 7.5 Comparison of Stiffness of Different Types of Matrix @ 50 rad. / sec

The comparison reconfirms that the stiffness of SGC FAM mixtures depends on the density and the air void content in them. There is an increase of standard deviations with the increase of air void content or the decrease of density, and vice versa. Similarly, the deviations are a bit higher for the circumferential samples than those for central samples, but still they are ignorable.

7.3 Results from Experimental Characterization of Aggregates

First, the effect of Poisson's ratio of the indenter in the elastic modulus of test samples was studied. The study showed that the elastic modulus is not affected a lot by the change of Poisson's ratio value. With a 0.12 value of Poisson's ratio, the average elastic modulus value from forty indents in limestone sample was determined as 69.1 G Pa ± 8.8 G Pa

with standard error of 12.7%. With 0.18 value of Poisson's ratio, the elastic modulus value changed into 67.9 G Pa ± 8.6 G Pa with same standard error of 12.7%. There was no more than 0.8 G Pa which is a very small value in comparison to the average elastic modulus value. Thus choosing a 0.15 value of Poisson's ratio, the average value of 68.6 G Pa ± 8.7 G Pa was determined for the Young's modulus of elasticity of limestone with a standard error of 12.7%.

Based on the recommendations of Aragão et al. (2010) to perform the experiments to determine the elastic modulus of aggregates rather than depending on literature, nanoindentation tests were performed in asphalt concrete samples too. The individual values of nanoindentation tests in the aggregates in two samples of SP4-Special asphalt concrete mixtures were selected and an average value of the elastic modulus of their aggregate phase was determined as 60.9 ± 11.2 G Pa (Figure 7.6).

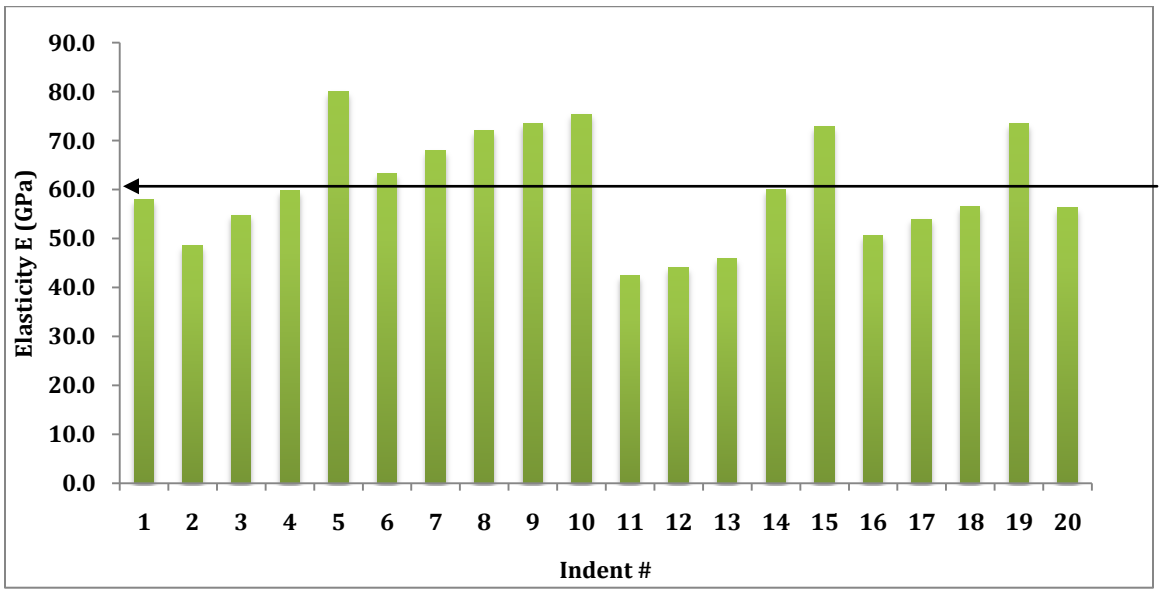

Figure 7.6 Elastic Modulus Values of Aggregates in AC Mixtures

7.4 Results from Computational Characterization of Asphalt Concrete Mixtures

The same samples used in dynamic modulus tests were used to generate the mesh required for FEM simulations of those tests. The master curves of dynamic modulus obtained from FEM simulations for the asphalt concrete mixtures, which contained the two extreme cases of air void contents in this study, are compared in Figure 7.7.

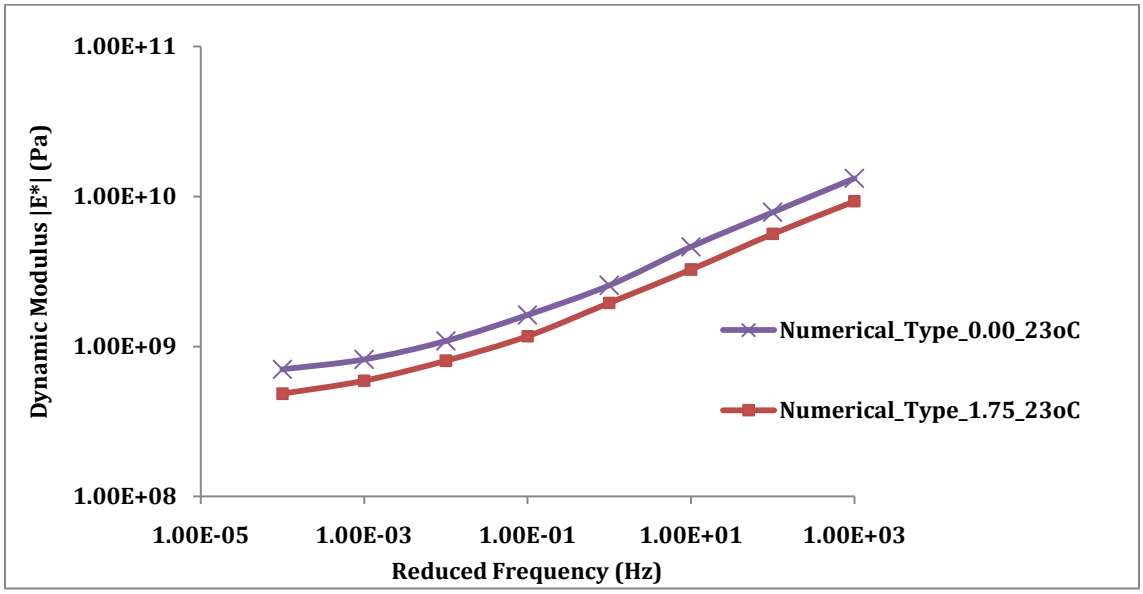

Figure 7.7 Dynamic Moduli from FEM Simulations: V a = 0.00%, 1.75%

It is obvious from above Figure 7.7 that the stiffness of FAM mixtures increases with increase in loading rate and decreases with decrease in loading rate in a similar trend as shown by stiffness in the laboratory tests. Similarly, with the increase in air void contents, the simulation results show an increase in the stiffness as observed earlier in the case of fine aggregate matrix mixtures. The simulations were performed at several frequencies comprising very low and high frequencies, even at those frequencies which are practically hard to achieve in the laboratory.

7.5 Comparison between Experimental Method and Computational Model

The master curves for the dynamic modulus obtained from the experimentation and FEM simulations were compared one to one for all five combinations of different types of fine aggregate matrix mixtures and aggregates in order to identify the particular value of air void content in fine aggregate matrix which when used in numerical simulation would give the best match with the experimental master curve of asphalt concrete. That particular value of air voids would be the air content in fine aggregate matrix to be fabricated in future. The master curves obtained by the numerical simulations of dynamic modulus tests of all the five types of fine aggregate matrix mixtures and aggregates, and the one obtained by the time-temperature superposition of the dynamic modulus curves obtained by laboratory tests of asphalt concrete mixtures are compared in the following Figure 7.8.

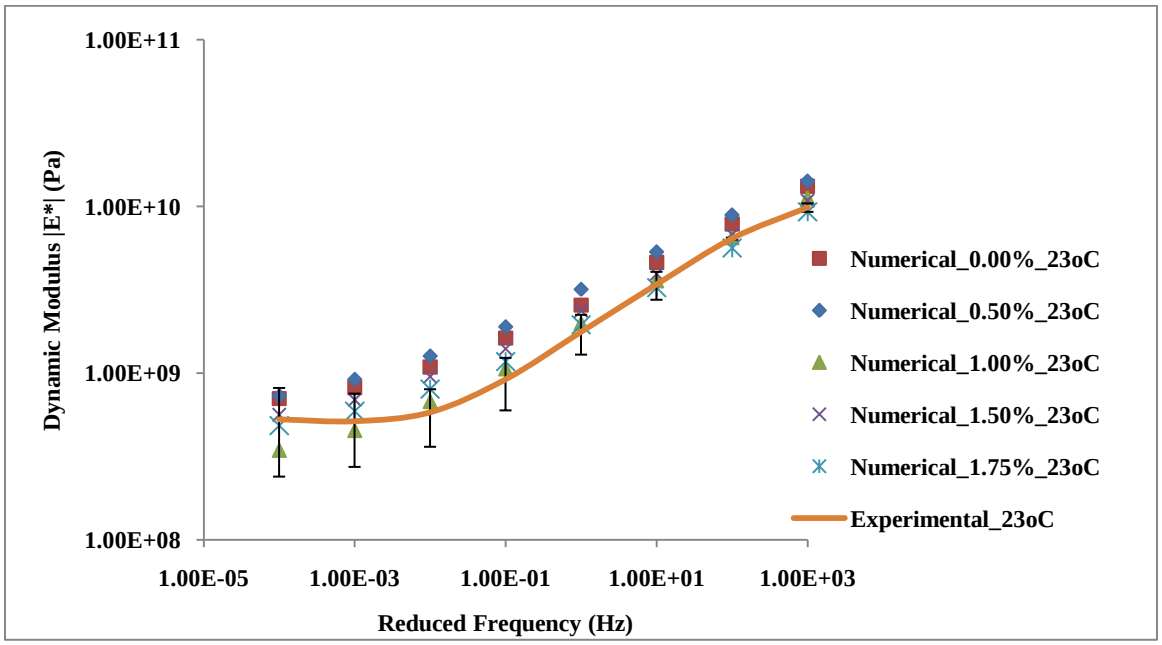

Figure 7.8 Comparison of Stiffness from Tests and FEM Simulations

As shown in Figure 7.8, none of the master curves obtained from FEM simulations converge exactly with experimentally obtained master curve. This can be attributed to the fact that there were many assumptions involved in the computational micromechanics model such as isotropy of the materials, homogeneity of the two phases and a single value of film thickness around coarse aggregates. Similarly, the diffusion of binder through the materials and the influence of pre-existing cracks were not considered. But even with the use of a two- dimensional microstructure, the model could predict the dynamic modulus which was close to the experimentally determined dynamic modulus. Provided a three-dimensional microstructure is used by incorporating the real scenario of individual phases and their interactions, the model can be made more accurate.

The model also suggests that air voids must be considered while simulating the tests with asphalt concrete samples. The simulations with no or low value of air voids were clearly outside the experimental range.

According to AASHTO PP 61, the coefficient of variation for dynamic modulus tests is approximately 13 %. So, it was decided to look for the best combination of fine aggregate matrix and aggregates whose dynamic modulus was inside the envelope of allowable upper and lower limits of experimentally determined dynamic modulus.

The master curves for the allowable lower and the upper limits of experimental values of dynamic modulus and the master curves of each combination of fine aggregate matrix and aggregates are shown in Figure 7.9.

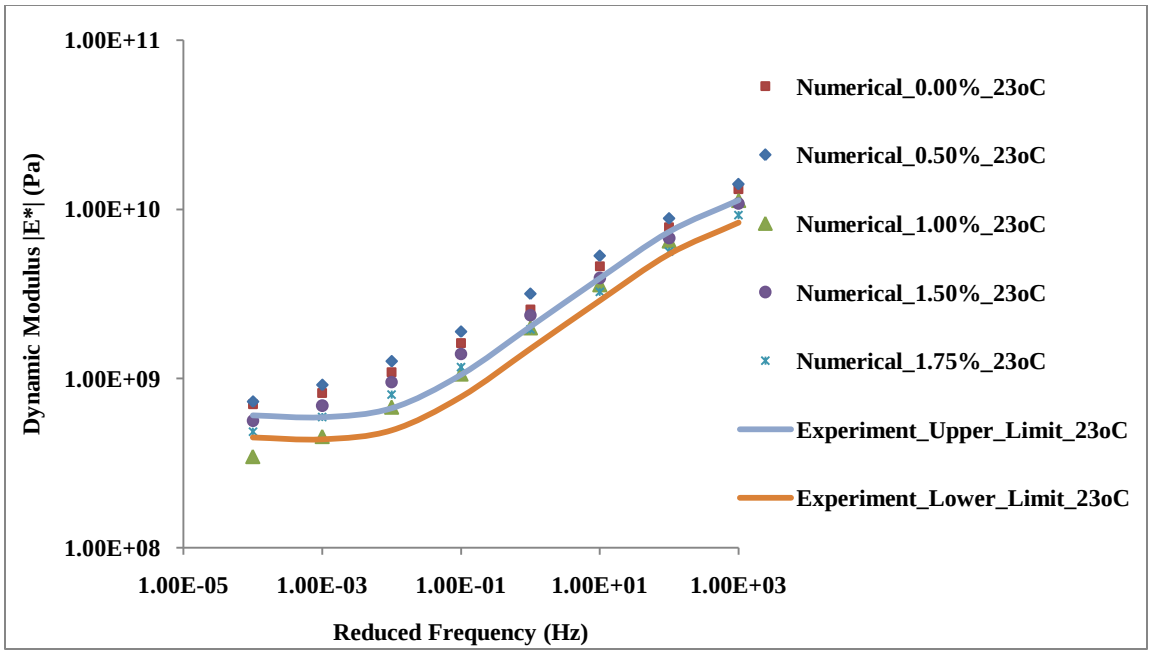

Figure 7.9 Simulation Results within the Allowable Limits of Experimental Results

It is obvious from Figure 7.9 that the master curves of asphalt concrete mixtures containing FAM phases with 1.00-1.75 % air voids were lying more closely in the region bound by the upper and the lower limits of the experimental values of dynamic modulus than the FAM phases with lower level of air voids (0.00 -0.50%). The simulation results with a very low value of air voids such as 0.00 % and 0.50% were clearly outside the experimental range. This fact reconfirms that the model must be incorporated with air voids that account for the air voids in the asphalt concrete mixtures to a certain extent.

CHAPTER EIGHT

CONCLUSIONS AND RECOMMENDATIONS

8.1 Conclusions

This study presented two different methods of determining dynamic modulus of asphalt concrete mixtures at different loading frequencies and temperatures. The first method was based on the laboratory tests of Superpave gyratory compacted asphalt concrete cylindrical samples while the second method was based on the finite element analysis of computational micromechanics model of the same samples.

Dynamic Modulus of asphalt concrete mixtures obtained from FEM simulations and the laboratory tests agreed fairly with each other. The model was able to predict the dynamic modulus of mixtures by using the properties of the fine aggregate matrix phase and the coarse aggregate phase in their microstructure. This observation once again proved that the fine aggregate matrix, but not just the binder, is responsible for viscoelastic properties of asphalt concrete. The results also showed that experimentally determined elastic properties of aggregates are required for predicting the dynamic modulus accurately. Since the master curves of asphalt mixtures containing the fine aggregates matrix with lower air voids (0.00-0.50%) were not so close to the experimentally determined master curve, it is obvious that air voids must be incorporated in the fine aggregate phase to predict the dynamic modulus of asphalt concretes accurately.

The entire process of performing the laboratory tests of dynamic modulus consisted of several steps in sequence from material selection to the data analysis taking almost two weeks for one sample in this study. The tests also required several machines and their accessories for the sample fabrication and the tests in a well-equipped laboratory setting.

In contrary, the dynamic modulus test simulations based on micromechanics computational model took less time, and required fewer steps and machines than the laboratory tests. The construction of a complete master curve by using the computational micromechanics model took just one day in contrast to almost three days of laboratory tests and temperature equilibrium for a single sample. Provided we have a virtually generated representative volume element with enough data base of the properties of its constituents, the computational micromechanics model can be a better, faster and cheaper substitute of the current experimental procedure.

In the due process, a new mix design of fine aggregate matrix was also proposed in this study to produce the fine aggregate matrix mixtures with the same properties of matrix phase of asphalt concrete mixtures with respect to compaction method, compaction density, and air voids. Superpave gyratory compaction was successfully implemented in fabricating the cylindrical fine aggregate matrix samples from which multiple torsional bars were extracted. The small discrepancy of dynamic shear modulus of cylindrical torsional bars extracted from different locations of Superpave gyratory compacted fine aggregate matrix mixtures illustrated the consistent properties irrespective of the locations of the sample extraction. Unlike the dynamic modulus tests of SGC asphalt concrete mixtures, the oscillatory frequency sweep tests of cylindrical bars were faster and more repeatable due to higher degree of homogeneity and smaller size of samples. It took less than two hours to determine the viscoelastic properties of a fine aggregate matrix sample in a dynamic shear rheometer. For the SP4-Special mixtures, an air void content of 1.000-1.75 % was required in fine aggregate matrix to predict the dynamic modulus of HMA mixtures inside the allowable limits of experiments.

Similarly, the workability, repeatability, accuracy and efficiency of using nanoindentation were also established for the asphalt concrete and the aggregate samples. The average elastic modulus of aggregates used in SP4-Special asphalt concrete mixtures in this study was determined as 60.9 G Pa, with a 0.15 value of Poisson's ratio.

The computational micromechanics model; however, could not provide an exact match of the master curve obtained from dynamic modulus tests. This is because the model did not address the issues such as anisotropy and heterogeneity of the fine aggregate matrix and coarse aggregates. Even if the model incorporated heterogeneity by assuming two different phases in the system, the model still ignored the heterogeneity due to different types of aggregates. Similarly, the finite element method used in the computation did not address the issues of pre-existing cracks, cohesive zone, adhesion between the binder and aggregates as well as the diffusion of binder. The model assumed a single value of binder film around all types and sizes of aggregates in contrast to the reality of variable film thickness.

In spite of the limitations of the model, the dynamic modulus values predicted by the model agreed fairly with the dynamic modulus values obtained from experiments. This fact signifies that the model can be more accurate once its limitations are addressed. Once the virtual image generation technique replaces the physical sample fabrication, the model can be faster and cheaper.

8.2 Recommendations

More research should be done with multiple types of asphalt concrete mixtures containing several types and proportions of aggregates and binders. The computational micromechanics should be verified with the asphalt concrete mixtures containing one

type of binder and only one type of aggregates of known properties. The range of air void content of fine aggregate matrix mixtures should be narrowed down by conducting the FEM simulations with multiple samples of the same type of mixtures used in this study.

Unless simpler, faster and cheaper method of obtaining statistically supported values for elastic modulus of aggregates is available, nanoindentation tests should be conducted for extracting the exact values of elastic modulus of aggregates.

The manual treatment of digital image analysis of asphalt concrete mixtures should be replaced with an automatic procedure to reduce the processing time as well as errors. While performing the image treatment, the volume fraction as well as the gradation of aggregates should be taken care of. The image treatment should be modified to identify the different types of aggregates and air voids in the mixtures.

The model should be refined by obtaining the elasticity of each type of aggregates and using them in the computational micromechanics model according to their proportions and distribution. A thorough analysis of influence of thermal drift, initial penetration depth, instrument compliance, indenter geometry, pile-ups, sink-ins, indentation size, surface roughness, tip rounding, residual stress, specimen preparation, etc. in the elastic modulus of aggregates should also be conducted. For the time being, the model should be improved by taking the weighted average of the elastic modulus values of aggregates rather than simple average used in this study.

Similarly, the model should be refined to address the issues such as diffusion, cohesion, adhesion, crack, anisotropy and heterogeneity.

BIBLIOGRAPHY

1. AASHTO PP 60, *Standard Method for Preparation of Cylindrical Performance Test Specimens Using the Superpave Gyratory Compactor (SGC)*
2. AASHTO PP 62-09[1], *Standard Practice for Determining Modulus Master Curves for Hot Mix Asphalt Mixture (HMA)*
3. AASHTO PP 61-09[1,2], *Standard Practice for Determining Modulus Master Curves for Hot Mix Asphalt Mixture Performance tester (AMPT)*
4. AASHTO R 30-02, *Standard Practice for Mixture Conditioning of Hot Mix Asphalt (HMA)*
5. AASHTO R 35-04, *Standard Practice for Superpave Volumetric Design for Hot Mix Asphalt (HMA)*
6. AASHTO T 11, *Standard Method of Test for Materials Finer Than 75 – μm (No. 200) Sieve in Mineral Aggregates by Washing*
7. AASHTO T 166-05, *Standard Method of Test for Bulk Specific Gravity of Compacted Hot-Mix Asphalt Using Saturate Surface-Dry Specimens*
8. AASHTO T 209-05, *Standard Method of Test for Theoretical Maximum Specific Gravity and Density of Hot-Mix Asphalt Paving Mixtures*
9. AASHTO T 312-08, *Standard Practice for Preparing and Determining the Density of Hot Mix Asphalt (HMA) Specimens by Means of the Superpave Gyratory Compactor*
10. AASHTO T 315-08, *Standard Method of Test for Determining the Rheological Properties of Asphalt Binder Using a Dynamic Shear Rheometer (DSR)*
11. AASHTO TP 62-07[1], *Standard Method of Test for Determining Dynamic Modulus*

12. Abbas, A., Masad, E., Papagiannakis, T., and Shenoy, A. (2005), Modeling Asphalt Mastic Stiffness Using Discrete Element Analysis and Micromechanics-Based Modes, *International Journal of Pavement Engineering*, Volume 6, Issue 2, pp. 137-146.

13. Abbas, A., Masad, E., Papagiannakis, T., and Harman, T. (2007), Micromechanics Modeling of the Viscoelastic Behavior of Asphalt Mixtures Using the Discrete-Element Method, *International Journal of Geomechanics*, Volume 7, Issue 2, pp. 131–139.

14. Aboudi, J. (1991), *Mechanics of Composite Materials - A Unified Micromechanics Approach*, Elsevier, New York.

15. Andrei, D., Witczak, M. W., and Mirza, M. W. (1999), Development of A Revised Predictive Model for The Dynamic (Complex) Modulus of Asphalt Mixtures, *NCHRP 1-37A Inter Team Report*, University of Maryland, College Park, MD.

16. Aragão, F. T. S., Lee, J., Kim, Y. R., and Karki, P. (2010), Material - Specific Effects of Hydrated Lime on the Properties and Performance Behavior of Asphalt Mixtures and Asphaltic Pavement, *Journal of Construction and Building Materials*, Volume 24, Issue 4, pp. 538-544.

17. Aragão, F. T. S., Kim, Y. R., Karki, P. and Little, D. N. (2010), Semi-Empirical, Analytical and Computational Predictions of Dynamic Modulus of Asphalt Concrete Mixtures, *Accepted for publication by the Transportation Research Board of the National Academics*, Washington, D.C.

18. ASTM D 3497-79, *Standard Test Method for Dynamic Modulus of Asphalt Mixtures*, *American Society for Testing and Materials*, Withdrawn in 2009.

19. ASTM D 692 / D 692 M-09, *Standard Specification for Coarse Aggregate for Bituminous Paving Mixtures*

20. ASTM D 1073-07, *Standard Specification for Fine Aggregate for Bituminous Paving Mixture*

21. ASTM D 242 / D 242 M-09, *Standard Specification for Mineral Filler for Bituminous Paving Mixtures*

22. ASTM D 3381/ D 3381 M-09a, *Standard Specification for Viscosity-Graded Asphalt Cement for Use in Pavement Construction*

23. ASTM C 117-04, *Standard Test Method for Materials Finer than 75-μm (No. 200) Sieve in Mineral Aggregates by Washing*

24. Bari, J. and Witczak, M. W. (2006), Development of A New Revised Version of The Witczak E* Predictive Model for Hot Mix Asphalt Mixtures, *Journal of the Association of Asphalt Paving Technologists,* Volume 75, pp. 381-423.

25. Barksdale, R. D. (1993). *The Aggregate Handbook,* National Stone Association, Washington, D. C.

26. Bei, H., Z.P. Lu, and George, E.P. (2004), Theoretical Strength and the Onset of Plasticity in Bulk Metallic Glasses Investigated by Nanoindentation with a Spherical Indenter, Physical Review Letters, American Physical Society, Volume 93, Number 12

27. Shen, Y.L. and Tang, G. (2009), Effect of Material Heterogeneity on The Evolution of internal Deformation during Nanoindentation, *International Journal of Materials and Structural Integrity*, Volume 3, Number 2-3, pp. 102-113.

28. Berkovich, E.S. (1951), Three Faceted Diamond Pyramids for Micro-Hardness Testing, *Industrial Diamond Review,* Volume 11, No. 127, pp.129-132

29. Boussinesq, J. (1885), *Application Des Potentiels à l'Étude de l'Équilibre et du Mouvement des Solides Élastiques*, Gauthiers -Villars, Paris

30. Brinell, J.A., (1901), II Congrès Internationál des Méthodes d'Essai, *Iron and Institute Journal*, Volume 59, p. 243.

31. Bonnaure, F., Gest, G., Gravois, A. and Uge, P. (1977), A New Method of Predicting The Stiffness of Asphalt Paving Mixtures, *Journal of the Association of Asphalt Paving Technologists*, Volume 46, pp. 64–104.

32. Bulychev, S.I., V. P., Alekhin, M. Kh., Shorshorov A. P., Ternovskii and G.D. Shnyrev (1975), Determining Young's Modulus from The Indenter Penetration Diagram, *Zavod Lab,* Volume 41, No. 9, pp. 1137-1140.

33. Bulychev, S.I., V.P. Alekhin, M. Kh. Shorshorov and A.P. Ternovskii (1976), Mechanical Properties of Materials Studied from Kinetic Diagrams of Load Versus Depth of Impression During Microimpression, *Strength of Materials*, Volume 8, No. 8, pp. 1084–1089.

34. Buttlar W.G. and R. Roque (1996), Evaluation of Empirical And Theoretical Models to Determine Asphalt Mixture Stiffnesses at Low Temperatures, *Journal of Association of Asphalt Paving Technologists*, Volume 65, pp. 99–141.

35. Buttlar W. G., D. Bozkurt, G. G. Al-Khateeb and A. S. Waldhoff (1999), Understanding Asphalt Mastic Behavior through Micromechanics, In *Transportation Research Record 1681*, Transportation Research Board of the National Academics, Washington, D.C., pp. 157–166.

36. Campen, J.F., Smith, J.R., Erickson, L.G., and Mertz, L.R. (1959), The Relationships Between Voids, Surface Area, Film Thickness and Stability in Bituminous Paving Mixtures, *Proceedings of the Association of Asphalt Paving Technologists*, Volume 28, pp. 149-178

37. Christensen, R. M., and Lo, K. H. (1979), Solutions for Effective Shear Properties in Three Phase Sphere and Cylinder Models, Journal of the Mechanics and Physics of Solids, Volume 27, Issue 4, pp. 315–330.

38. Christensen, D. W., Pellinen, T., and Bonaquist, R. F. (2003), Hirsch Model for Estimating The Modulus of Asphalt Concrete, *Journal of the Association of Asphalt Paving Technologists,* Volume 72, pp. 97-121.

39. Christensen, D. W. and Anderson, D. A. (1992), Interpretation of Dynamic Mechanical Test Data for Paving Grade Asphalt Cements, *Proceedings of the Association of Asphalt Paving Technologists,* Volume 61, pp. 67–116.

40. Ceylan. H., Gopalakrishnan. K., Kim. S. (2009), Looking to The Future: The Next-Generation Hot Mix Asphalt Dynamic Modulus Prediction Models, *International Journal of Pavement Engineering,* Volume 10, Issue 5, pp. 341 – 352.

41. Ceylan, H., Schwartz, C. W., Kim, S, and Gopalakrishnan, K. (2009), Accuracy of Predictive Models for Dynamic Modulus of Hot-Mix Asphalt, *Journal of Materials in Civil Engineering*, American Society of Civil Engineers, Volume 21, No. 6, pp. 286-293.

42. Couto, U. J. (1964), The Effect of The Elastic Modulus of The Aggregate on The Elastic Modulus, Creep, and Creep Recovery of Concrete, *Magazine of Concrete Research*, Volume 16, No. 48, pp. 129–138

43. Dai, Q. and You, Z. (2008), Micromechanics Finite Element Framework for Predicting Viscoelastic Properties of Asphalt Mixtures, *Materials and Structures*, Volume 41, Number 6, 1025-1037.

44. Dai, Q. & You, Z (2007), Prediction of Creep Stiffness of Asphalt Mixture and Micromechanics Finite-Element and Discrete Models. *Journal of Engineering Mechanics*, American Society of Civil Engineers, Volume 133, Number 2, pp. 163–173.

45. Doerner, M.F., and Nix, W.D. (1986), A Method for Interpreting the Data from Depth-Sensing Indentation Instruments, *Journal of Material Research*, Volume 1, Issue 4, pp.601-609.

46. Druta, C. (2006), *A Micromechanics Approach for Predicting the Complex Shear Modulus and Accumulated Shear Strain of Asphalt Mixtures from Binder and Mastics*, Doctoral Dissertation, Louisiana State University and Agricultural and Mechanical College, Louisiana

47. Eriksen, K, and Wegan, V. (1993), Optical Methods for the Evaluation of Asphalt Concrete and Polymer-Modified Bituminous Binders, *Note 244*, Danish Road Institute, Roskilde, Denmark

48. Gillespie H.M. (1992), *A Century of Progress: The History of Hot Mix Asphalt*, National Asphalt Pavement Association, Landham, MD

49. Goode, J.F. and Lufsey, L.A. (1965), Permeability, Film Thickness vs. Asphalt Hardening, *Proceedings of Association of Asphalt Paving Technologists*, Volume 34, pp. 430-463.

50. Goodrich, J. L. (1988), Asphalt and Polymer Modified Asphalt Properties Related to The Performance of Asphalt Concrete Mixes, *Journal of the Association of Asphalt Paving Technologists*, Volume 57, pp. 116–175.

51. Goodrich, J. L. (1991), Asphaltic Binder Rheology, Asphalt Concrete Rheology, and Asphalt Concrete Mix Properties, *Journal of the Association of Asphalt Paving Technologists*, Volume 60, pp. 80–120.

52. Hashin, Z. (1962), The Elastic Moduli of Heterogeneous Materials, Journal *of Applied Mechanics*, American Society of Mechanical Engineers, Volume 29, pp. 143–150

53. Hashin, Z., and Shtrikman, S. (1963), A Variational Approach to The Theory of The Elastic Behavior of Multiphase Materials, *Journal of the Mechanics and Physics of Solids*, Volume 11, Issue 2, pp. 127–140

54. Hashin, Z. (1965), Viscoelastic Behavior of Heterogeneous Media, *Journal of Applied Mechanics*, Volume 9, pp. 630–636.

55. Hertz, H. (1881), Über die Berührung Fester Elastischer Körper, *Journal für die Reine und Angewandte Mathematik*, Volume 92, pp. 156-171.

56. Hinrichsen, J. A., and Heggen, J. (1996), Minimum Voids in Mineral Aggregate in Hot-Mix Asphalt Based on Gradation and Volumetric Properties, *Transportation Research Record 1545*, Transportation Research Board of the National Academics. Washington, D.C., pp. 75-79.

57. Hirsch, T. J. (1962), Modulus of Elasticity of Concrete Affected by Elastic Moduli of Cement Paste Matrix and Aggregate, *Journal of American Concrete Institute*, Volume 59, No. 3, pp. 427-451.

58. Kandhal, P.S., and Chakraborty, S. (1996), Effect of Asphalt binder film Thickness on Short and Long Term Aging of Asphalt Paving Mixtures, *NCAT Report 96-01*, National Centre for Asphalt Technology, Auburn, AL

59. Kandhal, P.S., Foo, K.Y., and Mallick, R.B. (1998), A Critical Review of VMA Requirements in Superpave, *NCAT Report 98-01*, National Centre for Asphalt Technology (NCAT), Auburn, AL

60. Kim, Y. R., Daniel, J. S., & Wen, H. (2002), Fatigue Performance Evaluation of WesTrack and Arizona SPS-9 Asphalt Mixtures Using Viscoelastic Continuum Damage Approach, *Final Report FHWA/NC/2002-004* submitted to North Carolina Department of Transportation.

61. Kim, Y.R., Little D.N., Lytton R.L. (2002), Use of Dynamic Mechanical Analysis (DMA) to Evaluate The Fatigue And Healing Potential of Asphalt Binders in Sand Asphalt Mixtures, *Journal of the Association of Asphalt Paving Technologists*, Volume 71, pp.176–206.

62. Kim, Y. R., Little, D. N., and Lytton, R. L. (2003), Fatigue and healing characterization of asphalt mixtures." *Journal of Materials in Civil Engineering*, American Society of Civil Engineers, Volume 15, Issue 1, pp. 75–83.

63. Kim, Y. R, D. N. Little and R. L. Lytton (2004), Effect of Moisture Damage on Material Properties and Fatigue Resistance of Asphalt Mixtures, Transportation Research Record 1891, Transportation Research Board of the National Academics, Washington, DC, pp. 48-54.

64. Kim, Y. R., Allen, D. H., and Little, D. N. (2007), Computational Constitutive Model for Predicting Nonlinear Viscoelastic Damage and Fracture Failure of Asphalt Concrete Mixtures, *International Journal of Geomechanics*, American Society of Civil Engineers, Volume 7, No. 2, pp. 102-110.

65. Kim, Y. R., Lee, J. and Lutif, J. (2010), Geometrical Evaluation and Experimental Verification to Determine Representative Volume Elements of Heterogeneous Asphalt Mixtures, *Journal of Testing and Evaluation*, (In Print).

66. Kumar, A. and Goetz, W.H. (1977), Asphalt Hardening as Affected by Film Thickness, Voids and Permeability in Asphaltic mixtures, *In Proceedings of The Association of Asphalt Paving Technologists*, Volume 46.

67. Kushch, V.I., Dub, S.N., Litvin , P.M. (2007), Determination of the Young Modulus from Elastic Section of the Berkovich Indenter Loading Curve, *Journal of Superhard Materials*, Volume 29, No. 4, pp. 228-234.

68. Loubet, J. L. , Georges, J. M., Marchesini, O., Meille, G. (1984), Vickers Indentation Curves of Magnesium Oxide (MgO), *Journal of Tribology*, Volume 106, pp. 43-48

69. Loubet, J. L., Georges, J. M., Meille, G., (1986), Vickers Indentation Curves of Elastoplastic Materials, *Microindentation Techniques in Materials Science and Engineering*, pp. 72-89.

70. Love, A.E.H. (1929), The Stress in A Semi-Infinite Solid by Pressure on Part of the Boundary, *Philosophical Transactions of the Royal Society of London*, Series A, Volume 228, pp. 377-420.

71. Love, A.E.H. (1939), Boussinesq's Problem for A Rigid Cone, *Quarterly Journal of Mathematics*, Oxford University Press, Volume 10, pp. 161–175.

72. Masad, E., Muhunthan, B., Shashidhar, N. and Harman, T. (1999), Internal Structure Characterization of Asphalt Concrete Using Image Analysis, *Journal of Computing in Civil Engineering*, American Society of Civil Engineers, Volume 13, No. 2, pp. 88-95.

73. Masad, E., Niranjanan, S. (2002), Microstructural Finite-Element Analysis of Influence of Localized Strain Distribution on Asphalt Mix Properties, *Journal of Engineering. Mechanics*, American Society of Civil Engineers, Volume 128, Issue 10, pp. 1105-1114

74. McLeod, N.W. (1956), Relationships between Density, Bitumen Content and Voids Properties of Compacted Bitumen Paving Mixtures, *Proceedings of Highway Research Board*, Volume 35, pp. 327-404.

75. McLeod, N.W. (1959), Voids Requirements for Dense-Graded Bituminous Paving Mixtures, *Special Technical Publication 252*, American Society of Testing Materials.

76. Meyer, E. (1908), Untersuchungen über Härteprüfung und Härte, *Zeitschrift des Vereines Deutscher Ingenieure*, Volume 52, pp. 645-654.

77. MS-2, (1984), *Mix Design Methods for Asphalt Concrete and Other Hot-Mix Types (1984)*, Asphalt Institute.

78. MS-2, (1993), *Mix Design Methods for Asphalt Concrete and Other Hot-Mix Types (1993)*, Asphalt Institute, Sixth Edition

79. Mori, T., and Tanaka, K. (1973), Average Stresses in Matrix and Average Energy of Materials with Misfitting Inclusions, *Acta Metallurgica*, Volume 21, pp. 571–574

80. National Stone, Sand and Gravel Association (2009), Accessed online at http://nssga.org/communications/whoweare.cfm, Accessed on February 17, 2010.

81. Newey, D., Wilkins, M. A, and Pollock, H. M. (1982), An Ultra-Low-Load Penetration Hardness Tester, *Journal of Physics E: Scientific Instruments*, Volume 15, Number 1, pp. 119–122

82. Oliver, W.C. and Pharr, G.M. (1992), An Improved Technique for Determining Hardness and Elastic Modulus Using Load and Displacement Sensing Indentation Experiments, *Journal of Material Research*, Volume 7, No. 6, pp. 1564–1583

83. Oliver, W. C. and Pharr, G. M. (2004), Review: Measurement of Hardness and Elastic Modulus by Instrumented Indentation: Advances in Understanding and Refinements to Methodology, *Journal of Material Research*, Volume 19, No. 1, pp. 3-20

84. Papagiannakis, A. T., Abbas, A., and Masad, E. (2002). Micromechanics Analysis of Viscoelastic Properties of Asphalt Concretes, *Transportation Research Record 1789*, Transportation Research Board of the National Academics, pp. 113-120.

85. Pethica, J.B., Hutchings, R., Oliver, W.C. (1983), Hardness Measurement at Penetration Depths as Small as 20 nm, *Philosophical magazine* A, Volume 48, Issue 4, pp. 593–606.

86. Prowell, B. D., Zhang, J., & Brown, E. R. (2005), Aggregate Properties and the Performance of Superpave-Designed Hot Mix Asphalt, *NCHRP Report-539*, National Cooperative Highway Research Program, Transportation Research Board of the National Academics, Washington, D.C.

87. Radovskiy, B. (2003), Analytical Formulas for Film Thickness in Compacted Asphalt Mixture, *Transportation Research Record 1829*, Transportation Research Board of the National Academics, Washington, D.C., pp. 26-32.

88. Reese, R. (1997), Properties of Aged Asphalt Binder Related to Asphalt Concrete Fatigue Life, *Journal of the Association of Asphalt Paving Technologists*, Volume 66, pp. 604–632.

89. Roberts, F. L., Kandhal, P. S., Brown, E. R., Lee, D. Y., & Kennedy, T. W. (1996), *Hot Mix Asphalt Materials, Mixture Design and Construction*, National Center for Asphalt Technology, Auburn University, Second Edition.

90. Shashidhar, N. and Shenoy, A. (2002), On Using Micromechanics Models to describe Dynamic Mechanical behavior of Asphalt Mastics, *Mechanics of Materials*, Volume 34, Issue 10,

91. Shu, X. and Huang, B. (2008), Dynamic Modulus Prediction of HMA Mixtures Based on The Viscoelastic Micromechanics Model, *Journal of Materials in Civil Engineering*, American Society of Civil Engineers, Volume 20, No. 8, pp. 530-538.

92. Shu, X. and Huang, B. (2008), Micromechanics-Based Dynamic Modulus Prediction of Polymeric Asphalt Concrete Mixtures, *Composites - Part B: Engineering*, Volume 39, Issue 4, pp. 704-713

93. Sneddon, I.N, (1946), Boussinesq's Problem for A Flat-ended Cylinder, *Mathematical Proceedings of the Cambridge Philosophical Society*, Volume 42, pp. 29-49.

94. Sneddon, I.N, (1948), Boussinesq's problem for a rigid cone, *Mathematical Proceedings of the Cambridge Philosophical Society*, Volume 44, pp. 492-507.

95. Sneddon, I.N (1965), The Relation Between Load and Penetration in The Axisymmetric Boussinesq Problem for A Punch of Arbitrary Profile, *International Journal of Engineering Science*, Volume 3, pp. 47-57

96. Ternovskii, A.P., Alekhin, V.P., Shorshorov, M.K., Khrushchov, M.M., Skvortsov, V.N. (1973), Micromechanics Testing of Materials by Depression, *Industrial Laboratory*, Volume 39, No. 10, pp. 1242-1247.

97. Uddin, W. (2001), A Micromechanics Model for Prediction of Creep Compliance and Viscoelastic Analysis of Asphalt Pavements, National Centre for Asphalt Technology, Second International Symposium on Maintenance and Rehabilitation of Pavements and Technological Control, Auburn, AL.

98. Voigt, W. (1889), Ueber die Beziehung zwischen den beiden Elasticitatsconstanten isotroper Korper, *Annalen der Physik und Chemie (Leipzig)*, Volume 38, pp. 573–587.

99. You, Z. (2003), Development of a Micromechanics Modeling Approach to Predict Asphalt Mixture Stiffness Using the Discrete Element Method, *Ph. D. Dissertation*, University of Illinois at Urbana-Champaign, Urbana, IL.

100. You, Z. and Buttlar, W. G. (2006), Micromechanics Modeling Approach to Predict Compressive Dynamic Moduli of Asphalt Mixture Using the Distinct Element Method, *Transportation Research Record 1970*, Transportation Research Board of National Academics, pp. 73-83.

101. You, Z., Adhikari, S., and Kutay, M. E. (2008), Dynamic Modulus Simulation of The Asphalt Concrete Using The X-Ray Computed Tomography Images, *Materials and Structures*, Volume 42, No. 5, pp. 617-630.